12-2020

# Behavior of Concrete Structures Reinforced with High Strength Steel

Rahman S. Kareem
*University of Arkansas, Fayetteville*

Behavior of Concrete Structures Reinforced with High Strength Steel


A dissertation submitted in partial fulfillment
of the requirements for the degree of
Doctor of Philosophy in Engineering with a concentration in Civil Engineering


by


Rahman S. Kareem
University of Basrah
Bachelor of Science in Civil Engineering, 2007
University of Basrah
Master of Science in Civil Engineering, 2010


December 2020
University of Arkansas


This dissertation is approved for recommendation to the Graduate Council.


_____
Micah Hale, Ph.D.
Dissertation Director


_____                   _____
Gary Prinz, Ph.D.                                  Cameron Murray, Ph.D.
Committee Member                                   Committee Member


_____                   _____
Mark Arnold, Ph.D.                                 Canh Dang, Ph.D.
Committee Member                                   Committee Member

# ABSTRACT

The structural strength and corrosion resistance of concrete members are improved when A1035 steel is used as the main reinforcement.  The enhancement of A1035 is achieved by the modification of the composition and microstructure of the steel.  Therefore, the behavior of concrete structures reinforced with high-performance steel (A1035) is different from those reinforced with the regular steel (A615).  Concrete bridge decks reinforced with different amounts of A1035 were studied in this research program.  The structural behavior of twelve concrete bridge decks reinforced with A615 Grade 420 (60 ksi) and A1035 Grade 830 (120 ksi) steel was investigated at both service and strength limit states.  The tensile strain of steel and compressive strain of the concrete were measured in each load step.  In addition to measuring the deflection, a microscope was used to measure the maximum crack width during testing.  Then, the finite element method was used to model the concrete bridge decks.  ABAQUS software was used to represent the model.  The concrete material was represented by C3D8 elements, and the steel material was modeled by T3D2 elements.  Concrete Damaged Plasticity Model was used to represent the nonlinear behavior of concrete.  The plastic behavior of the reinforcing steel was represented by Plasticity option.  The final part of the dissertation focuses on investigating the structural behavior of concrete beams reinforced with A1035 and cast with different concrete strengths.  The structural behavior of eight reinforced concrete beams was investigated.  Two types of reinforcement were used, regular steel (A615) and high-performance steel (A1035).  Three different concrete strengths were used, normal, high, and ultra-high strength.  The deflection, maximum crack width, compressive strain of concrete, and tensile strain of steel were measured during testing.

## DEDICATION

I dedicate this dissertation to my mother for her constant unconditional love and to the memory of my father.

**TABLE OF CONTENT**

# LIST OF FIGURES

# LIST OF TABLES

# A LIST OF PUBLISHED JOURNAL ARTICLES

**Chapter 2:** Rahman S. Kareem; Casey Jones; Canh N. Dang; Gary S. Prinz; and W. Micah Hale, "Structural Performance of Concrete Bridge Decks Reinforced with Grade-830 Steel Bars," Journal of Structures. V. 27, 2020, pp. 1396-1404.

**Chapter 3**: Rahman S. Kareem; Canh N. Dang; Gary S. Prinz; and W. Micah Hale, "Flexural Performance of Bridge Decks Reinforced with High-Strength Steel: Finite Element Analysis Approach," Journal of Structures. 2020 (Submitted).

**Chapter 4**: Rahman S. Kareem; Canh N. Dang; and W. Micah Hale, "Flexural Behavior of Concrete Beams Cast with High-Performance Materials," Journal of Building Engineering.  2020 (Submitted).

# CHAPTER 1: INTRODUCTION AND RESEARCH OBJECTIVES

## 1.1 INTRODUCTION

For several years, reinforced concrete structures were designed by using reinforcing steel that was limited to a yield strength 420 MPa (60 ksi) or less. Currently, the reinforcing steel, most widely used to design concrete structures, conforms to ASTM A615 steel [1]. This steel has a well-defined yield strength and yield plateau, and includes Grade 280 MPa (40 ksi), Grade 420 MPa (60 ksi) and Grade 520 MPa (75 ksi) [2]. The behavior of concrete structures reinforced with regular steel (A615) has been investigated for decades. However, engineering designers have faced some problems when they design structures reinforced with regular steel. In addition to the corrosion problems of regular steel, congestion of reinforcement is another major problem. Also, the demands of transportation and high buildings have been increasing due to rapid urbanization and population growth. As a result, the service life of concrete structures is reduced, and the life-cycles costs is increased.

Concrete structures exposed to severe environments may have corrosion problems [3]. The Federal Highway Administration predicts that deficient bridges in the USA require an additional investment of approximately $7.7 billion annually in order to eliminate the deficient bridges by 2028 [4]. One of the major contributors to the bridge deficiency is the corrosion of reinforcement. Corrosion of the steel reinforcement leads to deterioration of concrete structures [5]. When reinforcing steel expands due to corrosion, these bars create a great inner pressure on the adjacent concrete. The internal pressure continues increasing until exceeding the tensile strength of concrete; then, this pressure causes the concrete to crack, which leads to spalling of the concrete and debonding of the reinforcing bar [6]. Consequently, the corrosion problems of

reinforcing steel in concrete structures reduce their service life and increases their life-cycle costs.

The major components of reinforced concrete members, reinforcing steel and concrete, have improved which has reduced the structural problems and increased the construction quality. The development of high strength materials can be used in concrete members to reduce cross sections, avoid steel congestion, reduce cost, improve corrosion resistance, and increase ultimate strength [7]. Researchers have investigated the influence of corrosion on infrastructure. The corrosion problems in reinforced concrete can be reduced by using high-performance steel because of its improved corrosion resistance [3]. High-performance steel, such as A1035 reinforcing bars, can also reduce the reinforcement ratio, increase the durability, and extend the service life of concrete structures [8].

## 1.2   ASTM A1035 STEEL OVERVIEW

The interest of using A1035 steel as the reinforcement in concrete structures is increasing because of the billions of dollars that could be saved in the U.S. [9,10,11]. Due to the enhanced properties of A1035 steel, the use of this steel in concrete structures can reduce cross-section dimensions, save materials and labor costs, and extend periodic maintenance intervals. High-performance steel bars conforming to A1035 are different in composition and microstructure from the regular reinforcing steel (A615). These changes improve the properties of A1035 in comparison to regular steel, such as a higher yield strength and improved corrosion resistance. The manufacture requirements of A1035 are considerably simpler than epoxy-coated reinforcing bars which are typically used in highly corrosive environments. Therefore, A1035 steel has started to be used in concrete members exposed to aggressive environments, such as bridge decks and underground tunnels [9].

2

Recently, researchers and designers have started to use A1035 steel as main reinforcement in concrete structures due to the improved corrosion resistance [12,13]. Reducing corrosion problems and increasing the ultimate strength of the structures are major advantages of using A1035 as main reinforcement. The corrosion resistance of A1035 steel is 5 to 6 times greater than A615 steel [12]. The concrete structures reinforced with A615 steel may need repair after 30 to 40 years of service, while the use of A1035 steel can extend the service life for the structures over 100 years [14,15].

In addition to the improved corrosion resistance, A1035 steel reinforcement is distinguished by a greater tensile strength and having no clear yield strength in its stress-strain relationship [16]. The yield strength of A1035 is determined by the offset method (0.2 % offset) [17,18]. The nominal yield strength for A1035 steel is 690 MPa (100 ksi) or 830 MPa (120 ksi), which is around 1.7 to 2 times greater than that of A615 Grade 420 (60 ksi) steel [13]. The carbon content in A1035 steel is specified at a maximum of 0.15 percent, while the chromium content is specified 8 to 10.9 percent [17].

The replacement of regular steel (A615) with high-performance steel (A1035) in concrete structures as a one-to-one ratio is considered a very conservative approach. The premium cost of A1035 is approximately 175% of regular steel [19]. In addition to the increased material costs, the direct replacement of regular steel with high-performance steel may lead to some problems such as, over-reinforcement and therefore members with less ductility. The full strength of A1035 has not been used in the design of concrete structures because of the lack of information on the behavior of concrete structures reinforced with this steel [11,20]. Recently, many researchers and several institutions have begun studying the applications of A1035 in concrete

structures [20]. Concrete structures designed using the total strength of A1035 can lead to reductions in steel, labor, cross-sections sizes, and shipping and placement costs [12].

## 1.3 MOTIVATION

The use of high-performance steel (A1035) improves the structural behavior of concrete members. Using A1035 in concrete structures reduces the effect of reinforcement corrosion, increases the structural durability, and extends the service life. However, concrete structures reinforced with high-performance steel are subject to greater service loads, which increases crack width. Additionally, the type of failure is different from that of structures reinforced with regular steel (A615). A better understanding of the structural behavior of concrete members reinforced with high-performance steel is one of the goals of this study. This research program investigates the material and cost saving that can be realized when using A1035 steel. A finite element model is also developed in this program for studying the behavior of concrete structures reinforced with A1035 which can provide an alternative method to experimental research.

## 1.4 RESEARCH OBJECTIVES

The objectives of the research project are as follows:

1. Investigate the structural behavior of concrete bridge decks, reinforced with A615 steel and A1035 steel, at the service and strength limit states.

2. Investigate the effect of reducing concrete cover of concrete bridge decks.

3. Examine the effect of reducing the quantity of reinforcement (reinforcement ratio) in concrete structures reinforced with A1035.

4. Document the material and cost savings associated with using A1035 reinforcement.

5. Examine the structural behavior of concrete beams reinforced with A1035 and cast with different concrete strengths.

6. Predict the analytical moment-deflection relationship of flexural members cast with A1035 reinforcement.

7. Develop a finite element model for concrete members reinforced with A1035.

## 1.5 DISSERTATION ORGANIZATION

This dissertation is a compilation of three journal articles which support the main idea and the primary objectives of this research. This dissertation contains five chapters. Chapter 1 is the introduction, overview of A1035 steel, objectives, and motivation for the presented research. Chapter 2 describes the investigation of structural performance of concrete bridge decks reinforced with Grade 830 steel bars. Chapter 3 summarizes the finite element model of bridge decks reinforced with high-performance steel. Chapter 4 focuses on studying the flexural behavior of concrete beams cast with high-performance materials. Chapter 5 presents a list of conclusions, scientific contributions of the research, and recommendations for further research.

## REFERENCES

[1] Mandadi, S., "Analytical Study of the Behavior of Beams Reinforced with High Strength Reinforcing Bars," Master Thesis in Civil Engineering, University of Texas at San Antonio, 2016, USA.

[2] Yosefani, A., "Flexural Strength, Ductility, and Serviceability of Beams that Contain High-Strength Steel Reinforcement and High-Grade Concrete," Doctor Dissertation of Philosophy in Civil Engineering, Portland State University, 2018, USA.

[3] Seliem, H., Lucier, G., Rizkalla, S., and Zia, P., "Behavior of Concrete Bridge Decks Reinforced with High-Performance Steel," ACI Structural Journal, V. 105, No. 1, 2008, pp. 78-86.

[4] American Society of Civil Engineers (ASCE), "Report Card for America's Infrastructure: 2013 Progress Report," 2013, Retrieved from www.asce.org/reportcard/2013.

[5] Hassan, T., Abdelrahman, A., Tadros, G., and Rizkalla, S., "Fibre Reinforced Polymer Reinforcing Bars for Bridge Decks," Canadian Journal of Civil Engineering, V. 27, No. 5, 2000, pp. 839-49.

[6] Broomfield, J.P., "Corrosion of Steel in Concrete: Understanding, Investigation and Repair," Taylor & Francis, United Kingdom, 2007.

[7] Bishaw, B.B., "Effect of High Strength Materials on the Seismic Performance of Reinforced Concrete Moment Resisting Frames," Doctor Dissertation of Philosophy in Civil Engineering, University of Utah, 2016, USA.

[8] Munikrishna, A., Hosny, A., Rizkalla, S., and Zia, P., "Behavior of Concrete Beams Reinforced with ASTM A1035 Grade 100 Stirrups Under Shear," ACI Structural Journal, V. 108, No. 1, 2011, pp. 1-34.

[9] Desalegne, A.S., Lubell, A.S., "Shear in Concrete Beams Reinforced with High-Performance Steel. ACI Structural Journal, V. 112, No. 6, 2015, pp. 783-792.

[10] Reis. H., Ervin, B.L., Kuchma, D.A., and Bernhard, J.T., "Estimation of Corrosion Damage in Steel Reinforced Mortar Using Guided Waves," Journal of Pressure Vessel Technology, V. 127, No. 3, pp. 255-261.

[11] Darwin, D., Browning, J., Nguyen, T.V., and Locke, C., "Mechanical and Corrosion Properties of a High-Strength, High Chromium Reinforcing Steel for Concrete," SM Report No. 66, University of Kansas, Lawrence KS, 2002.

[12] Faza, S., Kwok, J., and Salah, O., "Application of High-Strength and Corrosion-Resistant ASTM A1035 Steel Reinforcing Bar in Concrete High-Rise Construction," CTBUH 8th World Congress, Council on Tall Buildings and Urban Habitat, Chicago, Illinois, Dubai, 2008.

[13] Shahrooz, B.M., Reis, J.M., Wells, E.L., Miller, R.A., Harries, K.A., and Russell, H.G., "Flexural Members with High-Strength Reinforcement: Behavior and Code Implications," Journal of Bridge Engineering, V. 19, No. 5, 2014, pp. 1–7.

[14] Tikalsky, P.J., and Beh, D.E., "The Synthesis of Design Guidelines for Corrosion Resistant Reinforced Concrete," UT- 08-27, Utah Department of Transportation 4501 South 2700 West Salt Lake City, Utah 84114-8410, 2008

[15] Bowen, G.E., "Service and Ultimate Limit State Flexural Behavior of One-Way Concrete Slabs Reinforced with Corrosion-Resistant Reinforcing Bars," Thesis Master of Science in Civil Engineering, Virginia Polytechnic Institute and State University, 2013.

[16] Harries, K.A., Shahrooz, B.M., Soltani, A., "Flexural Crack Widths in Concrete Girders with High-Strength Reinforcement. Journal of Bridge Engineering. V. 17, No. 5, 2011, pp. 804-812.

[17] Wiss, Janney, Elstner Associates, Inc. Mechanical Properties of ASTM A1035 High Strength Steel Bar Reinforcement. WJE No. 2008.9901.0. Chicago, Illinois, 2008.

[18] Standard Specification for Deformed and Plain, Low-Carbon, Chromium, Steel Bars for Concrete Reinforcement, ASTM A1035/A1035M – 14.

[19] Bridge Design and Drafting Manual – May 2017, Oregon Department of Transportation.

[20] Hassan, T.K., Seliem, H.M., Dwairi, H., Rizkalla, S.D., and Zia, P., "Shear Behavior of Large Concrete Beams Reinforced with High-Strength Steel," ACI Structural Journal, V. 105, No. 2, 2008, pp. 173-179.

# CHAPTER 2: STRUCTURAL PERFORMANCE OF CONCRETE BRIDGE DECKS REINFORCED WITH GRADE-830 STEEL BARS

Rahman S. Kareem[1], Casey Jones[1], Canh N. Dang[2,3*], Gary S. Prinz[1], W. Micah Hale[1]

[1] University of Arkansas, Department of Civil Engineering, 4190 Bell Engineering Center

Fayetteville, AR 72701, USA

[2] Department for Management of Science and Technology Development, Ton Duc Thang

University, Ho Chi Minh City, Vietnam

[3] Faculty of Civil Engineering, Ton Duc Thang University, Ho Chi Minh City, Vietnam

* Corresponding author:

Emails: canhdang@tdt.edu.vn

Phone +1-479-575-6348

## ABSTRACT

High-performance reinforcement, which is known by its high-corrosion resistance and high-strength, is advantageous in the design and construction of concrete bridge decks. This research investigates the structural behavior of concrete bridge decks reinforced with either high-performance A1035M (Grade 830) or ASTM A615M (Grade 420) reinforcing steel at both the service and strength limit states. The tensile strain of the reinforcing steel, the compressive strain of the concrete, and the deflection of the specimens were monitored continuously during testing. A crack width microscope was used to measure the maximum crack width and the number of cracks. The results indicated an increased serviceability and flexural strength for the decks containing Grade 830 reinforcing steel.

**KEYWORDS:** High-performance reinforcement; bridge deck; serviceability; flexural resistance.

## 2.1 INTRODUCTION

According to the Report Card of the American Society of Civil Engineers (ASCE), there are two hundred million daily trips across insufficient bridges in the USA [1]. The Federal Highway Administration predicts that $20.5 billion should be invested annually to eliminate the nation's deficient bridges by 2028, whereas only $12.8 billion is currently being invested [1]. Corrosion of reinforcement in bridge decks is one of the major contributors to bridge deterioration. Bridge decks can be exposed to severe environments and subjected to a number of freezing-thawing cycles [2]. The deterioration mechanism of reinforcing steel corrosion within bridge decks is known [3]. When corrosion occurs, the reinforcing steel expands, which produces pressure on the adjacent concrete. When the pressure exceeds the concrete's tensile strength, concrete cracking occurs along with spalling of the concrete cover and debonding of the reinforcing steel [4]. However, these deficits can be prevented if the corrosion resistance of the reinforcing steel can be enhanced. The enhanced corrosion resistance can then increase the service life of concrete bridges and reduce the life-cycles costs of bridge decks.

Researchers have investigated the effects of corrosion on infrastructure for many years [5]. Corrosion problems in reinforced concrete can be reduced by using high-performance reinforcing steel, such as ASTM A1035M reinforcement [2]. The composition and microstructure of this steel has been modified which increases its corrosion resistance. For ASTM A615M (here after referred as Grade 420), the phosphorus content is specified up to 0.06%, and there is not minimum chromium content [6]. On the other hand, A1035M steel includes a maximum carbon and phosphorus content of 0.15% and 0.035%, respectively, and the chromium content shall be between 8% and 10.9% [7]. When compared to A615M steel, the corrosion resistance of A1035M steel is 5 to 6 times higher, which can extend periodic

maintenance intervals or extend the service life of the bridge decks. In particular, concrete structures reinforced by Grade 420 steel may require maintenance after 20 to 30 years of service [8]. On the other hand, A1035M steel can extend the service life for the structure to over 100 years [9].

ASTM A1035M steel has two grades, Grade 690 (or equivalent to Grade 100 in U.S. practice) and Grade 830 (or equivalent to Grade 120 in U.S. practice). The use of Grade 830 reinforcement in concrete structures can reduce the reinforcement ratio because of its higher yield strength [10]. Grade 830 steel is distinguished from Grade 420 steel by its greater tensile strength and no apparent yield plateau in its stress-strain relationship [11]. The offset method (0.2% offset) is used to determine the nominal yield strength for Grade 830 steel [12]. The nominal yield strength of Grade 830 steel is 1.7 to 2 times greater than that of Grade 420 steel. Due to its greater yield strength, the amount of reinforcement can be decreased, when compared to the same structure using Grade 420 steel, which can decrease the overall cost [13].

In summary, the use of Grade 830 steel is advantageous for bridge decks based on the improved corrosion resistance and the higher yield strength, which can reduce the overall amount of steel needed in the deck. It has been estimated that using Grade 830 steel can result in a savings of 40% in reinforcement costs when compared to Grade 420 steel [13,14,15]. This assessment is based on an equivalency in tension force of the reinforcement. Due to the lower reinforcement ratio that can be achieved with Grade 830 reinforcement when compared to Grade 420 steel, further experimental testing is necessary to better understand the structural performance (i.e., moment capacity, deflection, crack width) of bridge decks reinforced with these higher grades of steel. Although the concrete structure reinforced with Grade 830 steel may be stiffer, there is less reinforcement in the bridge when compared to a similar bridge deck containing Grade 420

steel, and this could affect the deck performance. The project will also examine the material savings involved when using Grade 830 reinforcement in bridge decks. The reduction in reinforcement content discounts the additional cost of Grade 830 reinforcement and reduces both the labor cost and time for placing the reinforcement.

## 2.2 LITERATURE REVIEW

The use of A1035M reinforcement has several advantages when compared to Grade 420 reinforcement. In 2002, Ansley [16] investigated the behavior of four beams reinforced with Grade 690 or Grade 420 reinforcing steel. The authors concluded that the beams reinforced with Grade 690 steel resisted greater applied loads than the beams reinforced with Grade 420 steel at failure. Yotakhong [17] also investigated the flexural behavior of rectangular concrete beams reinforced with conventional steel stirrups and longitudinally reinforced with Grade 830 steel or Grade 420 steel. It was found that all concrete beams reinforced with Grade 830 steel had higher ultimate strengths and comparable ductility to the control beams reinforced by Grade 420 steel. The shear strength of reinforced concrete structures can also be increased by using Grade 830 steel as shear reinforcement (stirrups). In 2011, Munikrishna et al. [18] investigated the shear strength of large-sized concrete beams reinforced with Grade 830 steel stirrups. The performance of these beams was compared to that of similar beams reinforced with Grade 420 steel stirrups. The study indicated that by using Grade 830 stirrups with a reduced reinforcement ratio, the beams can achieve shear strengths that were similar to the beams reinforced with Grade 420 steel. In addition, Desalegne and Lubell [19] tested eight beams, which were longitudinally reinforced with Grade 830 steel and transversely reinforced with either Grade 830 or Grade 420 steel. The experimental results showed that the failure modes are different for specimens which

11

have various types of transverse reinforcing steel. Specimens transversely reinforced with Grade 420 steel failed in a shear mode due to the lower yielding strength of steel. However, specimens transversely reinforced with Grade 830 steel failed in a different mode. The beams showed significant nonlinear response of the longitudinal reinforcement before failure due to the higher yielding strength of the Grade 830 steel. This resulted in a flexural failure of beams transversely reinforced with Grade 830 steel.

Crack widths and crack patterns are also different in concrete members reinforced with Grade 830 steel when compared to those reinforced with Grade 420 steel. This is important because cracking in concrete members affects the structures' durability. The steel stress at the service state in concrete structures reinforced with higher strength reinforcement is anticipated to be greater than those reinforced by conventional steel. Thus, the steel strains at service loads are greater and affects crack behavior. Yotakhong [20] tested four large-scale concrete beams. Three beams were reinforced by Grade 830 steel, and one beam was reinforced by Grade 420 steel. The author investigated the beams' behavior during the pre-cracking, cracking, post-cracking, ultimate capacities, and modes of failure. Beams reinforced with Grade 830 steel showed higher ultimate strength in comparison to beams reinforced with Grade 420 steel. Also, the beams experienced smaller cracks widths and a reduced number of cracks in comparison to beams reinforced by Grade 420 steel at the same load level.

As previously mentioned, using Grade 830 steel can increase the corrosion resistance of concrete structures [11,13]. Naaman and Chandrangsu [21] stated that the major problem plaguing bridges is deck deterioration. The deck deterioration can be caused by corrosion resulting from severe environmental conditions [2]. Seliem [22] examined the improved corrosion resistance of Grade 830 steel in comparison to Grade 420 steel. The author investigated the corrosion rate and

the effect of corrosion on the tensile strength of Grade 830 steel bars. An accelerated corrosion test was conducted in Seliem's research. The results showed that the corrosion rate for Grade 830 steel is 87% less than that of Grade 420 steel. The author also investigated the behavior of concrete bridge decks reinforced with Grade 830 steel, and these decks were compared to others reinforced with the conventional Grade 420 steel. However, it was concluded that a direct replacement of Grade 420 steel with Grade 830 steel in bridge decks is conservative in terms of structural performance. In 2014, Salomon and Moen [15] tested 36 concrete decks reinforced with different types of corrosion-resistant steel. The authors stated that decks reinforced with corrosion-resistant steel can meet the requirements of serviceability and strength in addition to the advantage of enhanced corrosion resistance.

The improved corrosion resistance and higher strength of Grade 830 steel not only extend the service life of concrete structures but also reduce the total construction cost. Faza et al. [13] used Grade 830 steel to redesign a concrete mat foundation of a parking structure and shear walls in a building in Las Vegas, Nevada, USA. The structure was designed and constructed with Grade 420 steel. The authors proved that the total cost of the concrete members reinforced with Grade 830 steel could be reduced by 12 to 15% due to the reduction in the total amount of reinforcing steel and the reduced labor cost since fewer bars were used.

In summary, the use of Grade 830 steel can reduce rebar congestion, increase site safety, and result in improved constructability and quality. Thus, to widen the applications of Grade 830 steel in design and construction of concrete structures, additional studies are necessary to increase the reliability and structural understanding in the steel performance. In fact, due to Grade 830 steel has no apparent yield plateau, the warning signs prior to failure of concrete structures reinforced with Grade 830 steel are less visible than that of structures reinforced with

Grade 420 steel. This structural behavior is not preferable. Therefore, this research focuses on bridge decks reinforced with Grade 830 steel and Grade 420 steel. A systematic testing matrix was developed to identify the structural behaviors of the decks. Twelve concrete decks were cast and reinforced with Grade 420 and Grade 830 steel. The load was applied incrementally. In each load step, the tensile strain of the steel, the compressive strain of the concrete, deflection, and crack width were measured. The decks were loaded until failure. Structural performance of decks at service and strength limit states are summarized and reported. The replacement cost of Grade 420 with Grade 830 steel is also discussed.

## 2.3    EXPERIMENTAL PROGRAM

### 2.3.1   Materials Properties

2.3.1.1 Concrete

Conventional concrete was used for casting the bridge decks and was provided by a local ready-mix company. All bridge decks were cast using the mixture proportion as shown in **Table 2-1**. Fly ash Class C was used 35% as a percentage of cementitious materials. The replacement percentage 35% was chosen because this percentage represents the highest rate specified by Federal Highway Administration [23]. The compressive strength ranged from 38 MPa to 44 MPa at 28 days of age. The average strength was approximately 41 MPa, which is in the recommended compressive strength range for bridge deck structures of 28 to 42 MPa at 28 days of age.

14

**Table 2-1** – **Concrete mixture proportions.**

| Materials | Quantity per cubic meter |
|---|---|
| Cement | 231.4 kg |
| Fly ash | 124.6 kg |
| Coarse aggregate | 1008.6 kg |
| Fine aggregate | 818.7 kg |
| Water | 167.3 L |
| Water / Cementitious ratio | 0.47 |

For each concrete batch, 18 cylinders, 100 mm by 200 mm, were cast to evaluate the

compressive strength at 1, 7, 28, 56 and 90 days of age as shown in **Table 2-2**. The modulus of

elasticity was additionally measured at 28 days of age. The measured fresh concrete properties

shown in **Table 2-2** included slump, unit weight, air content, and temperature. During casting, a

mechanical vibrator was used to consolidate the concrete. The decks were cured for 15 days and

covered by a layer of sand to reduce the water evaporation as shown in **Figure 2-1**.

**Table 2-2** – **Concrete properties.**

| Compressive Strength (MPa) | |
|---|---|
| 1 day | 12 |
| 7 days | 27 |
| 28 days | 41 |
| 54 days | 48 |
| 90 days | 52 |
| Modulus of elasticity at 28 days | 35.4 GPa |
| Slump | 160 mm |
| Unit weight | 2338.7 kg/m$^3$ |
| Air content | 1.8 % |
| Concrete Temperature | 26.0ºC |

**Figure 2-1. Curing of bridge decks.**

2.3.1.2 Reinforcing Steel

Grade 420 and Grade 830 steel were used to reinforce the concrete bridge decks. Two rebar

sizes, #16 and #19, were used for each reinforcement steel type. **Figure 2-2** shows the

experimental stress-strain curve of the Grade 420 steel, and the analytical stress-strain curve of

the Grade 830 steel using a Ramberg-Osgood (R-O) function and a set of coefficients proposed

by Shahrooz et al. [24]. It should be noted that the Grade 830 steel has no apparent yielding

plateau, which can be a concern in terms of structural design as aforementioned. Typically, a

flexural member reinforced with Grade 420 steel achieves the nominal capacity as the concrete

reaches maximum compressive strain and the reinforcement reaches the yielding plateau. The

reinforcement continues to yield, and the concrete member shows visible warnings before

failure. For a member reinforced with Grade 830 steel, the steel stress may continue to increase

gradually as the concrete reaches its maximum compressive strain. Therefore, for concrete

members reinforced with Grade 830 steel, there can be fewer visible warning signs before failure when compared to members reinforced with Grade 420 steel. In this study, the failure of bridge decks, reinforced with both steel grades, was observed, and the amount of deflection at failure was measured.
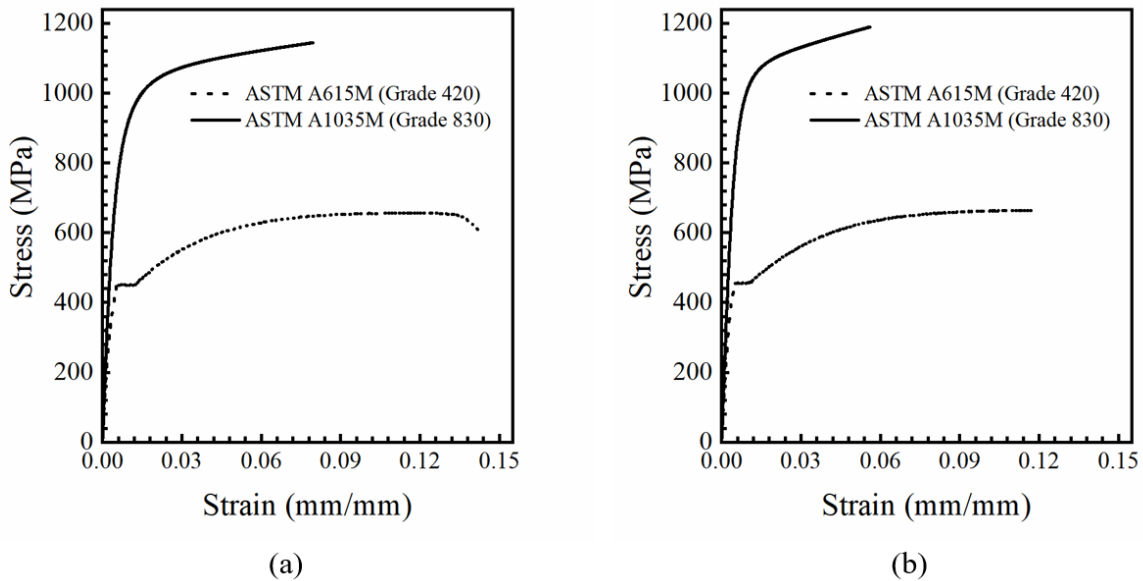


**Figure 2-2**. **Stress-strain curves for Grade 420 and Grade 830 steel.**
(Note: (a) for #16 bar; (b) for #19 bar)

### 2.3.2   Test Specimens and Testing Matrix

The test specimens were 900-mm wide, 200-mm thick, and 4200-mm long. The reinforcement detail is shown in **Figure 2-3**. The span-to-depth ratio of concrete decks was 19.5, and the deck was designed as a flexural member. The bridge decks were designed based on AASHTO LRFD Bridge Design Specifications [25]. The nominal shear strength is 136 kN for the bridge deck, and the nominal flexural strengths are 91 kN-m and 110 kN-m for bridge decks reinforced by #16 @150 mm and #19 @ 200 mm, respectively as shown at **Appendix 2A**. For bridge decks, there are two common design practices. Bridge decks can be designed to fail in shear, with a low

span-to-depth ratio. The shear resistance is mainly provided by the concrete, so that the reinforcement has minimal contribution. The other practice further utilizes the flexural capacity of the decks, with a high span-to-depth ratio. The selection of the design practices varies. In general, the second one can be more advantageous as it fully utilizes the deck capacity in both flexure and shear, requires a fewer number of deck-supporting girders, and reduces the dead load to the substructure.
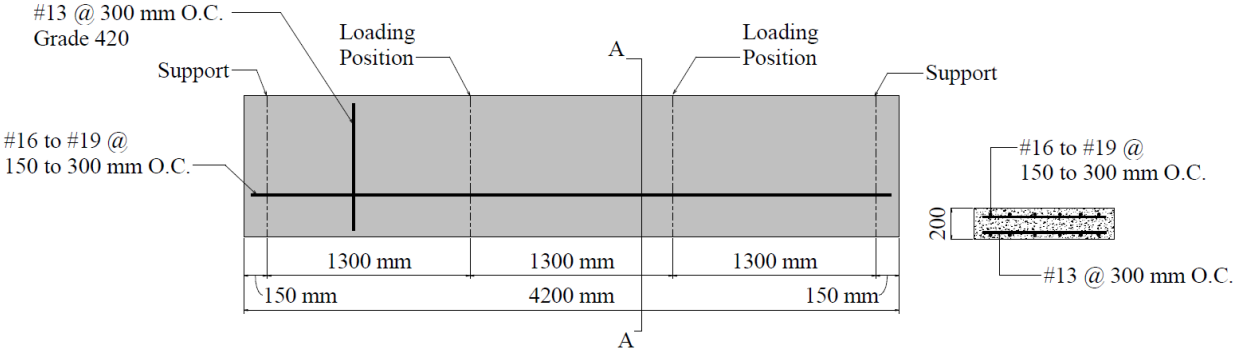


**Figure 2-3**. **Bridge deck dimension and reinforcement detail.**
(Note: O.C. = on center)

**Table 2-3** shows the testing matrix for the 12 concrete decks. For each bar diameter, the testing matrix consists of one control deck cast with Grade 420 steel, three bridge decks cast with Grade 830 steel, and two more representative tests. For the bridge decks containing #16 bars, the control deck No. 5-1 uses Grade 420 steel as the main reinforcement. The deck No. 5-2 uses the same amount of reinforcement as the deck No. 5-1 to evaluate the effect of a direct one-to-one replacement of Grade 420 steel with Grade 830 steel. The decks No. 5-3 and No. 5-4 are conducted to assess the behavior of the bridge decks when the amount of reinforcement is reduced by 25% and 40%, respectively. Based on the experimental results, two additional

representative decks (No. 5-R and No. 5-R1-C1.5) were further investigated to confirm the

experimental results and study the effect of reducing concrete cover. The first representative

deck (No. 5-R1) was the deck No. 5-4. The other (No. 5-R1-C1.5) was identical to deck No. 5-

R1, but the concrete cover was reduced from 50 mm to 38 mm. The texting matrix of #19 bars is

similar to that of #16 bar, as presented in **Table 2-3**.

**Table 2-3** – **Testing matrix of concrete bridge decks.**

| Test designation | Bar Grade | Bar quantity | Reinforcement ratio $\rho$ | Test description |
|---|---|---|---|---|
| No. 5 group (50-mm concrete cover) | | | | |
| No. 5-1 | Grade 420 | #16@150 mm | 0.86% | Control |
| No. 5-2 | Grade 830 | #16@150 mm | 0.86% | One-to-one replacement |
| No. 5-3 | Grade 830 | #16@200 mm | 0.65% | 25% reduced reinforcement ratio |
| No. 5-4 | Grade 830 | #16@250 mm | 0.52% | 40% reduced reinforcement ratio |
| No. 6 group (50-mm concrete cover) | | | | |
| No. 6-1 | Grade 420 | #19@200 mm | 0.98% | Control |
| No. 6-2 | Grade 830 | #19@200 mm | 0.98% | One-to-one replacement |
| No. 6-3 | Grade 830 | #19@250 mm | 0.78% | 20% reduced reinforcement ratio |
| No. 6-4 | Grade 830 | #19@300 mm | 0.65% | 35% reduced reinforcement ratio |
| Representative deck (50-mm concrete cover) | | | | |
| No. 5-R1 | Grade 830 | #16@250 mm | 0.52% | A representative of No. 5 |
| No. 6-R2 | Grade 830 | #19@300 mm | 0.65% | A representative of No. 6 |
| Representative deck (with reduced concrete cover to 38-mm) | | | | |
| No. 5-R1-C1.5 | Grade 830 | #16@250 mm | 0.52% | A representative of No. 5 |
| No. 6-R2-C1.5 | Grade 830 | #19@300 mm | 0.65% | A representative of No. 6 |

### 2.3.3   Test Setup

The flexural capacity of the bridge decks was evaluated using a four-point bending test as shown

in **Figure 2-4**. The concrete deck was simply-supported. The load was applied with a 445 kN

hydraulic actuator and applied incrementally until failure. The mid-span deflection was

measured using a linear cable encoder during loading.
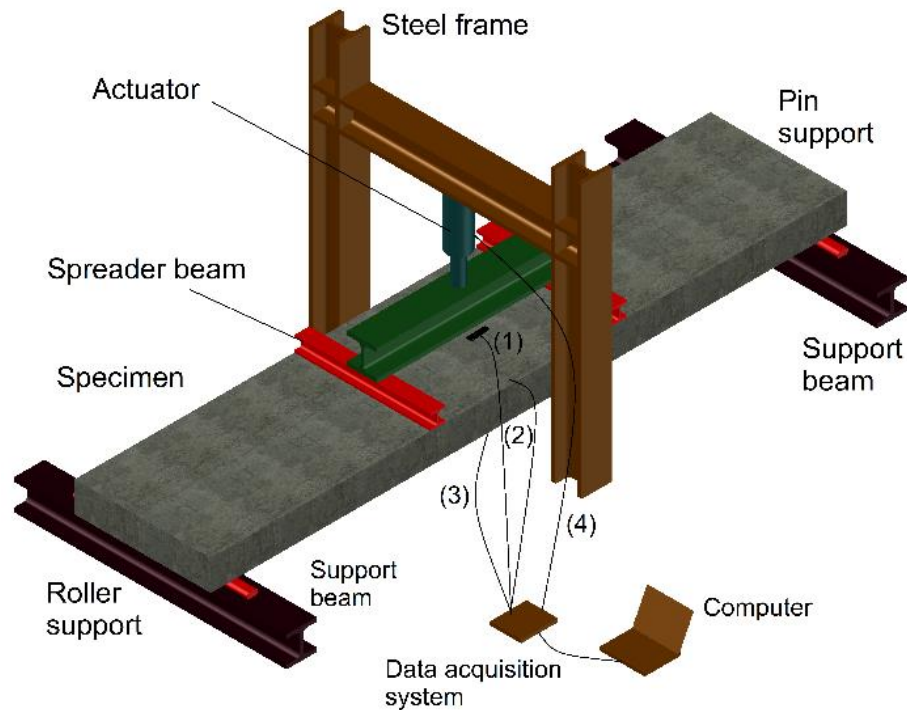


**Figure 2-4. Four-point bending test.**
(Note: (1) for two wires connecting to concrete strain gauges; (2) and (3) for two wires
connecting to steel strain gauges; (4) for one wire connecting to load cell)

To monitor the tensile stress in the reinforcement, two vibrating wire strain gauges were attached

to the reinforcing steel prior to casting the concrete. **Figure 2-5 (A)** and **Figure 2-5 (B)** show

steel cage before casting concrete and setting up a flexural test, respectively. The strain gauges

are shown in **Figure 2-5 (A)**. Two additional wire lead strain gauges (Linear Strain Gauges)

were attached to the top surface of the deck to evaluate concrete compressive strain, as shown in

**Figure 2-5 (B)**. During the flexural test, a crack-width microscope was used to measure the crack width and to count the number of cracks.



**Figure 2-5. Steel and concrete strain gauges.**
(Note: (A) Steel cage before casting concrete; (B) Setting up a flexural test)

## 2.4    EXPERIMENTAL RESULTS AND DISCUSSION

### 2.4.1    Flexural Capacity

The replacement of Grade 420 steel with Grade 830 steel increases the flexural capacity of the specimens. As shown in **Figure 2-6**, the moments at failure at mid-span for control decks, No. 5-1 and No. 6-1, are 106 kN-m and 127 kN-m, respectively. On the other hand, the moments at failure for No. 5-2 and No. 6-2 decks were 146 kN-m and 176 kN-m, respectively, which were 37% and 38% greater than those of the control decks. This was expected since it was a one to one replacement of Grade 420 steel with Grade 830 steel. A similar increase in failure moment was also observed by Salomon and Moen [15]. No. 5-3 and No. 5-4 decks were reinforced with

Grade 830 steel, but their reinforcement ratios were 25% and 40% less when compared to deck

No. 5-2, respectively. The failure moments for those decks were also 29% and 24% greater than

the control deck No. 5-1. Similarly, the failure moments for decks No.6-3 and No. 6-4 were 25%

and 19% greater than the control deck No. 6-1, respectively, regardless of the fact that their

reinforcement ratios were 20% and 35% less.
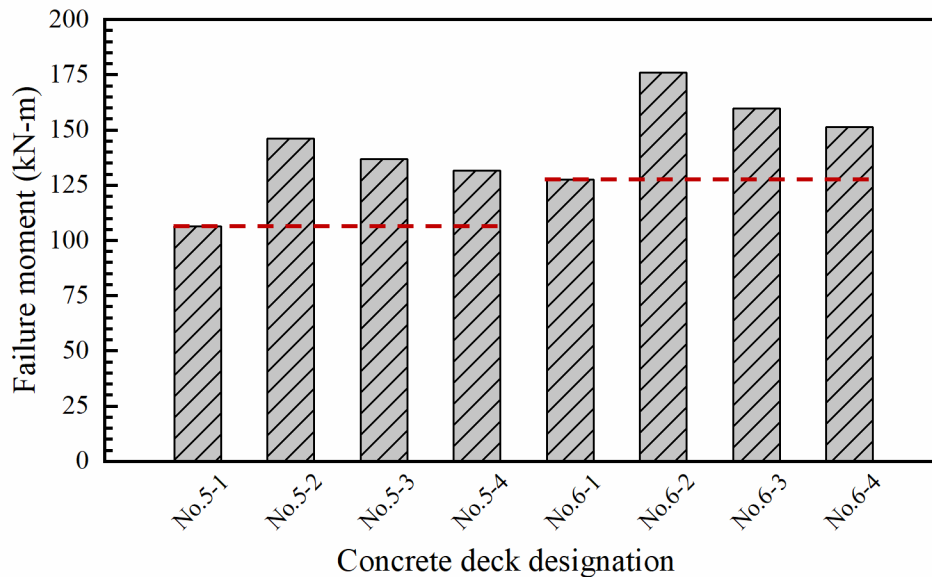


**Figure 2-6**. **Failure moments of decks No. 5-1 to No. 5-4 and No. 6-1 to No. 6-4**.

When using Grade 830 steel, the reinforcement ratio can be decreased from 35% to 40%, without

reducing the flexural capacity of concrete members. This result confirms the material savings

realized when using Grade 830 steel when compared to Grade 420 steel. In addition, by using a

lower reinforcement ratio, the issues caused by steel congestion are also resolved. For bridge

decks, reinforcement congestion may be observed at the connection to bridge girders. For

general concrete components (i.e., columns, walls, beam-column or beam-wall joints, or mat

foundations) reinforcement congestion can be a significant issue and be more severe when there are seismic requirements.

### 2.4.2   Deflection

The relationship between the deflection at mid-span and applied loads is shown in **Figure 2-7**. All decks exhibited visible deflection as the applied load increased.  At a certain load magnitude, the deflection of the control decks (No. 5-1 and No. 6-1) was greater than the deflection of decks No. 5-2 and No. 6-2, respectively.  This result was attributed to the higher tensile strength of Grade 830 in comparison to Grade 420 steel even though both types of steel have same modulus of elasticity.  However, these decks (No. 5-2 and No. 6-2) have greater deflection at the last load step because they resisted a greater ultimate load.
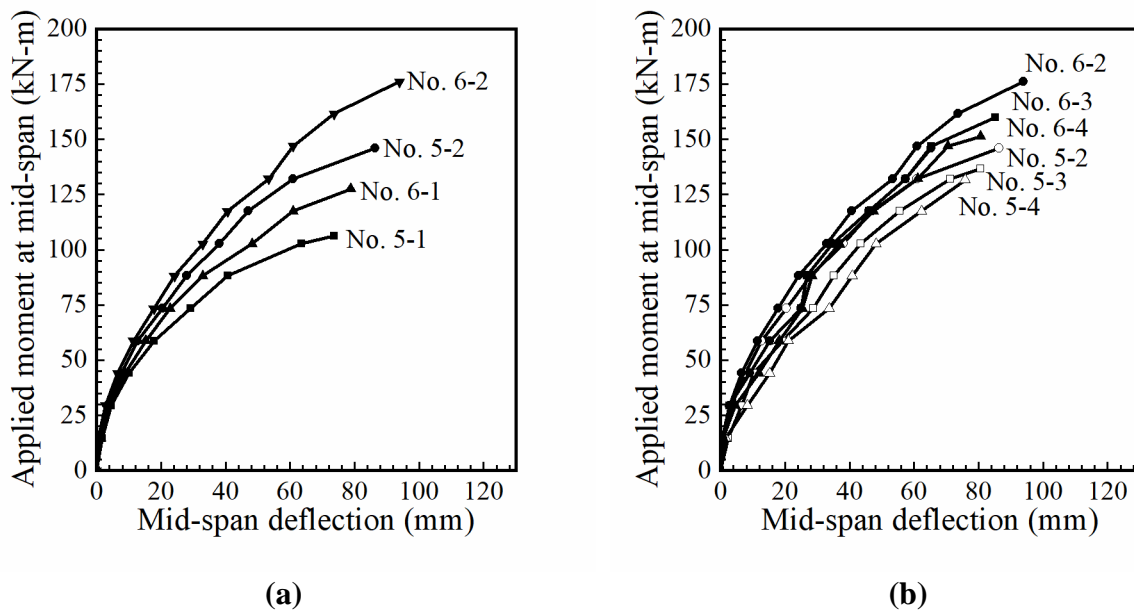


**(a)**                                                                 **(b)**
**Figure 2-7**. **Relationship between mid-span deflection and applied load.**
(Note: (a) Comparison of No. 5-1 vs. No. 5-2 decks and No. 6-1 vs. No. 6-2 decks; (b) Comparison of No. 5-2 to No. 5-4 decks and No. 6-2 to No. 6-4 decks)

The one-to-one replacement of Grade 420 steel by Grade 830 steel decreased deflection at the service state but increase deflection at failure due to the greater ultimate load. The degree of deflection or deformability up to failure, a suitable indictor for ductility, of all decks reinforced with Grade 830 was greater than that of decks reinforced with Grade 420 steel even though the amount of Grade 830 steel was reduced by 35%-40%. During the service life, bridge decks primarily resist service-loads, while greater loads only occur under extreme circumstances. A lower deflection at the service-load level minimizes the number and the width of the cracks in the concrete, which can reduce the ingress of harmful chemicals into the concrete.

### 2.4.3   Steel Tensile Strain

Shown in **Figure 2-8** is the relationship of steel tensile strain to the applied moments. The tensile strain was measured until the steel yielded. The reinforcement in deck No. 5-1 yielded at a moment of approximately about 95 kN-m, while the reinforcement in No. 6-1 deck yielded at approximately 115 kN-m. The reinforcement in deck No. 5-1 yielded at a moment slightly before the reinforcement in deck No. 6-1. This was due to the deck No. 5-1 containing less steel than the deck No. 6-1. On the other hand, tensile steel in decks No. 5-2 and No. 6-2 yielded at a moment of approximately 135 kN-m and 154 kN-m, respectively. It was found that the required moment for tensile steel yielding in concrete decks increased by approximately 40% when Grade 830 steel was used as one to one replacement of Grade 420 steel. This increment is due to the higher yield strength of Grade 830 steel which is approximately two times that of Grade 420 steel.
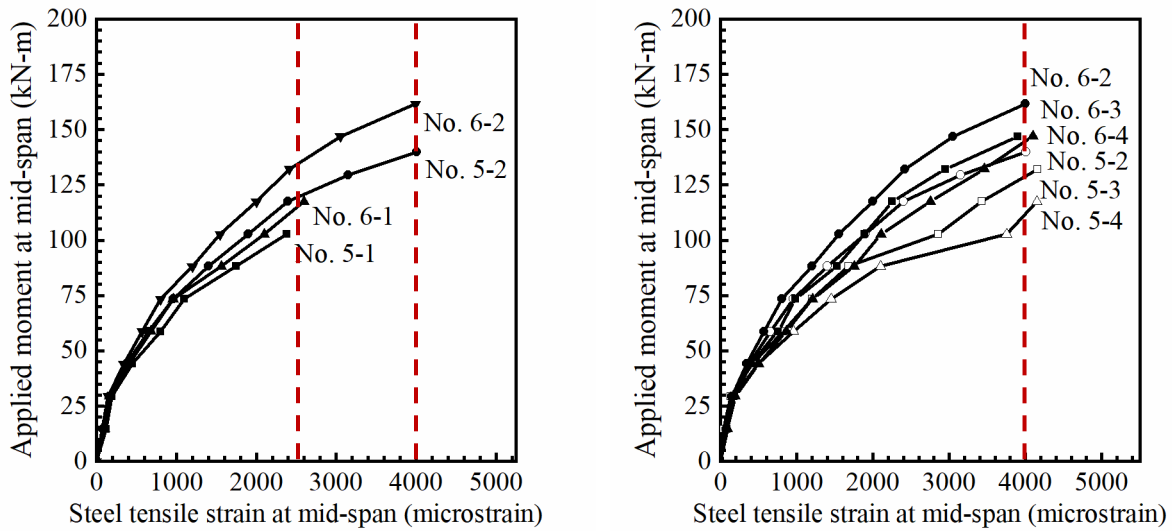
**(a)** **(b)**
**Figure 2-8**. **Relationship between tensile steel strain and applied moment.**
(Note: (a) Comparison of No. 5-1 vs. No. 5-2 decks and No. 6-1 vs. No. 6-2 decks; (b)
Comparison of No. 5-2 to No. 5-4 decks and No. 6-2 to No. 6-4 decks)

### 2.4.4 Concrete Compressive Strain

**Figure 2-9** illustrates the relationship of concrete compressive strains with applied moments for

concrete decks. The compressive concrete strains were measured at mid-span at the top surface

of the specimen and were measured continuously until failure. The compressive strains of decks

No. 5-2 and No. 6-2 were less than those of the control decks (No. 5-1 and No. 6-1) during

loading as shown in **Figure 2-9 (a)**. However, the maximum compressive strain for all decks

was approximately 2.8‰, even though the difference between the ultimate applied moments for

decks No. 5-1 and No. 5-2 is 37%, and for decks No. 6-1 and No. 6-2 is about 38%. **Figure 2-9**

**(b)** shows the applied moments producing the maximum compressive strains of tested decks

increase with reducing Grade 830 steel. The maximum compressive strain of all decks is close

to the theoretically maximum compressive strain of concrete (3‰) [26].

25
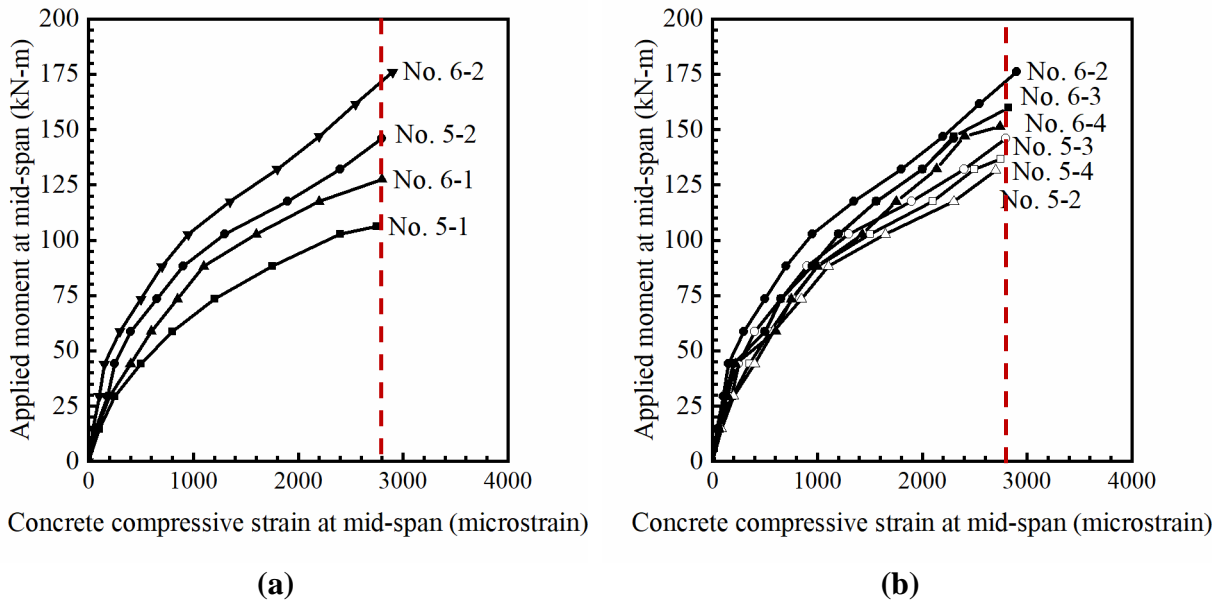
**Figure 2-9**. **Relationship between compressive concrete strain and applied moment.**
(Note: (a) Comparison of No. 5-1 vs. No. 5-2 decks and No. 6-1 vs. No. 6-2 decks; (b)
Comparison of No. 5-2 to No. 5-4 decks and No. 6-2 to No. 6-4 decks)

In terms of structural engineering applications, there is no difference in the maximum concrete
strains for the decks reinforced with either Grade 420 or Grade 830 steel. It is generally
understood that the compressive strain is dependent on concrete properties. In the study, all
decks were cast with normal-strength concrete and did not contain steel fibers. Therefore, the
measured values were close to the theoretical threshold.

### 2.4.5   Crack Width

The width and number of cracks were measured throughout testing using a microscope. The
service moment was defined using the AASHTO LRFD Bridge Design Specifications [25]. This
moment results from the dead load (5.1 kN-m/m) plus the live loads (30.7 kN-m/m), and these
loads are unfactored. The applied moment on the decks at the service limit was 32.2 kN-m. This

value was determined by multiplying the total moment (35.8 kN-m/m) by the deck width (900-mm as shown in **Figure 2-3**).

2.4.5.1 Cracks Width at Service

**Table 2-4** shows the maximum crack width and number of flexural cracks for the eight decks at the service moment. The maximum flexural crack width of deck No. 5-1 was 0.2 mm, and four cracks formed at the service limit 32.2 kN-m. Both the width and the number of cracks for the decks reinforced with the Grade 830 steel are less than those of decks containing Grade 420 steel. The crack widths of decks No. 5-2, No. 5-3, and No. 5-4 were 0.05 mm, 0.13 mm, and 0.18 mm which are less than that of deck No. 5-1 (0.2 mm). Likewise, the number of cracks for the three decks with the Grade 830 steel was two, two, and three cracks compared to the 4 cracks in the control deck containing Grade 420 steel. A similar trend was observed on the No. 6 deck group. The maximum crack width of deck No. 6-1 was 0.18 mm, and there were three cracks. For decks No. 6-2, No. 6-3, and No. 6-4 containing Grade 830 steel, the cracks widths decreased by 71%, 43%, 14%, and the number of cracks decreased to one, two cracks, and two cracks, respectively. The use of Grade 830 steel reduced the number of cracks and the cracks widths which are two significant parameters affecting reinforcement corrosion and durability. The maximum crack width of all decks was less than the maximum allowable crack width (0.32 mm) specified by AASHTO LRFD Bridge Design Specifications [25].

**Table 2-4** – **Maximum crack width and number of cracks at service state.**

| Test designation | Maximum crack width (mm) | Number of cracks |
|---|---|---|
| No. 5 group | | |
| No. 5-1 | 0.20 | 4 |
| No. 5-2 | 0.05 | 2 |
| No. 5-3 | 0.13 | 2 |
| No. 5-4 | 0.18 | 3 |
| No. 6 group | | |
| No. 6-1 | 0.18 | 3 |
| No. 6-2 | 0.05 | 1 |
| No. 6-3 | 0.10 | 2 |
| No. 6-4 | 0.15 | 2 |

2.4.5.2 Cracks Width at Failure

**Figure 2-10** shows the crack pattern for deck No. 5-1 at failure.  The cracks were concentrated

between the applied loads.  For deck No. 5-2, the crack widths decreased by 75%, and the

number of cracks decreased by 50% when compared to deck No. 5-1 at failure.  **Figure 2-11**

shows the cracks pattern for deck No. 5-2 at failure.  By moving from loading points to mid-

span, the cracks angles decrease.  The crack patterns were similar to that of deck No. 5-1.  Decks

reinforced by Grade 830 steel provide adequate warning through large deformation and extensive

cracking.

**Figure 2-10**. **Cracks patterns of deck No. 5-1 at failure.**



**Figure 2-11**. **Cracks patterns of deck No. 5-2 at failure.**

The use of Grade 830 steel can reduce cracking in bridge decks when loaded to their service

moments. The reduction in crack width is more significant as the number of cracks is dependent

29

on the applied load configuration. Experimental data indicate that the one-to-one replacement of

Grade 420 steel by Grade 830 steel reduces crack widths and the total number of cracks at the

service moment which increases durability and extends the service life. When using Grade 830

steel, the reinforcement ratio can be decreased by 35% to 40% and still provide comparable

performance to a deck containing Grade 420 steel at a greater reinforcement ratio.


### 2.4.6 Representative Deck Behavior

After evaluating the results of the first eight decks (No. 5-1 to No. 5-4 and No. 6-1 to No. 6-4),

four additional decks were cast and tested. This included two representative decks (No. 5-R1

and No. 6-R2), which had the same reinforcement as decks No. 5-4 and No. 6-4. Also, two

additional decks (No. 5-R1-C1.5 and No. 6-R2-C1.5) which had reduced concrete cover (C)

were evaluated. For these decks, the top and bottom cover were reduced from 50 mm to 38 mm.

Research results have shown that the reduction in concrete cover is an effective way to reduce

cracking bridge decks [6]. However, there is little research on the behavior of decks reinforced

with Grade 830 steel with reduced cover. The testing of decks No. 5-R1-C1.5 and No. 6-R1-

C1.5 are aimed at evaluating the effect of reduced concrete cover on the performance of the

decks reinforced with Grade 830 steel.

**Table 2-5** shows the maximum compressive and tensile strains and maximum crack width at the

service limit and failure moments for decks No. 5-R1, No. 6-R2, No. 5-R1-C1.5, and No. 6-R2-

C1.5. At service limit moment, the concrete compressive strains were 0.32‰ and 0.29‰, while

the steel tensile strains were 0.26‰ and 0.22‰ for decks No. 5-R1 and No. 6-R2, respectively.

The steel strains were low due to the higher strength of Grade 830 steel. The decks No. 5-R1-

C1.5, and No. 6-R2-C1.5 decks had greater flexural capacity, which was expected due to the

larger moment arm which resulted from the smaller concrete cover.  For deck No. 5-R1-C1.5, the

moment at failure was 2% greater than that of the similar deck with 50 mm cover. Also, the

maximum compressive and tensile strains at the service limit moment decreased to 0.26‰ and

0.20‰ when compared to the deck with standard cover of 50 mm.  For deck No. 6-R2-C1.5, the

maximum compressive and tensile strains decreased to 0.19‰ and 0.17‰ at the service limit

moment, and the moment was 5% greater at failure than that of control with 50 mm cover.  For

crack width at service limit, the reduction in concrete cover decreases the crack width by 33%

and 20% for decks No. 5-R1-C1.5 and No. 6-R2-C1.5, respectively.

**Table 2-5** – **Maximum strains and cracks widths at service state and failure moments.**

| Test designation | Compressive concrete strain at service limit (microstrain) | Tensile steel strain at service limit (microstrain) | Max. crack width at service limit (mm) | Failure moment (kN-m) |
|---|---|---|---|---|
| No. 5-R1 | 328 | 267 | 0.06 | 133 |
| No. 5-R1-C1.5 | 260 | 203 | 0.04 | 136 |
| No. 6-R2 | 289 | 221 | 0.05 | 149 |
| No. 6-R2-C1.5 | 191 | 170 | 0.04 | 157 |

**Figure 2-12** shows the relationship between mid-span deflection and applied moment for the

four representative decks.  At moments of 70 kN-m and greater, the deflection of decks No. 5-R1

and No. 6-R2 decks was greater than those of decks No. 5-R1-C1.5, and No. 6-R2-C1.5 decks,

respectively.  These results are attributed to the greater effective depths of decks No. 5-R1-C1.5

and No. 6-R2-C1.5 decks, which additionally lead to greater resistance to the applied loads.
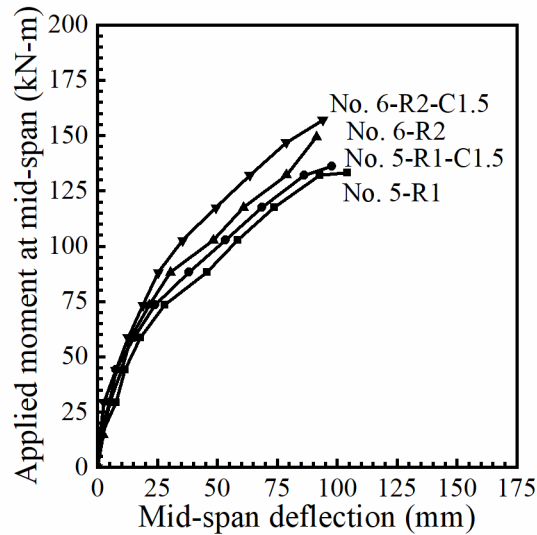
**Figure 2-12. Relationship between deflection and applied moment for representative decks.**

### 2.4.7 Replacement Cost

The replacement of Grade 420 steel, by the high corrosion resistance, Grade 830 steel in concrete

structures increases the total cost of structures when the replacement rate is one-to-one. The cost

of Grade 830 steel is approximately 175% more than Grade 420 steel [14]. However, similar

performance can be achieved using 35 to 40% less Grade 830 steel when compared to a deck

reinforced with Grade 420 steel. This reduction in reinforcement reduces the increase due to the

differences in material costs. Additionally, the labor costs associated with placing the steel can

be also reduced due to the reduction of overall amount of Grade 830 steel.

### 2.5 CONCLUSIONS

Based on the test results of 12 concrete decks, reinforced with either Grade 420 steel or high-

performance Grade 830 steel, the following conclusions can be drawn:

1. The replacement of Grade 420 by Grade 830 steel reduced the maximum crack width, the number of cracks, and deflection. The reduction level is dependent on the replacement rate of Grade 830 steel to Grade 420 steel. The performance of concrete bridge decks reinforced with Grade 420 or Grade 830 steel are comparable when the amount of Grade 830 steel is 35 to 40 percent less than that of Grade 420 steel.

2. The flexural resistance of the concrete decks increases by 37% when Grade 420 steel is replaced by Grade 830 steel at a 1:1 replacement ratio. The improvement in flexural resistance was 19-24% when the replacement ratio of Grade 830 steel to Grade 420 steel was 1:0.35-0.45.

3. When the concrete cover of decks reinforced with Grade 830 steel was reduced from 50 mm to 38 mm, the maximum crack widths at service limit are reduced by 20-33%. Likewise, the maximum compressive concrete strain and tensile steel strain at service limit state decreased by 28% and 24%, respectively.

4. The use of a lower reinforcement ratio of Grade 830 steel, as compared to Grade 420 steel, reduces the total cost and time for constructing concrete bridge decks. When using reinforcement ratio that is 60% to 70% of that of Grade 420 steel, which can offset the additional cost due to the increased material costs of Grade 830 steel.

**ACKNOWLEDGMENTS**

**REFERENCES**

[1] American Society of Civil Engineers (ASCE), "2013 Report Card for America's Infrastructure," March 2013.

[2] Seliem, H., Lucier, G., Rizkalla, S., Zia, P., "Behavior of Concrete Bridge Decks Reinforced with High-Performance Steel," ACI Structural Journal, V.105, No. 1, 2008, pp. 78–86.

[3] Hassan, T., Abdelrahman, A., Tadros, G., Rizkalla, S., "Fibre Reinforced Polymer Reinforcing Bars for Bridge Decks," Canadian Journal of Civil Engineering, V. 27, No. 5, 2000, pp. 839–849.

[4] Broomfield, J. P., "Corrosion of Steel in Concrete: Understanding, Investigation and Repair," Taylor & Francis, United Kingdom, 2007.

[5] Tahershamsi, M., "Structural Effects of Reinforcement Corrosion in Concrete Structures," Dissertation of PhD. in Chalmers University of Technology, Department of Civil and Environmental Engineering; Gothenburg, Sweden 2016.

[6] Otieno, A., "Sensitivity of Chloride-Induced Corrosion Rate of Steel in Concrete to Cover Depth, Crack Width and Concrete Quality," Materials and Structures Journal, V. 50, No. 1, 2017, pp. 1-10.

[7] Graham, S. K., Paulson, C., "Mechanical Properties of ASTM A1035 High Strength Steel Bar Reinforcement," WJE No.2008.9901.0, 2008, pp. 1-47.

[8] Tikalsky, P. J., Beh, D. E., "The Synthesis of Design Guidelines for Corrosion Resistant Reinforced Concrete," UT- 08-27, Utah Department of Transportation 4501 South 2700 West Salt Lake City, Utah 84114-8410, 2008.

[9] Bowen, G. E., "Service and Ultimate Limit State Flexural Behavior of One-Way Concrete Slabs Reinforced with Corrosion-Resistant Reinforcing Bars," Thesis Master of Science in Civil Engineering, Virginia Polytechnic Institute and State University, May 2013.

[10] Munikrishna, A., Hosny, A., Rizkalla, S., Zia, P., "Behavior of Concrete Beams Reinforced with ASTM A1035 Grade 100 Stirrups Under Shear. ACI Structural Journal, V. 108, No. 1, 2011, pp. 34-41.

[11] Harries, K. A., Shahrooz, B. M., Soltani, A., "Flexural Crack Widths in Concrete Girders with High-Strength Reinforcement," Journal of Bridge Engineering, V. 17, No. 5, 2001, pp. 804-812.

[12] ASTM A1035/A1035M−14, "Standard Specification for Deformed and Plain, Low-Carbon, Chromium, Steel Bars for Concrete Reinforcement," ASTM International, West Conshohocken, PA, 2014.

[13] Faza, S., Kwok, J., Salah, O., "Application of High-Strength and Corrosion-Resistant ASTM A1035 Steel Reinforcing Bar in Concrete High-Rise Construction," CTBUH 8th World Congress, Council on Tall Buildings and Urban Habitat, Chicago, Illinois, Dubai, 2008, pp. 1-6.

[14] Bridge Design and Drafting Manual, Oregon Department of Transportation, Section 1, May 2017.

[15] Salomon, A. L., Moen, C. D., "Structural Design Guidelines for Concrete Bridge Decks Reinforced with Corrosion- Resistant Reinforcing Bars," FHWA/VCTIR 15-R10, 2014, pp. 1-51.

[16] Ansley, M. H., "Investigation into the Structural Performance of MMFX Reinforcing," Florida Department of Transportation, 2002.

[17] Yotakhong, P., "Flexural Performance of MMFX Reinforcing Rebars in Concrete Structures," Master's Thesis, North Carolina State University, Raleigh, NC., 2003.

[18] Munikrishna, A., Hosny, A., Rizkalla, S., Zia, P., "Behavior of Concrete Beams Reinforced with ASTM A1035 Grade 100 Stirrups Under Shear," ACI Structural Journal, V. 108, No. 1, 2011, pp. 34-41.

[19] Desalegne, A. S., Lubell, A. S., "Shear in Concrete Beams Reinforced with High-Performance Steel," ACI Structural Journal, V. 112, No. 6, 2015, pp. 783-792.

[20] Yotakhong, P., "Flexural Performance of MMFX Reinforcing Rebars in Concrete Structures," Master Thesis of Science in Civil, Construction, and Environmental Engineering, North Carolina State University, 2003.

[21] Naaman, A. E., Chandrangsu, K., "Innovative Bridge Deck System Using High-Performance Fiber-Reinforced Cement Composites," Structural Journal, V. 101, No. 1, 2004, pp. 57-64.

[22] Seliem, H. M. A., "Behavior of Concrete Bridges Reinforced with High-Performance Steel Reinforcing Bars," Doctor Dissertation of Philosophy in Civil Engineering, North Carolina State University, 2007.

[23] Chesner WH, Collins RJ, Mackay MH. User guidelines for waste and by-product materials in pavement construction. FHWA-RD-97-148, 1998, p. 24

[24] Shahrooz, B. M., Harries, K. A., Russell, H. G., "Design of Concrete Structures Using High-Strength Steel Reinforcement," Rep. No. 12-77, Transportation Research Board, Washington, D.C., 2011.

[25] American Association of State Highway and Transportation Officials, "AASHTO LRFD Bridge Design Specifications," 8th Edition. American Association of State Highway and Transportation Officials, Washington, DC, 2017.

[26] ACI Committee 318, American Concrete Institute, "Building Code Requirements for Structural Concrete (ACI 318R-14): an ACI Standard: Commentary on Building Code Requirements for Structural Concrete," An ACI Report, Farmington Hills, MI: American Concrete Institute, 2014.

**APPENDIX 2A**

The concrete thickness of all tested bridge decks satisfies the requirement of minimum thickness (178 mm) specified by AASHTO LRFD Bridge Design Specifications [25].  The nominal shear strength and flexural strength are determined by **Eq. 2A-1** and **Eq. 2A-2**, respectively [25]:

$$V_c = 0.166(bd)\sqrt{f'_c} \qquad\qquad\qquad \textbf{(Eq. 2A-1)}$$

$$M_n = (A_s f_s)\left(d_s - \frac{a}{2}\right) - (A'_s f'_s)\left(d'_s - \frac{a}{2}\right) \qquad\qquad \textbf{(Eq. 2A-2)}$$

Where: $V_c$ is the nominal shear strength; $b$ is concrete width; $M_n$ is the nominal flexural strength; $A_s$ and $A's$ are the area of tension and compression reinforcement, respectively; $d$ and $d'$ are the distance from extreme compression fiber to the centroid of tensile and compression reinforcement, respectively; $a$ is the depth of equivalent stress block.

# CHAPTER 3:  FLEXURAL PERFOMANCE OF BRIDGE DECKS REINFORCED WITH HIGH-STRENGTH STEEL: FINITE ELEMENT ANALYSIS APPROACH

Rahman S. Kareem[1], Canh N. Dang[2,3*], Gary S. Prinz[1], W. Micah Hale[1]

[1] University of Arkansas, Department of Civil Engineering, 4190 Bell Engineering Center

Fayetteville, AR 72701, USA

[2] Department for Management of Science and Technology Development, Ton Duc Thang

University, Ho Chi Minh City, Vietnam

[3] Faculty of Civil Engineering, Ton Duc Thang University, Ho Chi Minh City, Vietnam

* Corresponding author:

Emails: canhdang@tdt.edu.vn

Phone +1-479-575-6348

## ABSTRACT

This paper numerically investigated flexural performance of concrete bridge decks reinforced

with high strength steel specified by ASTM A1035 (Grade 830 and Grade 690).  The decks

reinforced by ASTM A1035 (Grade 830) and ASTM A615 steel (Grade 420).  ABAQUS

software was used to develop the finite-element (FE) model.  The concrete material was

represented by 8-node brick elements (C3D8).  Concrete Damaged Plasticity (CDP) model was

used to capture the concrete nonlinear behavior.  The reinforcement steel was modeled by 2-node

truss elements (T3D2) and embedded in the concrete elements using the embedded element

technique.  The accuracy of the FE model was validated by the experimental results of 10

concrete bridge decks.  Parametric studies were performed to understand the flexural

performance of concrete bridge decks reinforced with ASTM A1035 (Grade 690) steel.  The

investigation revealed that one-to-one replacement of ASTM A615 by ASTM A1035 steel of

concrete bridge decks increases the flexural capacity up to 29%-41%, maximum deflection up to 21%-28%, and maximum crack width at service up to 58%-78%.

**KEYWORDS:** Concrete bridge decks; high-strength steel; finite element method; ABAQUS; Concrete Damaged Plasticity Model; embedded element technique

## 3.1    INTRODUCTION

Concrete bridge decks are prone to corrosion due to severe weather conditions and heavy vehicle volumes.  In recent years, the effect of climate change (i.e., extremely hot summers, longer winters, increased freeze-thaw cycles) on bridge decks is more profound [1].  On the other hand, due to the demand of transportation, the load and frequency of heavy vehicles on highway systems have increased exponentially [2].  All of these factors accelerate the deterioration of bridge decks.  Researchers and engineers have indicated that the utilization of high-performance reinforcing (HPR) steel in concrete bridge decks can enhance the service life and reduce the maintenance cost for the decks [2].  HPR steel is characterized by its high-strength and high-corrosion resistance [3].  ASTM A1035 is specifically designed for HPR steel consisting of two grades: Grade 690 and 830 or Grade 100 and 120 in US practice, respectively.

 **Figure 3-1** shows a typical cross section of bridge.  The concrete deck is assumed to act as one-way slab supported by steel girders.  Conventionally, the spacing between these girders is relatively small, so the design of the concrete deck is governed by shear (conceptually shown on **Figure 3-1 (A)** and (**B**)).  The use of high-strength steel (i.e., ASTM A1035 Grade 830 or 690) can enhance the flexural capacity of the concrete deck.  This enhancement provides an opportunity to extend the deck spans, in which the concrete deck can be fully utilized in flexure

and shear (conceptually shown on **Figure 3-1 (C)**).  The reduction in number of bridge girders is

another advantage for construction.  In fact, one disadvantage is that the concrete tends to

experience more flexural cracking, which can lead to water ingress and corrosion-related issues.
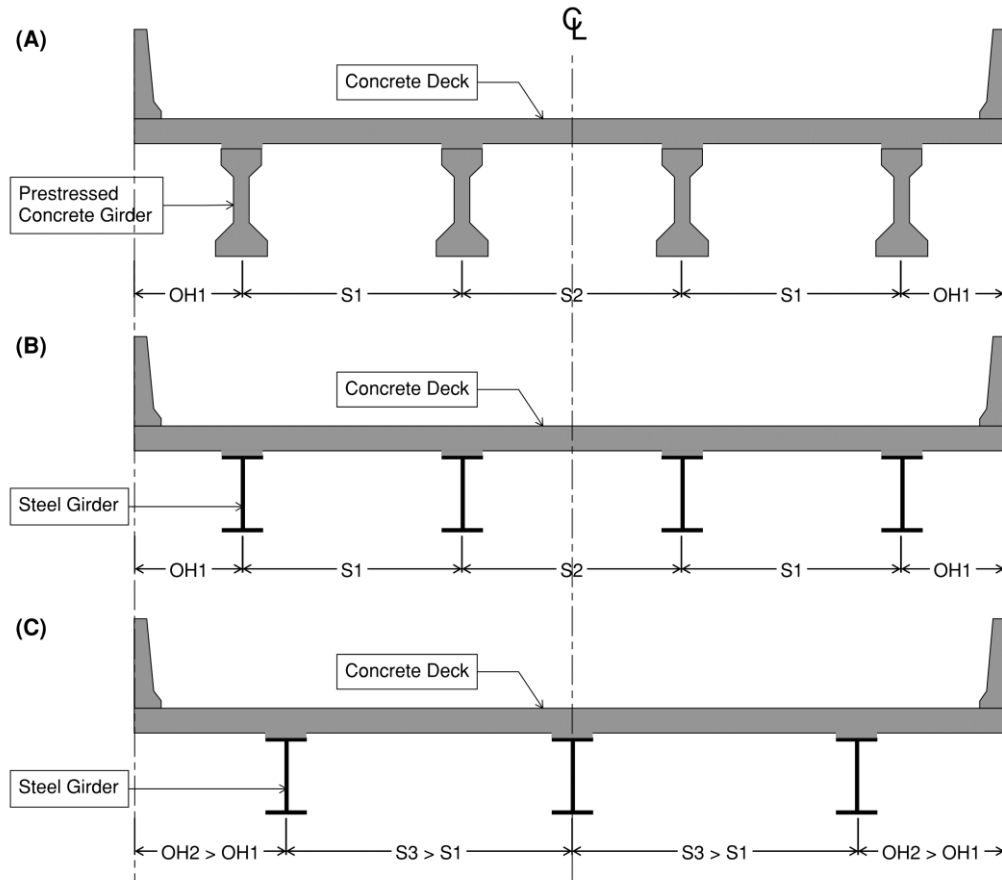


**Figure 3-1. Typical bridge cross section.**
(Notes: other bridge elements are not shown for simplification)

The ultimate tensile strength of HPR steel is approximately two times greater than that of regular

steel (ASTM A615).  Both grades of A1035 steel do not have clear yield plateau, so the offset

method is typically used to determine the yield strength ($f_y$) [4].  In addition to possessing high

tensile strength, HPR steel has improved corrosion resistance.  The enhanced properties are

achieved by altering the composition of the steel.  The carbon content of A1035 is not more than

0.15%, and the chromium content ranges from 8% to 10.9% [4].  The corrosion resistance of

A1035 is approximately five times greater than that of regular steel [5]. The service life of reinforced concrete structures can be extended by using A1035 steel as the main reinforcement [1,5]. Concrete structures reinforced by A615 can require maintenance after 20 to 30 years of service, whereas structures reinforced with A1035 may not require maintenance for up to 100 years [6].

Several experimental studies have been conducted on concrete members reinforced with A1035 steel [1,2,7]. The ultimate flexural strength of concrete members increases when A1035 steel is used as the main reinforcement [1]. In comparison to concrete members reinforced with A615, the ultimate strength of the concrete members reinforced with A1035 can be maintained with less steel ratio [7]. Decreasing the amount of reinforcing steel is an effective way to ease the placement of concrete and reduce the cost of labor, materials transportation, and site space for storage [5]. However, the ACI Committee 439 (ACI 439.6R-19), the committee developing the guide for the use of ASTM A1035/A1035M, indicates that the research data and experience of structural performance of concrete members reinforced with A1035 Grade 830 are still insufficient [8]. In other words, additional research is necessary to gain the reliability of A1035 steel for structural applications. To further understanding the structural behavior of concrete bridge decks, along with experimental investigations, numerical simulation is a feasible way to capture the deck behavior. This technique enables a thorough understanding on the variation in concrete stress and reinforcement yielding, which are significant to the deck performance at the service and ultimate limit stages. It should be noted that the A1035 steel has no apparent yielding plateau like A615 steel. Nonetheless, a flexural member reinforced with A1035 steel is expected to fail by steel yielding, not by concrete crushing, and to show visible warning signs before failure (i.e., visible cracking or large deflection). Therefore, several numerical models are

developed in this study for further understanding the behavior of concrete decks reinforced with A1035 steel and to investigate the difference in structural performance in comparison to the decks reinforced with A615 steel.

## 3.2 LITERATURE REVIEW

Numerical simulations of reinforced concrete structures have extensive applications, such as assessing the ultimate strength and crack patterns of the structures under different loading combinations. Finite-element programs, such as ABAQUS [9,], ANSYS [10], or ADINA [11], can model the linear and nonlinear behavior of concrete structures. The nonlinearity of concrete in compression and tension at pre-cracking and post-cracking states can be accurately captured through sophisticated concrete models, such as Concrete Damaged Plasticity [12], Willam and Warnke [13], and Smeared Crack [14]. For reinforcing steel, reinforcement yielding is typically simulated by Plasticity features in these programs [15]. The interaction of concrete and steel can be accomplished with fully bonding or a relative slip at the interface of the two materials [14]. Due to the advantages of numerical simulation versus experimental investigation, different finite element models have been proposed to simulate bridge decks for the last two decades. Razaqpur et al. [16] used finite-element method to investigate the behavior of steel-concrete composite bridges. An orthotropic nonlinear material model with the biaxial constitutive law was used to represent for concrete, while an elastic–plastic strain-hardening model was used to represent the steel and reinforcement. Likewise, Helba et al. [17] investigated the failure loads of composite skew bridges with slab-on-I-steel girders. The analytical results were validated with the experimental data. It was found that the finite-element method is a promising alternative method to costly experimental work.

43

The design of reinforced concrete structures proposed by design codes assumes a linear behavior for simplification. In fact, the behavior of reinforced concrete structures is nonlinear due to the nonlinearity of the steel and concrete, geometry, and boundary conditions [18]. Therefore, plastic performance of concrete structures must be considered in addition to the elastic behavior [9]. Thevendran et al. [19] used the nonlinear behavior of steel and concrete to investigate the ultimate load of simply supported composite steel beams curved in plan. Isoparametric thick and thin shell elements with 4-nodes were used to model the slab and girders, respectively. Shear connectors were represented by nonlinear spring elements. The results from the proposed finite element model and the experimental results showed an acceptable correlation. Also, Hu et al. [20] predicted the ultimate loading capacity of rectangular reinforced concrete beams by using the finite-element method. The beams were strengthened by fiber-reinforced plastics. The nonlinear behavior of reinforcement, concrete, and fiber-reinforced plastics was implemented. In 2017, Metwally [21] investigated twelve large scale concrete deep beams reinforced with glass fiber reinforced polymer bars. The author analytically examined the performance of beams by considering the elastic and plastic behaviors of materials. The simulation showed that the structural behavior of reinforced concrete deep beams is similar to the experimental data, such as the load–deflection behavior, crack propagation, and the strains in the reinforcement and concrete.

Among several general finite-element programs aforementioned, ABAQUS has been recognized as a feasible tool for finite-element modeling of reinforced concrete or composite structures. Barth et al. [22] investigated the behavior of concrete slabs on steel stringer bridge superstructures by using nonlinear finite element method under the effect of ultimate load. The concrete slab, steel girders, and stiffeners were modeled by using a general shell element with

reduced integration technique. One-dimensional rebar elements were used to represent the reinforcement. The connection between the reinforced concrete slab and steel girders was represented by multiple-point constraint beam elements. There was an excellent agreement between the finite-element results and the experimental data. Sinaei et al. [23], Ahmed [24], and Sihua et al. [25] also investigated the behavior of reinforced concrete beams by using finite-element model. The behavior of concrete was represented by Concrete Damage Plasticity. Full bond contact between the steel reinforcement and concrete was assumed by using the embedded element option. The results from the finite element model such as, displacement, compressive strain in the concrete, tensile strain in the reinforcing steel, and crack patterns were well matched with the experimental data.

## 3.3    RESEARCH OBJECTIVES

The serviceability, ultimate strength, and corrosion resistance of concrete bridge decks can be improved by using A1035 steel as the main reinforcement. Given the uncertainty around using A1035 steel due to the incompleteness or lack of supporting research data, the direct replacement of A615 steel with A1035 steel has been implemented for several bridge projects to demonstrate the enhancement of A1035 steel. In fact, this approach has two implications: (1) the concrete section is over-reinforced and less ductility as a result, and (2) the construction cost is increased. Therefore, this research aims at further understanding the structural behavior of concrete bridge decks cast with different A1035 steel grades (Grade 690 and Grade 830), steel ratios, and various concrete strengths. A general finite-element program, ABAQUS, was used for the investigation. The nonlinear properties of concrete and steel materials were considered to properly capture the behavior of the bridge decks. The accuracy of the numerical simulation was validated by the

45

experimental results of 10 concrete decks cast at the University of Arkansas. A number of findings are discussed and reported in the following sections.

## 3.4 EXPERIMENTAL DATA

For validation of the proposed FE model (presented in Section 3.5), the analytical results are compared against experimental results. The experimental program included casting and testing ten concrete bridge decks for investigating their structural behavior conducted by Kareem et al. [26]. The deck was 200-mm thick, 900-mm wide, and 4200-mm long. Two concentrated loads were applied at 1300 mm apart. The deck length was determined based on the load configuration and the anchorage length of Grade 830 steel. The anchorage length was designed to be longer than the development length $L_d$, which enables the application of a perfect bond between reinforcement and concrete material. According to ACI 318-19, the development length of reinforcing bar is the required length for which the reinforcement must be properly bonded to the concrete to attain the yield stress with no slip. The detailed calculation procedure of the development length of ASTM A1035 steel is summarized in **Appendix 3A**.

The concrete decks were reinforced with Grade 830 or Grade 420 steel. The structural performance of concrete decks was investigated at service and ultimate limit states. The tensile strains in reinforcement were monitored by vibrating wire strain gauges attached to reinforcing bars before casting concrete as shown in **Figure 3-2 (A)**. Also, the compressive strains in concrete were monitored by wire lead strain gauges attached to top surface of the deck as shown in **Figure 3-2 (B)**. The bridge decks were cast with normal-weight concrete. All of the ten bridge decks were cast in one batch for archiving the consistency in concrete properties.

Table 3-1 shows the concrete mix proportions.  Fly ash Class C was used 35% as replacement of cement.  This is a typical replacement range for the concrete mixtures used in bridge deck construction.  The compressive strength and modulus of elasticity were measured for the concrete mixture.  The compressive strength at 28 days of age was evaluated by testing three cylinders of 100 mm by 200 mm.  The test was conducted according to ASTM C39 [27].  The average compressive strength ( $f_c'$ ) was 41 MPa at 28 days of age.  Additional three concrete cylinders of 100 mm by 200 mm were cast to measure the modulus of elasticity.  ASTM C469 was used to determine modulus of elasticity [28].  The average modulus of elasticity ($E_c$) was 35.37 GPa at 28 days of age.



**Figure 3-2. Concrete deck fabrication and testing frame.**
(A) vibrating wire strain gauges attached to reinforcing bars before casting concrete, and (B) wire lead strain gauges attached to top surface of the deck.

**Table 3-1 – Concrete mixture proportions.**

| Materials | Quantity per cubic meter |
|---|---|
| Cement | 231.4 kg |
| Fly ash | 124.6 kg |
| Coarse aggregate | 1008.6 kg |
| Fine aggregate | 818.7 kg |
| Water | 167.3 L |
| Water / Binder ratio | 0.47 |

The decks were reinforced with 2 layers of steel either Grade 830 steel or Grade 420 steel and with different reinforcement ratios ($\rho$). The testing matrix is shown in **Table 3-2** . The testing objective of each deck is described in the table description. The control decks are typical of the designs used in bridge deck construction [2,29,30]. The replacement of Grade 420 by Grade 830 increases the flexural strength of concrete members. Therefore, the replacement ratio of steel can be decreased, and the concrete members can still achieve an equivalent strength and stiffness. This is investigated in the decks where the reinforcement decreases from 0.86 to 0.52 percent for the D.5-group of decks. A similar examination is in the D.6-group decks where the reinforcement ration decreases from 0.98 to 0.65 percent. Two decks were additionally cast at the lowest reinforcement ratio for the D.5 and D.6 group of decks.

**Table 3-2 – Testing Matrix.**

| Deck designation | Steel | Bar quantity | $\rho$ | Number of decks | Concrete cover | Description |
|---|---|---|---|---|---|---|
| D.5 group | | | | | | |
| D5-1 | Grade 420[a] | No. 16 @ 150 mm | 0.86% | 1 | 51 mm | Control deck, reinforced with Grade 420 steel. |
| D5-2 | Grade 830[b] | No. 16 @ 150 mm | 0.86% | 1 | 51 mm | Identical to D5-1, with one-by-one reinforcement replacement by Grade 830 steel. |
| D5-3 | Grade 830 | No. 16 @ 200 mm | 0.65% | 1 | 51 mm | Identical to D5-2, with 25% reduction in reinforcement ratio. |
| D5-4 | Grade 830 | No. 16 @ 250 mm | 0.52% | 2 | 51 mm | Identical to D5-2, with 40% reduction in reinforcement ratio. |

**Table 3-2 – Testing Matrix (cont.).**

| Deck designation | Steel | Bar quantity | $\rho$ | Number of decks | Concrete cover | Description |
|---|---|---|---|---|---|---|
| D.6 group | | | | | | |
| D6-1 | Grade 420 | No. 19 @ 200 mm | 0.98% | 1 | 51 mm | Control deck, reinforced with Grade 420 steel. |
| D6-2 | Grade 830 | No. 19 @ 200 mm | 0.98% | 1 | 51 mm | Identical to D6-1, with one-by-one reinforcement replacement by Grade 830 steel. |
| D6-3 | Grade 830 | No. 19 @ 250 mm | 0.78% | 1 | 51 mm | Identical to D6-2, with 20% reduction in reinforcement ratio. |
| D6-4 | Grade 830 | No. 19@ 300 mm | 0.65% | 2 | 51 mm | Identical to D6-2, with 35% reduction in reinforcement ratio. |

Note: [a] = ASTM A615 Grade 420 steel; [b] = ASTM A1035 Grade 830 steel.

A flexural-testing set up is shown in **Figure 3-3**. The decks were tested at 28 days of age. The loads were applied incrementally until failure. The deflection at the mid-span and cracking occurrence and propagation were recorded at each step. For each deck, two strain gauges were attached to reinforcing bars in mid-span of decks to monitor the tensile strains in the reinforcement. The concrete compressive strains were monitored by two additional strain gauges attached to the top surface of the deck.
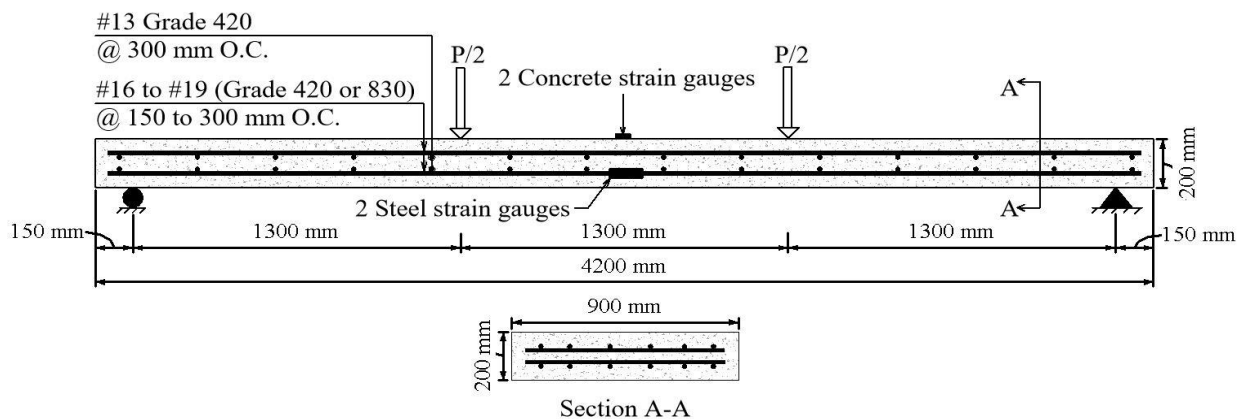


**Figure 3-3. Bridge deck dimension and the distribution of reinforcement.**
(Note: O.C. = on center)

### 3.5    FINITE-ELEMENT MODEL

### 3.5.1    General

The non-linear finite element software package, ABAQUS, was used to model the concrete

decks.  The concrete and steel materials were modeled by 8-noded brick elements (C3D8 type)

and 2-noded truss elements (T3D2 type), respectively.  These elements have three degrees of

freedom for each node.  The bond between concrete and reinforcing bars was simulated by

embedded method.  The steel elements were embedded and constrained with concrete elements

nodes [14,23].  As graphically illustrated in **Figure 3-4**, the elements of concrete and

reinforcement can be bonded without having to share the same node and occupied same regions

[31].  The embedded method overcomes the restrictions of concrete meshing since the stiffness

of reinforcing bars is calculated separately from the concrete elements.  Consequently, the

deformations of the reinforcing bars are compatible with the surrounding concrete.  The

embedded method is applicable for a perfect bond between the concrete and steel elements to

work together as one unit [23,32].  Therefore, the tension stiffening (stress-strain relationship) of

concrete was modified to consider the effects of bond slip with reinforcing bars [33].
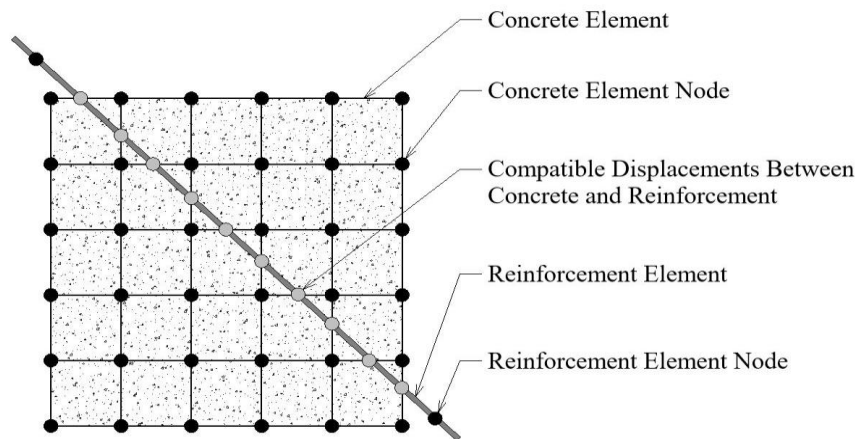


**Figure 3-4. Embedded reinforcement elements in concrete.**

Boundary conditions and loading configuration in the model were applied to simulate the experimental test setup of tested decks. **Figure 3-5** shows the applicable boundary conditions and loads. Decks were considered as simply supported. The roller support was analytically produced by restraining the movement in Y direction ($U_2 = 0$). Similarly, the pin support was produced by restraining the movements in Y and Z directions ($U_2 = U_3 = 0$). The two concentrated loads were divided by the area of loading plate, so the loads were applied as pressure in the model. A static analysis was used to numerically investigate the behavior of concrete bridge decks.
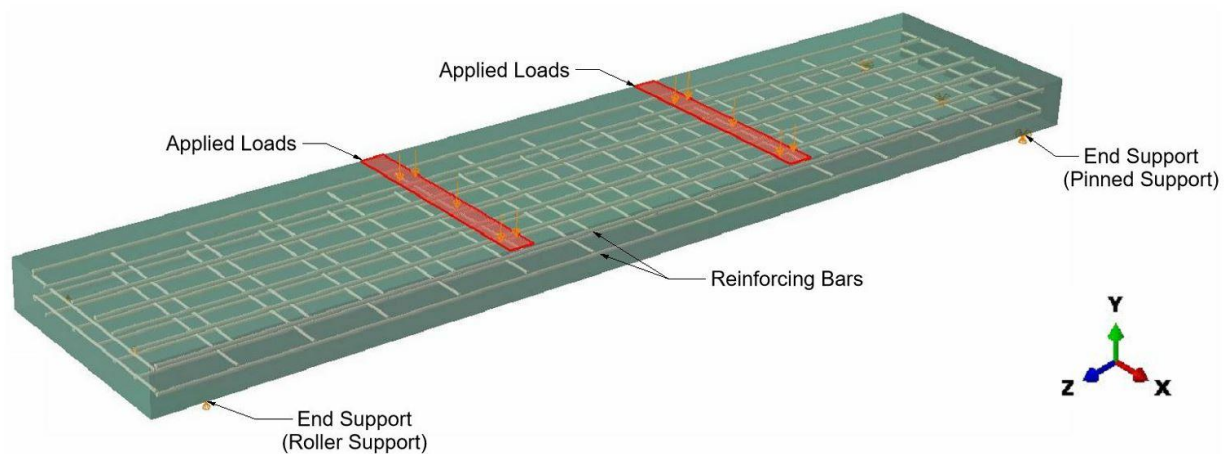


**Figure 3-5. Supports and applied loads on concrete decks.**

### 3.5.2    Concrete Material Definition

The behavior of concrete decks was simulated by modeling the elastic and plastic performance of concrete and steel materials. The modulus of elasticity and the Poisson's ratio were used to model the elastic behavior of concrete and steel [23]. For plastic performance of concrete, Concrete Damage Plasticity (CDP) model was used to simulate the damage. The model

51

considers the tensile cracking and the compressive crushing as the two main failure mechanisms

in concrete [33]. CDP model can simulate the complete inelastic behavior of concrete in both

tension and compression including damage characteristics [23]. The parameters of CDP model

were chosen according to the ABAQUS manual and research literature. The dilation angle ($\psi$)

and shape factor ($K_c$) are typically in a range of 31° to 42° and 0.5 to 1.0, respectively. As

recommended by Azam [14] and Abhaee [34], the values of 35° and 0.667 were selected for

dilation angle ($\psi$) and shape factor ($K_c$), respectively. The selection of the eccentricity ($m$) of 0.1

and stress ratio ($f_{b0}/f_{c0}$) of 1.16 was based on the ABAQUS manual. These values are typically

applicable for normal-weight normal-strength concrete. The viscosity parameter ($\mu$) is set to be

close to zero as it has minimal to no effect to the simulation [14,32]. In this study, the viscosity

parameter was 0.01. For reinforcement steel, the plastic behavior was modeled by the plasticity

option. When the stress in steel exceeds the yield limit, the plasticity definition governs the

element properties [15].

In additional to the parameters defined above, the behavior of concrete in compression and

tension is needed for the CDP model [33]. The model of Lu and Zhaoc [35] was used to capture

the compressive stress-strain relationship of concrete. The compressive stress of concrete ($f_c$) is

calculated by **Eq. (3-1)**, with supplementary equations shown in **Eq. (3-2)** to **Eq. (3-4)**; in which

$f'_c$ is the measured concrete strength at 28 days of age as aforementioned. For tensile stress, the

model of Hsu and Mo [36] was used to capture the stress-strain relationship of concrete. The

tensile stress of concrete ($f_t$) is calculated by **Eq. (3-5)**. The compressive and tensile stress-strain

relationships of concrete are presented in **Figure 3-6**. The peak compressive stress ($f'_c$) and

corresponding strain ($\varepsilon_{ut}$) are 41 MPa and 0.0022, respectively. It is noted that the compressive

stress-strain curve exhibits linear behavior up to a stress level of around $0.4 f_c'$. The peak tensile

stress ($f_{ut}$) and corresponding strain ($\varepsilon_{uc}$) are 2.5 MPa and 0.00021, respectively.

$$f_c = \begin{cases} f_c' \times \left\{ \dfrac{\left[ \left( \dfrac{E_{it}}{E_0} \right) \times \left( \dfrac{\varepsilon_c}{\varepsilon_0} \right) - \left( \dfrac{\varepsilon_c}{\varepsilon_0} \right)^2 \right]}{1 + \left( \dfrac{E_{it}}{E_0} - 2 \right) \times \left( \dfrac{\varepsilon_c}{\varepsilon_0} \right)} \right\} & 0 \le \varepsilon_c \le \varepsilon_L \\[4em] f_c' \times \left\{ \dfrac{1}{1 + 0.25 \times \left( \dfrac{\varepsilon_c}{\varepsilon_0} - \dfrac{\varepsilon_c}{\varepsilon_L} - 1 \right)^{1.5}} \right\} & \varepsilon_c > \varepsilon_L \end{cases}$$

Eq. (3-1)

$$\varepsilon_L = \varepsilon_0 \times \left[ \left( 0.1 \dfrac{E_{it}}{E_0} + \dfrac{4}{5} \right) + \sqrt{\left( 0.1 \dfrac{E_{it}}{E_0} + \dfrac{4}{5} \right)^2 - \dfrac{4}{5}} \right]$$

Eq. (3-2)

$$E_{it} = 19350 \times \left( \dfrac{f_c'}{10} \right)^{1/3}$$

Eq. (3-3)

$$\varepsilon_0 = 700 \times \left( f_c' \right)^{0.31} \times 10^{-6}$$

Eq. (3-4)

$$E_0 = \dfrac{f_c'}{\varepsilon_0}$$

Eq. (3-5)

$$f_t = \begin{cases} (\varepsilon_t \times E_c), & \varepsilon_t \le \varepsilon_{cr} \\[2em] 0.31 \times \sqrt{f_c'} \times \left( \dfrac{\varepsilon_{cr}}{\varepsilon_t} \right)^{0.4}, & \varepsilon_t > \varepsilon_{cr} \end{cases}$$

Eq. (3-6)

where: $\varepsilon_c$ and $\varepsilon_t$ are compressive and tensile strains, respectively; $\varepsilon_t$ is cracking strain of concrete (taken as 0.00008 [33]); $f_c'$, $E_{it}$, $E_0$, and $E_c$ are in MPa.
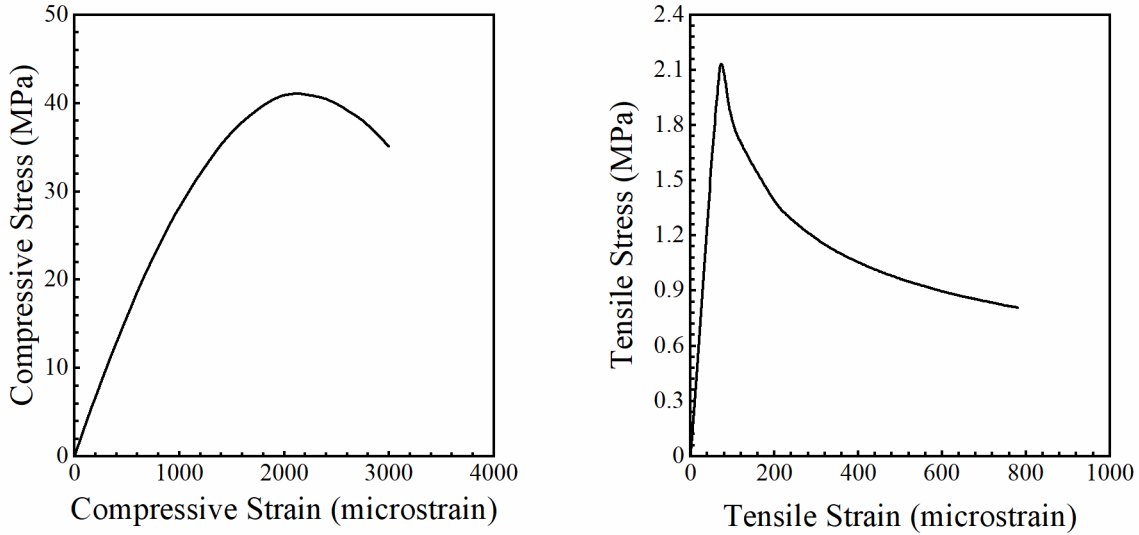


**Figure 3-6. Compressive and tensile stress-strain relationships of concrete.**

The nonlinear behavior of concrete can be attributed to two distinct material mechanical processes: plasticity and damage [33]. Therefore, it is important to consider both damage and plasticity in concrete materials for a more realistic modeling of the behavior of concrete. CDP model can simulate both plasticity and damage of concrete. The compressive and tensile behaviors of concrete are defined through a yield stress versus plastic strain relationship. CDP model can automatically consider and calculate the biaxial and degradation in concrete material by inputting the parameters of uniaxial stress-strain and damage. The uniaxial compressive stress ($\sigma_c$) is calculated by **Eq. (3-7)** [37]. For the tensile stress ($\sigma_t$), the stress is calculated by **Eq. (3-8)**, with supplementary equations shown in **Eq. (3-9)** to **Eq. (3-18)** [33]. The effect of bond slip between concrete and reinforcing bars is considered by modifying the tensile stress of concrete ($\sigma_t$). The tensile stress ($\sigma_t$) takes into account reinforcement steel ratio ($\rho$), yield

strength of steel ($f_y$), and mesh size of concrete elements ($L_c$). The plasticity-damage constitutive relationships of concrete under uniaxial compressive and tensile loading are shown in **Figure 3-7**. CDPM performs the simulation of nonlinear behavior of concrete by incorporating the isotropic-damaged elasticity with tensile and compressive plasticity [34].

$$\sigma_c = \frac{((f_c' \times E_c / \varepsilon_{uc})(\varepsilon_c / \varepsilon_{uc}) + (D-1)(\varepsilon_c / \varepsilon_{uc})^2}{1 + ((f_c' \times E_c / \varepsilon_{uc}) - 2)(\varepsilon_c / \varepsilon_{uc}) + D(\varepsilon_c / \varepsilon_{uc})^2} \times f_c'$$

Eq. (3-7)

$$\sigma_t = \begin{cases} (E_c \times \varepsilon_t), & \varepsilon_t \leq \varepsilon_{cr} \\ \\ 0.33 \times \sqrt{f_c'} \times \left(\frac{\varepsilon_{cr}}{\varepsilon_t}\right)^n, & \varepsilon_{ut} > \varepsilon_t > \varepsilon_{cr} \end{cases}$$

Eq. (3-8)

$$n = (A_n - B_n)D_n \times L_n$$

Eq. (3-9)

$$A_n = 0.48 - 0.0023 f_c'$$

Eq. (3-10)

$$B_n = (13.4 - 0.0834 f_c')(\rho - 0.012)$$

Eq. (3-11)

$$D_n = (1.64 - 0.0016 f_y)(f_y / 400)$$

Eq. (3-12)

$$L_n = (0.665 - 0.014 L_c)$$

Eq. (3-13)

$$\varepsilon_{ut} = \gamma \varepsilon_{cr}$$

Eq. (3-14)

$$\gamma = (A_\gamma + B_\gamma)D_\gamma$$

Eq. (3-15)

$$A_\gamma = 0.24(f_c')^2 - 20.8 f' + 548$$

Eq. (3-16)

$$B_\gamma = (68 f_c' + 8300)(\rho - 0.012)$$

Eq. (3-17)

$$D_n = (0.0022 f_y - 0.12)(f_y / 400)$$

Eq. (3-18)
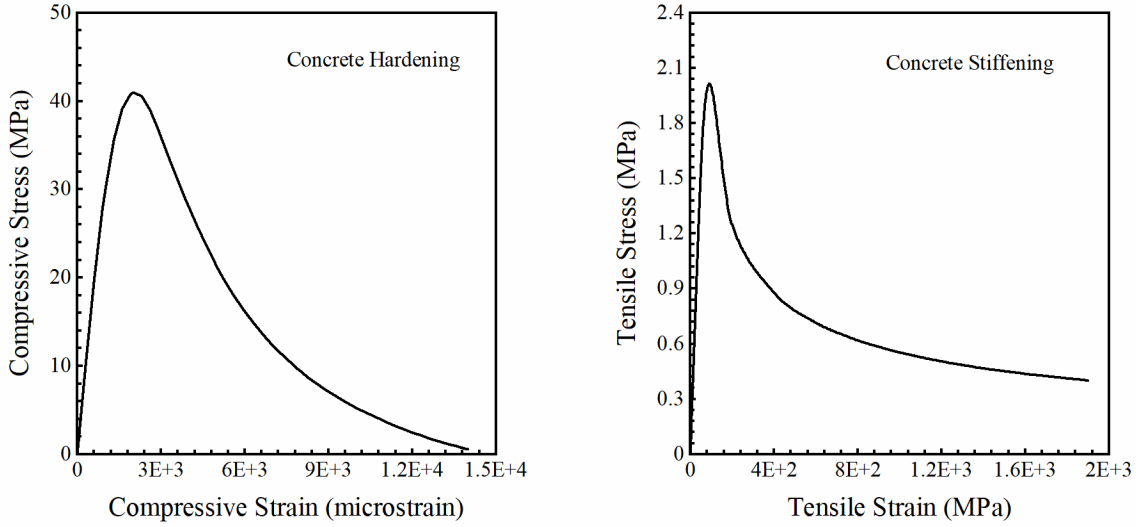
**Figure 3-7. Concrete uniaxial compression hardening and tension stiffening.**

In CDP model, the degradation of concrete is defined through the use of the damage with plastic strain curve [33]. The compressive damage ($d_c$) and tensile damage ($d_t$) are calculated by **Eq. (3-19)**, with supplementary equations shown in **Eq. (3-20)** to **Eq. (3-22)** [37]. The damage parameters for cracking and crushing of concrete are shown in **Figure 3-8**. The degradation of the elastic stiffness of concrete is different in compression than in tension. The concrete damage describes the reduction in the material stiffness [33,37].

$$d_{c/t} = 1 - \frac{\sigma_{true} \times E_c^{-1}}{(b_{c/t} \times \varepsilon^{in})(1/b_{c/t} - 1) + \sigma_{true} \times E_c^{-1}}$$

Eq. (3-19)

$$\varepsilon_{true} = \ln(1 + \varepsilon)$$

Eq. (3-20)

$$\sigma_{true} = \sigma(1 + \varepsilon)$$

Eq. (3-21)

$$\varepsilon^{in} = \varepsilon_{true} - \frac{\sigma_{true}}{E_c}$$

Eq. (3-22)

56

where: $b_c$ is equal to 0.7 for compressive damage; $b_t$ is equal to 0.3 for tensile damage.
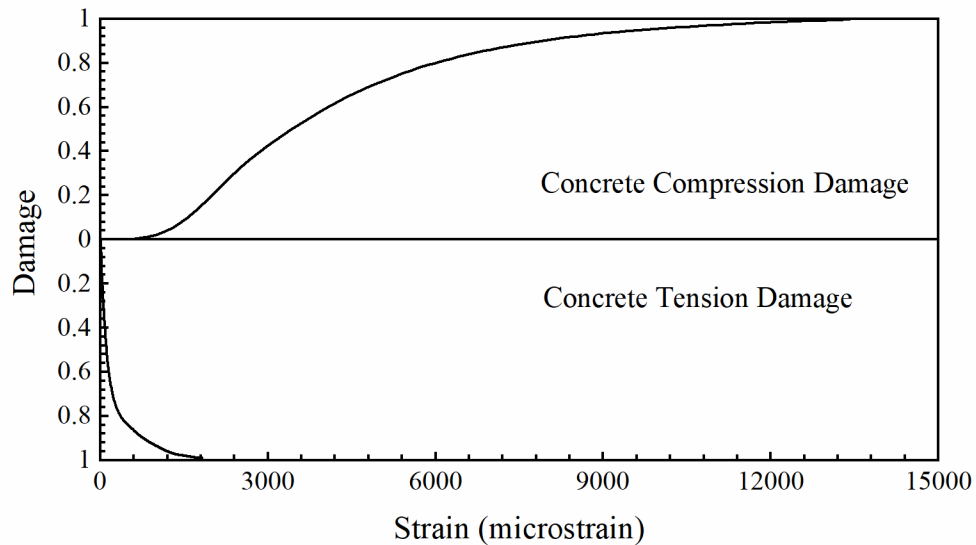


**Figure 3-8. Concrete damage of tension and compression.**

### 3.5.3 Steel Material Definition

The stress-strain relationship for Grade 420, Grade 690 and Grade 830 steel are analytically determined.  The modulus of elasticity ($E_s$) and Poisson's ratio ($\upsilon$) of the reinforcing steel were 200 GPa and 0.3, respectively.  The stress-strain relationship of the steel is captured by **Eq. (3-23)** for Grade 420 and by **Eq. (3-24)** for Grade 690 and Grade 830 [38,39].  The parameters $A$, $B$, and $C$ are 0.017, 205, and 2.4 for Grade 690 steel and 0.013, 184, and 2.5 for Grade 830 steel, respectively.  **Figure 3-9** shows the stress-strain relationship of the three steel grades.  For Grade 420 steel, the yielding plateau was explicit, so the plasticity region was defined from yielding strength to failure (end of the stress-strain curve).  For Grade 690 and Grade 830 steel, the yielding occurred gradually without an explicit yielding plateau like Grade 420 steel.  The yield strengths of Grade 690 and Grade 830 were determined by the offset method (technically termed

57

as 0.2% offset) [4]. The plasticity region of these steel grades was defined from the nominal yielding strength to failure.

$$f_s = \begin{cases} 200000 \times \varepsilon_s & 0 \le \varepsilon_s \le 0.002 \\ f_y & 0.002 < \varepsilon_s \le 0.0055 \\ f_y + (620 - f_y) \times \sqrt{\dfrac{\varepsilon_s - 0.0055}{0.0455}} & 0.0055 < \varepsilon_s \le 0.09 \end{cases}$$

Eq. (3-23)

$$f_s = 200000 \times \varepsilon_s \times (A + \frac{1 - A}{\left[1 + (B \times \varepsilon_s)^C\right]^{1/C}})$$

Eq. (3-24)

where: $f_s$ is steel stress; $f_y$ is yield strength of steel; $\varepsilon_s$ is steel strain;
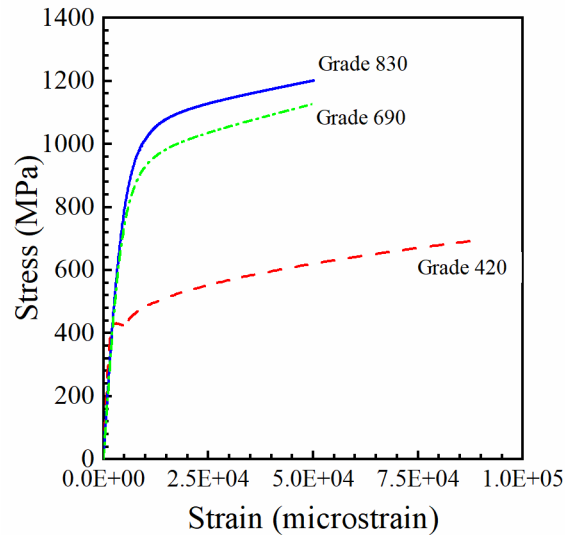


Figure 3-9. Stress-strain curve of Grade 420, Grade 690, and Grade 830 steel.

The elasticity and plasticity behavior of reinforcement were a function of the stress-strain relationship of steel. The modulus of elasticity ($E_s$) and Poisson's ratio ($v$) represented the steel elasticity behavior. On the other hand, the reinforcement elements were governed by the plasticity behavior when the stresses exceed the yield strength. The nonlinear behavior of the reinforcing steel was modeled by Plasticity option in ABAQUS. The material plasticity was defined by the stress-plastic-strain relationship. The initial stress value corresponded to the yield strength in which the plastic strain was set to be zero [15].

## 3.6 RESULTS AND DISCUSSION

### 3.6.1 Load-Deflection Curve

The results from the FE model are compared to the experimental data for the ten concrete decks. The comparison between the analytical and experimental load-deflection relationships is shown in **Figure 3-10**. **Figure 3-10 (A)** indicates a good agreement between the analytical and experimental results for the concrete decks reinforced by Grade 420 steel. However, the load-deflection curve produced by FE model is stiffer than the experimental load-deflection curve. The maximum analytical deflection and experimental deflection are 73 mm and 57 mm, respectively, for the decks reinforced with Grade 420 steel. Also, the analytical failure load to experimental failure load is 1.02 for D5-1 deck. **Figure 3-10 (B)**, **Figure 3-10 (C)**, and **Figure 3-10 (D)** show the analytical and experimental load-deflection relationships for concrete decks reinforced by Grade 830 steel. The figures indicate the relationship of deflection with applied load is similar between the analytical results and experimental data. **Figure 3-10 (B)** Figure 3-10. shows the analytical and experimental relationships are identical until 20 kN, then the analytical results are stiffer than the experimental data until failure. The maximum analytical deflection

and experimental deflection are 71 mm and 86 mm, respectively, and the maximum analytical

load to experimental load is 1.04 at failure.  For **Figure 3-10 (C)**, the analytical and experimental

results are very close until 175 kN, then the analytical results are more conservative.  **Figure 3-**

**10 (D)** shows the maximum analytical deflection and the average experimental deflection of two

tests are 88.0 mm and 91.5 mm.  For the maximum load, the ratio of the analytical load to the

average experimental load for the two tests is 1.03 at failure.
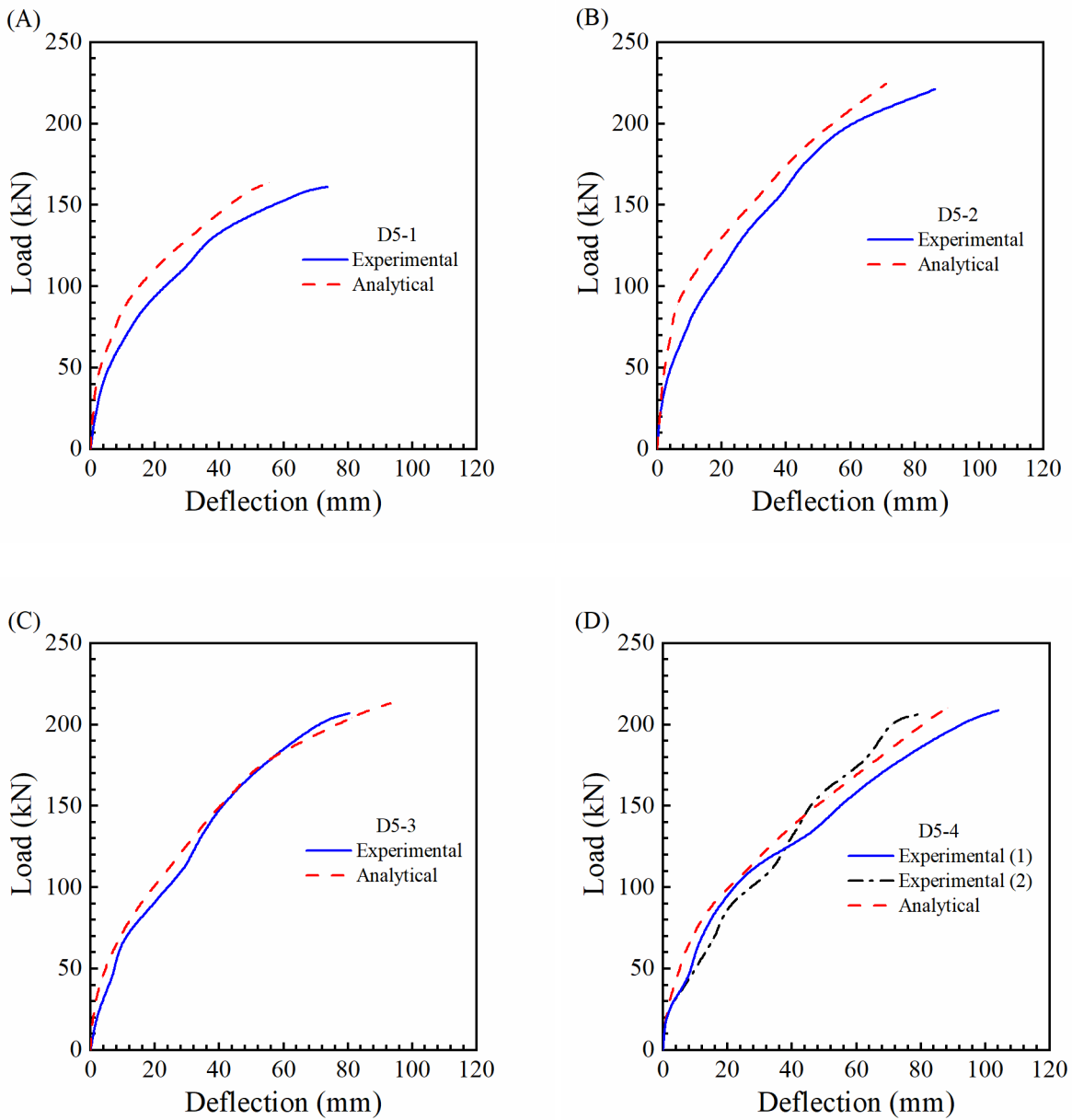
**Figure 3-10. Experimental and analytical load-deflection curves of D.5 group.**

The difference between the analytical and experimental results can be due to microcracking at

the interfaces between the cement paste and aggregate due to drying shrinkage in the concrete,

similar to the observation in Metwally's research [21]. On the other hand, these microcracks are

not present in the FE model. Another important reason leading to difference between the FE

model and the experimental results is that the FE model simulates the concrete as a uniform

isotropic material [21,25]. The uniform isotropic definition assumes the concrete has the same

properties in all directions. In fact, the concrete consists of three phases of materials with

different properties in different directions: hardened binder, interfacial transition zone, and

coarse aggregate. To simplify the development of FE model, only concrete compressive

strength, tensile strength, and modulus of elasticity were used to represent for the concrete

behavior. This is a typical practice in reinforced concrete modeling when overall performance of

concrete members is the point of interest rather than the micro performance of concrete material.

Additional concrete decks (D.6 group) reinforced with different amounts of reinforcing steel

were modeled and compared with the experimental data. The comparison between the analytical

and experimental load-deflection relationships is shown in **Figure 3-11**. **Figure 3-11 (A)** shows

the behavior of a concrete deck reinforced with Grade 420 steel, while the other figures are

related to concrete decks reinforced with Grade 830 steel. **Figure 3-11 (A)** shows the maximum

analytical deflection and experimental deflection are 79 mm and 69 mm, respectively. **Figure 3-11 (B)** and **Figure 3-11 (C)** show the maximum analytical deflections are less than the maximum

experimental deflections are by 4% and 7%, respectively. For the maximum load, the ratio of

analytical failure loads to experimental loads are 1.03, 1.04, and 1.02 as shown in **Figure 3-11 (A)**, **Figure 3-11 (B)**, and **Figure 3-11 (C)**, respectively. For **Figure 3-11 (D)**, the maximum

analytical deflection and load are greater by 11% and 3% than that of the average experimental

data for the two tests, respectively. **Figure 3-11** confirms the good agreement between the

analytical and experimental load-deflection relationship for the concrete deck.
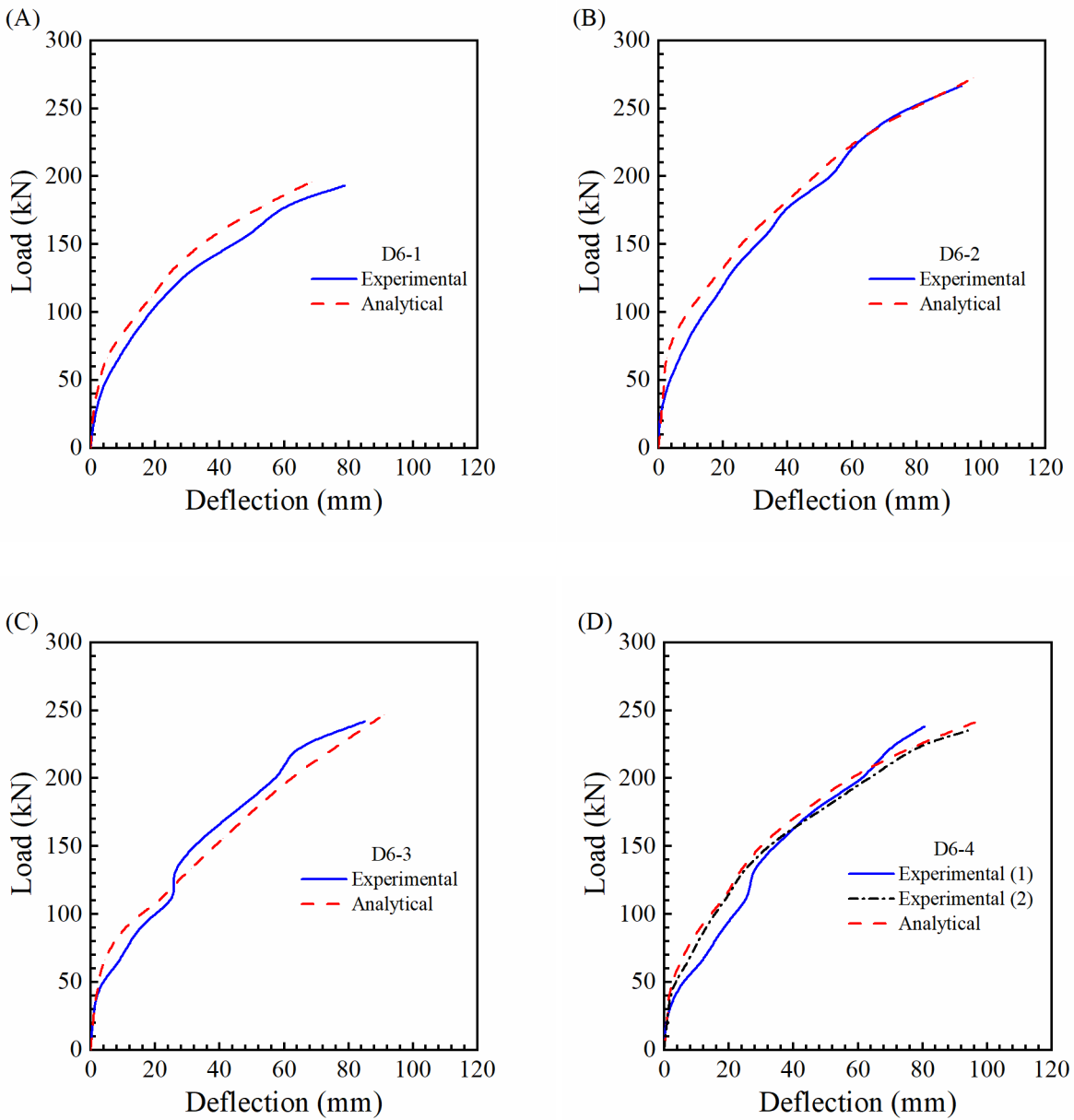
**Figure 3-11. Experimental and analytical load-deflection curves of D.6 group.**

### 3.6.2 Strain Variation

**Figure 3-12** illustrates the comparison of the analytical and experimental relationship of the

applied loads to strains. The relationship shows the steel and concrete strains for decks

reinforced with No. 16 bars. The concrete compressive strains were measured until failure, while steel tensile strains were measured until yielding.
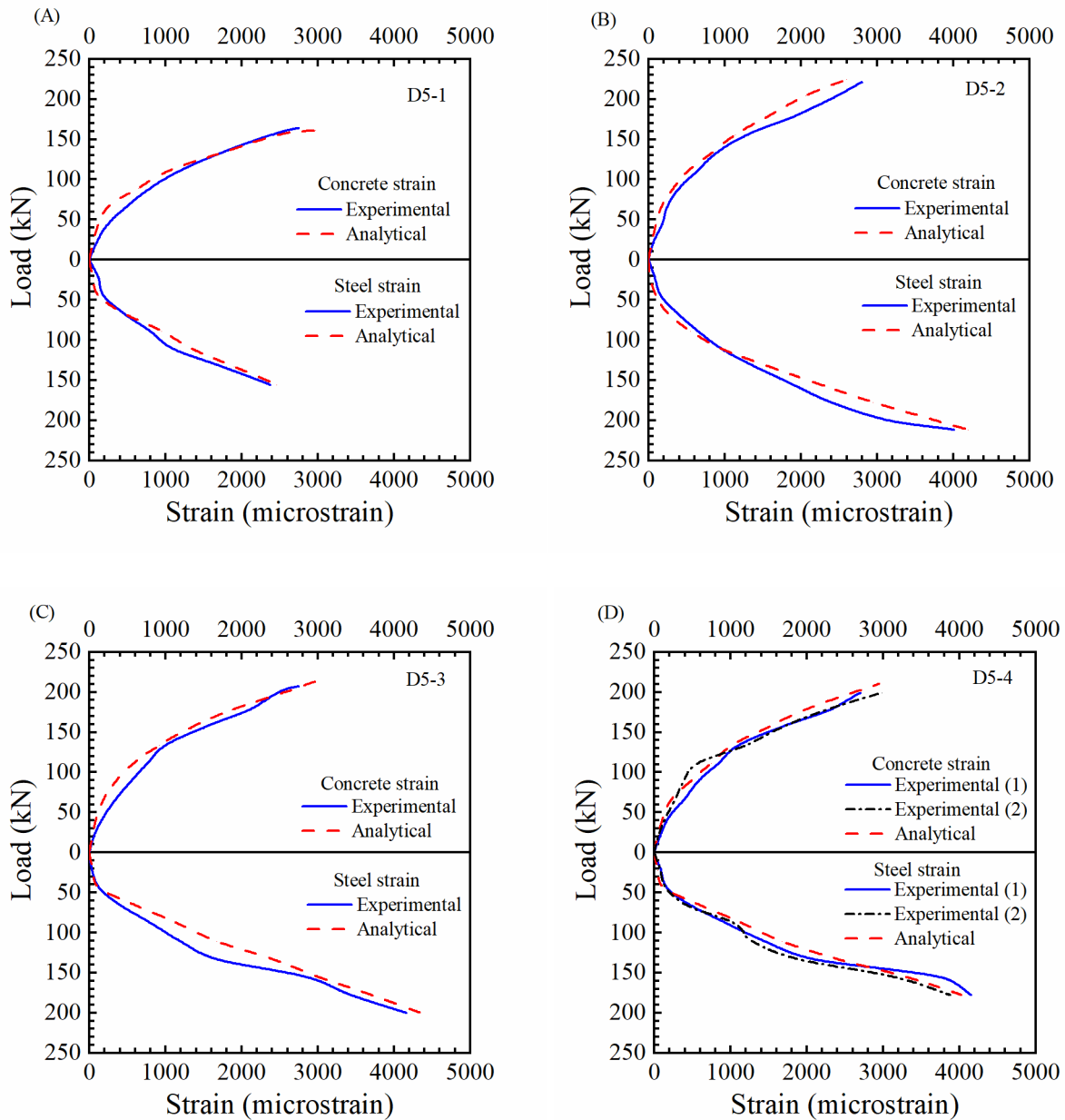


**Figure 3-12. Experimental and analytical load-concrete and steel strains curves of D.5 group.**

**Figure 3-12 (A)** shows a good agreement between the analytical strains and the measured results for D5-1. The maximum compressive strain of the concrete predicted by the analytical method was 8% greater than the experimental strain. Also, the analytical tensile strain of steel was 4% greater than the experimental results. **Figure 3-12 (B)**, **Figure 3-12 (C)**, and **Figure 3-12 (D)** represents the analytical and experimental results of D5-2, D5-3, and D5-4, respectively. The analytical results of the maximum compressive concrete strains are different from the experimental data by -9%, 7%, and 4% as shown in **Figure 3-12 (B)**, **Figure 3-12 (C)**, and **Figure 3-12 (D)**, respectively. All decks show the maximum compressive strain of concrete predicted by FEM was approximately 3000 microstrain. Also, the analytical tensile strains in the reinforcing steel are well related to experimental results. The analytical results of the reinforcing steel strains were 4%, 4%, and -1% different from the experimental results as shown in **Figure 3-12 (B)**, **Figure 3-12 (C)**, and **Figure 3-12 (D)**, respectively. Even with the replacement of Grade 420 with Grade 830 which reduced the reinforcement ratio by 40%, the required loads for steel yielding are still greater than that of decks reinforced with Grade 420.

**Figure 3-13** shows the comparison between the analytical and experimental load versus strain relationship for the concrete and reinforcing steel for the D.6 group. The strains were measured until failure for the concrete and until yielding for steel. Shown in **Figure 3-13 (A)** is the comparison of the experimental and analytical results of D6-1. The maximum concrete strain and steel strain predicted by FEM were 11% and 6% greater than that of experimental data. Shown in **Figure 3-13 (B)**, **Figure 3-13 (C)**, and **Figure 3-13 (D)** are the behavior of D6-2, D6-3, and D6-4, respectively. For maximum compressive concrete strains, the analytical results were 13%, 10%, and 8% greater than the experimental data as shown in **Figure 3-13 (B)**, **Figure 3-13 (C)**, and **Figure 3-13 (D)**, respectively. For steel strains, the analytical results are differed

from the experimental results by 3%, 7%, and 5% as shown in **Figure 3-13 (B)**, **Figure 3-13 (C)**, and **Figure 3-13 (D)**, respectively. The maximum concrete strains predicted by FEM for the decks reinforced with Grade 420 or 830 were near the theoretically ultimate strain of concrete. On the other hand, the tensile strain curves in all figures were close to linear change. This is because the variations of reinforcement steel were calculated until yielding. The analytical results from the FEM related well to the experimental tests. Both the experimental and analytical results of steel tensile strains show that D6-4 decks required additional loads to reach steel yielding in comparison to D6-1 due to the higher yielding strength of Grade 830 in comparison to Grade 420.
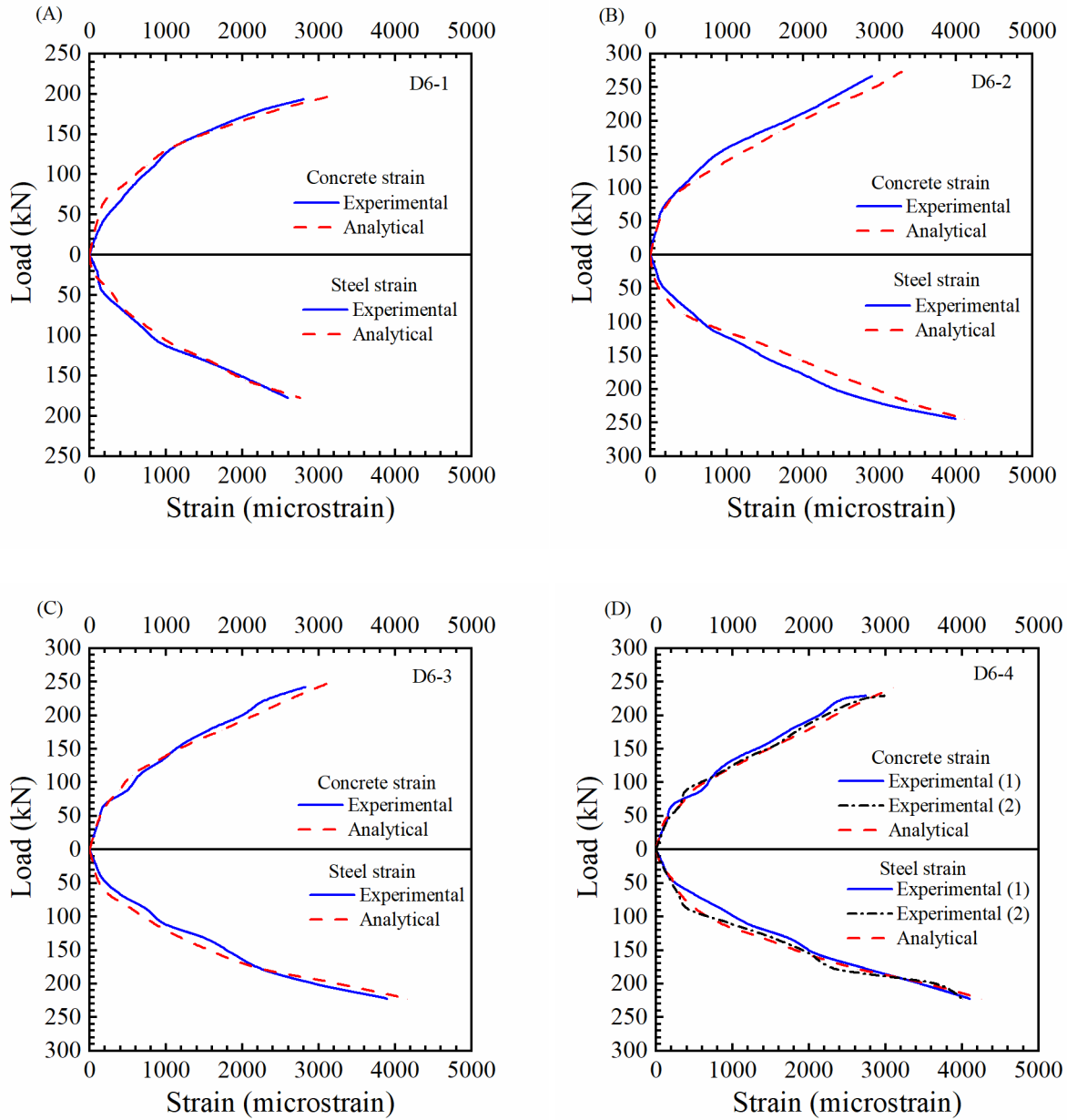
**Figure 3-13. Experimental and analytical load-concrete and steel strains curves of D.6 group.**

### 3.6.3 Crack Pattern

Cracks in concrete occur when the tensile stresses exceed the tensile strength of concrete. In the CDPM, cracks can be visualized by assuming they initiate at points where the tensile stress is greater than tensile strength of concrete. Cracks initiate at points where the tensile plastic strains

are greater than zero.  Therefore, crack propagation in the finite element model can be tracked

through the maximum principal plastic strains in the concrete [40].  **Figure 3-14** shows the

analytical and experimental crack patterns for D5-3 and D6-3.  **Figure 3-14 (A)** show the

experimental cracks patterns in concrete decks.  **Figure 3-14 (B)** show the distribution of plastic

strains in concrete decks, while **Figure 3-14 (C)** display the direction of plastic strains.  The

cracks were concentrated in the middle of the decks.  This is because of the high of tensile strains

at this region.  The crack pattern of the finite element model is similar to that of the experimental

pattern.  The crack directions are considered to be perpendicular to plastic strains.  The

experimental crack patterns **Figure 3-14 (A)** are well related to the visualization by FEM as

shown in **Figure 3-14 (B)**.  Also, the maximum plastic strains are 0.04232 and 0.04920 for decks

D5-3 and D6-3 as shown in **Figure 3-14 (D5B)** and **Figure 3-14 (D6B)**, respectively.  Therefore,

the crack widths of D6-3 are wider than that of D5-3.  This is because of the greater applied

loads on D6-3 than that on D5-3.
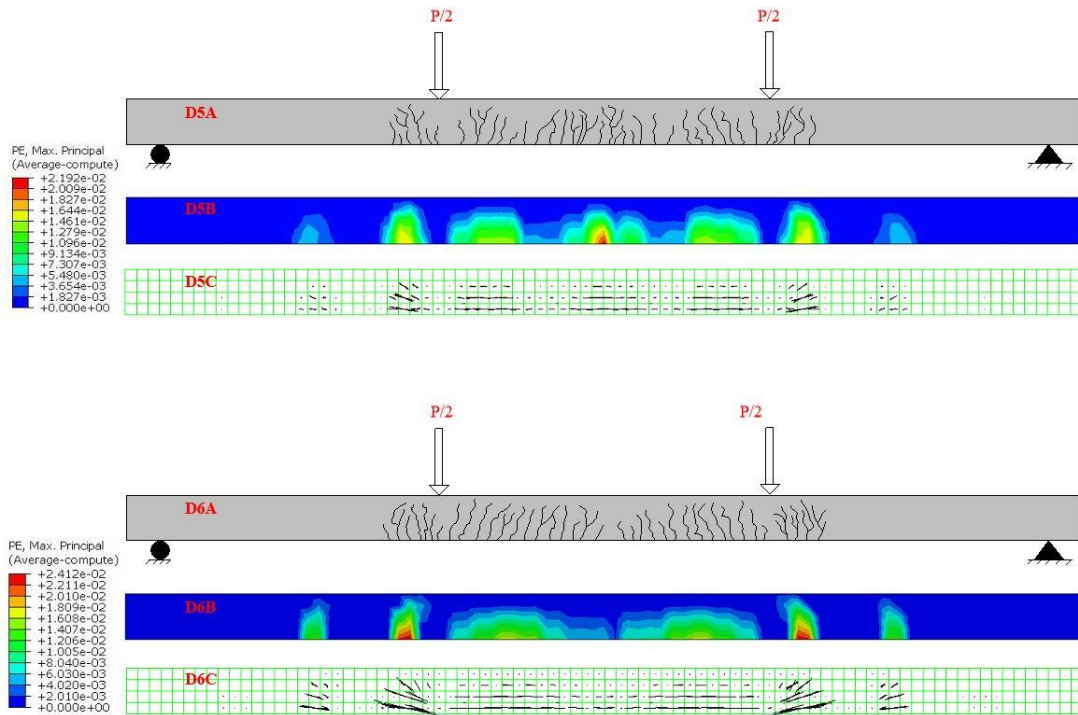
**Figure 3-14. Experimental crack pattern and analytical plastic strain.**

The experimental cracks patterns were visualized until 0.01 mm depending on the accuracy and precision of the crack-microscope. However, the FEM can visualize all plastic strains, which represent the analytical cracks patterns. **Figure 3-15** shows the maximum crack width at service load and at yielding load. The service loads are considered as the loads developing steel stress ($f_s$) at reinforcing bars less than $0.6f_y$ [39]. The yielding loads are considered as the loads corresponding to steel yielding at concrete decks. The crack widths were analytically calculated by **Eq. (3B-1)** [41]. The cracks widths created at concrete decks reinforced with Grade 830 are greater than that developed at decks reinforced with Grade 420. This is because of the greater service loads applied on decks reinforced with Grade 830 in comparison to deck reinforced with Grade 420. At service loads, the maximum crack width of D5-1 is 0.09 mm, while the crack widths are increased by 78%, 111%, and 156% for D5-2, D5-3, and D5-4, respectively. For D6-

69

1, the maximum crack width is 0.12 mm, and the maximum crack widths are increased by 58%, 92%, and 125% for D6-2, D6-3, and D6-4, respectively.  At yielding loads, the maximum crack width of D5-1 is 0.44 mm, while the crack widths are increased by 95%, 143%, and 193% for D5-2, D5-3, and D5-4, respectively.  For D6-1, the maximum crack width is 0.54 mm, and the maximum crack widths are increased by 98%, 139%, and 189% for D6-2, D6-3, and D6-4, respectively.
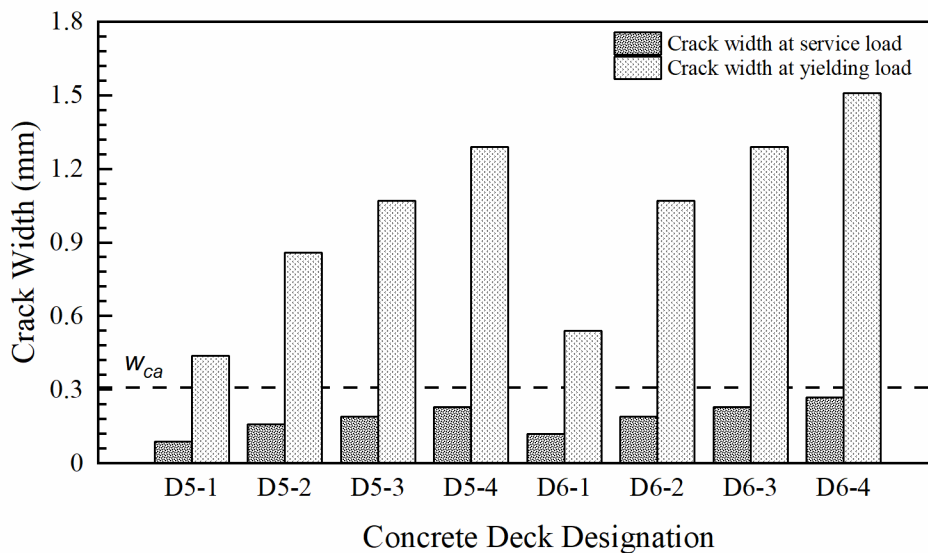


**Figure 3-15. Maximum crack width at service and yielding loads.**

Cracks width adversely affects concrete members at service limit state.  In addition to increasing the risk of corrosion, the greater cracks widths reduce the bond between concrete and reinforcing bars, increase deflection, and decrease stiffness [6].  AASHTO LRFD Bridge Design Specifications have specified that the maximum allowable crack width ($w_{ca}$) is 0.32 mm [29].  At service loads, the maximum crack width of all decks was less than the maximum allowable crack

width.  At yielding loads, decks reinforced with Grade 830 provide adequate warning through large deformation and extensive cracking.

### 3.6.4    Parametric Studies 1: Grade 690 Steel

The analytical results of the proposed model showed a good agreement with the experimental data of the concrete decks reinforced with Grade 830 and Grade 420 steel.  Therefore, the model can be adopted to study additional concrete decks.  **Table 3-3** summarizes the parametric studies. Decks reinforced with Grade 690 and Grade 830 are investigated and compared to decks reinforced with Grade 420.  The concrete decks are also reinforced with one or two layers of steel to investigate the reduction in the amount of steel.  Moreover, the effects of concrete strength on the performance of deck reinforced with Grade 830 are investigated.

**Table 3-3 – Parametric studies.**

| Deck designation | Steel | Bar quantity | Number of steel layers | Description |
|---|---|---|---|---|
| D.P.5 group | | | | |
| D.P.5-1 | Grade 690 | No. 16 @ 150 mm | 2 | Identical to D5-2, with replacing Grade 830 by Grade 690. |
| D.P.5-2 | Grade 830 | No. 16 @ 150 mm | 1 | Identical to D5-2, with reducing number of steel layers. |
| D.P.6 group | | | | |
| D.P.6-1 | Grade 690 | No. 19 @ 200 mm | 2 | Identical to D6-2, with replacing Grade 830 by Grade 690. |
| D.P.6-2 | Grade 830 | No. 19 @ 200 mm | 1 | Identical to D6-2, with reducing number of steel layers. |

**Figure 3-16** shows the load-deflection relationship for decks reinforced with Grade 830, 690, and Grade 420.  **Figure 3-16** (**A)** and **Figure 3-16** (**B)** show the analytical results for concrete decks D.P.5-1 and D.P.6-1, which have same amount and distribution of steel as D5-1 (#16 @ 150mm) and D6-1 (#19 @ 200mm), respectively, but the reinforcement steel grade was Grade

690.  **Figure 3-16** shows that the deflection of the concrete decks reinforced was Grade 830 and Grade 690 was greater in comparison to the decks reinforced with Grade 420.  **Figure 3-16 (A)** shows the maximum deflection of D.P.5-1 was 69 mm.  The failure load of D.P.5-1 was 28% greater and 6% less when compared to decks D5-1 and D5-2, respectively.  **Figure 3-16 (B)** also confirms the load-deflection relationship of concrete decks reinforced with Grade 690 (D.P.6-1).  The maximum deflection of D.P.6-1 was 96 mm.  The failure load of D.P.6-1 was 29% greater and 7% less when compared to D6-1 and D6-2, respectively.  It is noted that the failure load of concrete decks decreased when Grade 830 is replaced with Grade 690.  However, the flexural strength of concrete decks reinforced by Grade 690 is greater than that of decks reinforced with Grade 420 steel.  The average failure load of decks reinforced with Grade 690 was 29% greater than that of decks reinforced with Grade 420.
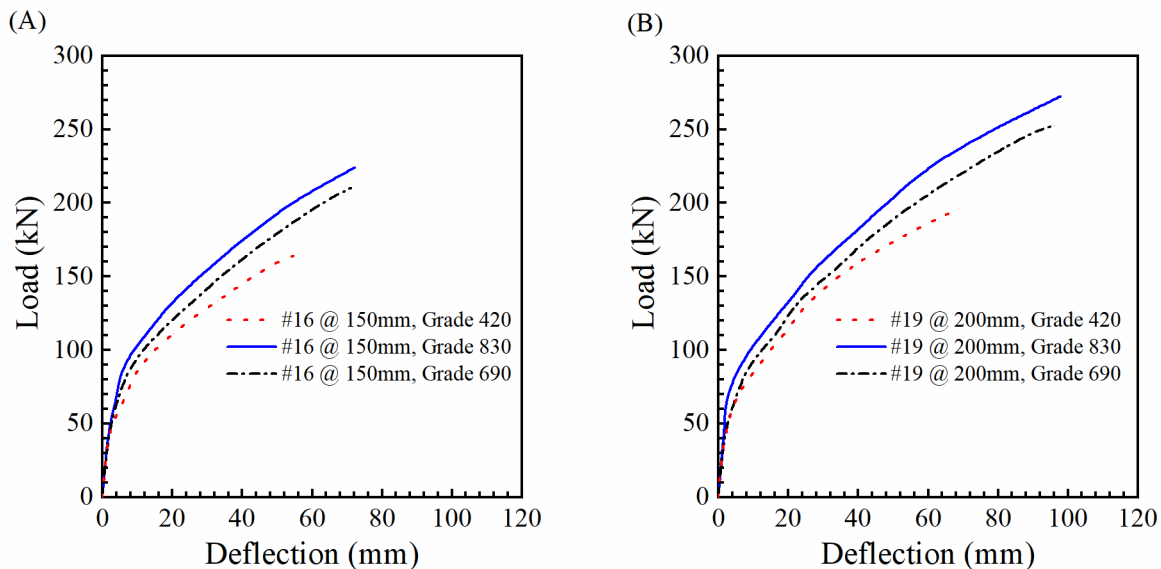


**Figure 3-16. Load-deflection curves of decks reinforced with different steel grades.**

Shown in **Figure 3-17** is the load-deflection relationship of concrete decks reinforced with one or two layers of reinforcement. D.P.5-2 and D.P.6-2 have one layer of reinforcement, while D5-2 and D6-2 have two layers of reinforcement. The reinforcement layer for D.P.5-2 and D.P.6-2 has the same distribution of reinforcement bars of D5-2 and D6-2, respectively. **Figure 3-17 (A)** shows the failure load of D.P.5-2 is 27% greater than that of D5-1 and 7% less than that of D5-2. **Figure 3-17 (B)** indicates that the failure load of D.P.6-2 is 30% greater than that of D6-1 and 7% less than that of D6-2. On the other hand, the maximum deflections of D.P.5-2 and D.P.6-2 are 71 mm and 95 mm, respectively. The flexural resistance of concrete decks reinforced with one layer of reinforcement of Grade 830 was greater than that of decks reinforced with two layers of Grade 420.
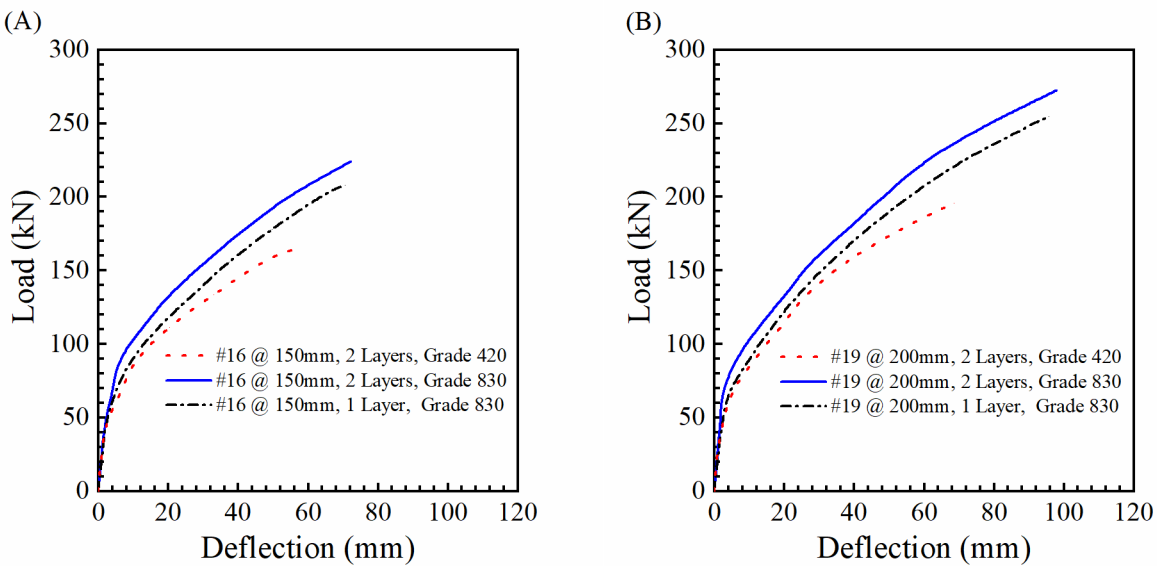


**Figure 3-17. Load-deflection curves of decks reinforced with one or two layers of steel.**

### 3.6.5　Parametric Studies 2: Concrete Compressive Strength

The proposed model was also used to investigate the effects of concrete strength on the performance of deck reinforced with Grade 830. **Figure 3-18** shows the effect of concrete strength on decks reinforced with Grade 830. Three different concrete strengths, 30 MPa, 40 MPa, and 50 MPa, were used to model D.P.5-2. **Figure 3-18 (A)** shows load-deflection relationship. It is noted that the flexural strength is improved by increasing the concrete strength. The ultimate flexural resistance of D.P-2 increases by 5.2% and 10.4% when the concrete strength is increased from 30 MPa to 40 MPa and 50 MPa, respectively. Moreover, the maximum deflection was increased by 5.7% and 11.4%. **Figure 3-18 (B)** shows load-crack width relationship. The crack widths were calculated until steel yielding. The yielding loads are increased by 3.4% and 6.8% when the concrete strength was increased by 33.3% and 66.7%, respectively. It is noted that the crack width is reduced by increasing concrete strength. Generally, the steel stress of reinforcing bars at service load does not exceed 0.6 times yield strength [39]. The service load was assumed as 0.6 times yield load of deck casted by concrete strength 30 MPa to investigate the effect of increasing concrete strength on crack width. The maximum crack width was reduced by 20.7% and 41.4% at service load when concrete strength increased by 33.3% and 66.7%, respectively.
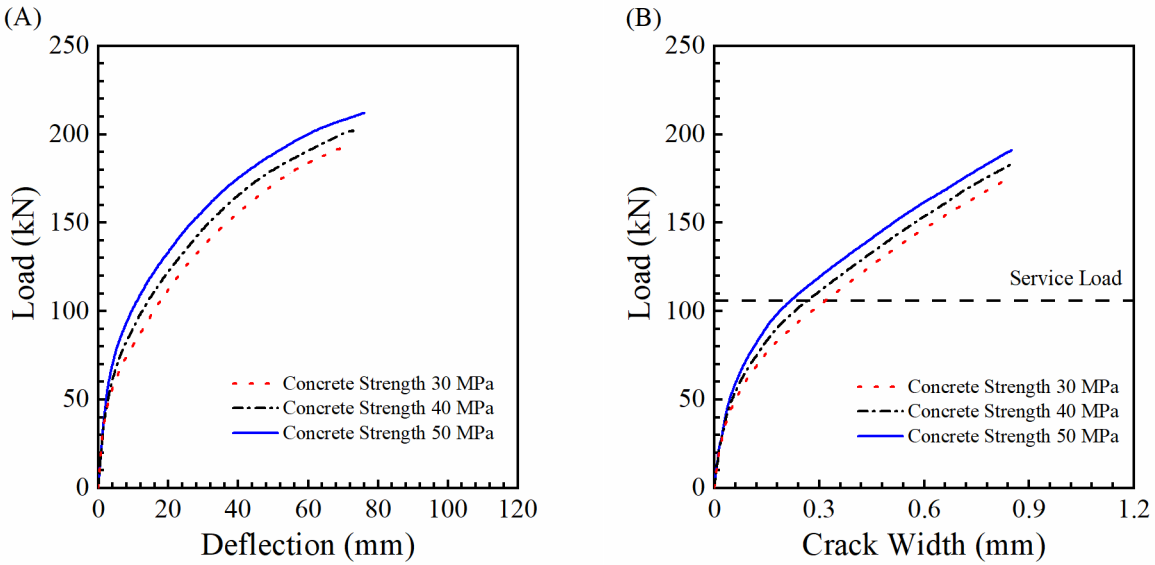
**Figure 3-18. Load-deflection and crack width curves of decks casted by different concrete strengths.**

### 3.6.6    Research Limitations

The numerical modeling of reinforced concrete structures has been progressively advanced for the last three decades back to the 1990s with a significant milestone in the development of computer-aided design (CAD) programs.  At the current state of the art, several sophisticated FE models have been developed to accurately capture the behavior of the structures.  The reinforcing bar can be simply represented by truss elements or alternatively modeled by solid elements.  The consideration of the deformation of the reinforcing bar is doable with the support from three-dimensional graphic programs.  For concrete material, it is typically modeled by 8-node brick elements, indeed several constitutive models have been successfully implemented in which the concrete damage plasticity model is a typical one.  The interaction between the reinforcing bar and concrete can be modeled by a perfect bond between the two materials or alternatively by a bond stress-slip model, which allows the reinforcing bar to slip in relative to the concrete during loading application.  The incorporation of a bond model is particularly

needed in the investigation of bond-related parameters (i.e., development length or lap length of reinforcing bar). This study, in fact, focused on the global behavior of the concrete bridge decks. This is the source of the simplifications in the reinforcement and the bond of the reinforcing bar and concrete to minimize the computational effort without compromising the accuracy of the results.

## 3.7 CONCLUSIONS AND RECOMMENDATIONS

In this paper, a nonlinear finite element analysis of concrete decks reinforced with Grade 420, Grade 690, and Grade 830 steel was investigated by ABAQUS software. Based on the analytical results and the validation with the experimental data, the following conclusions may be drawn:

1. In comparison to the experimental data, the analytical results show that the nonlinear behavior of concrete material and yielding of Grade 420 steel (with an apparent yielding plateau) and Grade 830 steel (without an apparent yielding plateau) can be suitably modeled by ABAQUS. The analytical load-deflection relationship, compressive strains of concrete, and tensile strains of reinforcement analyzed by the finite-element models are in a good agreement with the experimental data.

2. The analytical results indicate the replacement of Grade 420 steel by Grade 690 and Grade 830 steel increases the maximum deflection of concrete decks by 21% and 28%, respectively.

3. In comparison to the concrete decks reinforced with Grade 420 steel, the failure loads of decks reinforced by Grade 690 and Grade 830 steel are greater by 29% and 41%, respectively.

4. Minimal crack pattern of decks can be better visualized by finite element model than the experimental testing. In comparison to decks reinforced with Grade 420 steel, the maximum

76

crack width at the service loads is increased 58%-78% for decks reinforced with Grade 830 steel.

5.   The flexural resistance of concrete decks reinforced with one layer of Grade 830 steel is greater by 29% than that of decks reinforced with two layers of Grade 420 steel.


Based on the results, the following suggestions should be considered when A1035 steel is used for concrete bridge decks as main reinforcement:

1.  Direct replacement of Grade 420 steel with A1035 steel (Grade 690 or Grade 830) is a very conservative method.  The amount of steel can be reduced by 40% when replacing Grade 420 steel with A1035 (Grade 830) steel.

2.  The flexural strength of the concrete decks reinforced with A1035 steel is greater than that of decks reinforced with Grade 420 steel because of the increased tensile strength of A1035 steel.  As a result, the high stresses created in the concrete develop more cracks that are also wider.

3.  The failure load and maximum deflection of concrete decks reinforced with Grade 830 are 6.5% and 2.5% greater than that of decks reinforced with Grade 690, respectively.

4.  The crack width of decks reinforced with Grade 830 reduces by increasing concrete strength. The maximum crack width at service limit state can be reduced up to 41.4% when concrete strength increases from 30 MPa to 50 MPa


**ACKNOWLEDGMENTS**

University of Arkansas at Fayetteville, the Higher Committee for Education Development in Iraq

(HCED), and The Ton Duc Thang University is thankful.

# REFERENCES

[1] Seliem, H., Lucier, G., Rizkalla, S., Zia, P., "Behavior of Concrete Bridge Decks Reinforced with High-Performance Steel," ACI Structural Journal, V. 105, No. 1, 2008, pp. 78–86.

[2] Salomon, A.L., Moen, C.D., "Structural Design Guidelines for Concrete Bridge Decks Reinforced with Corrosion- Resistant Reinforcing Bars," Virginia Center for Transportation Innovation and Research, Charlottesville, Rep. No. FHWA/VCTIR 15-R10, VA, USA, 2014, pp. 1-51.

[3] Xia, J., Mackie, K.R., Saleem, M.A., Mirmiran, A., "Shear Failure Analysis on Ultra-High Performance Concrete Beams Reinforced with High Strength Steel," Engineering Structure Journal, V. 33, No. 12, 2011, pp. 3597–3609

[4] ASTM A1035/A1035M−14, "Standard Specification for Deformed and Plain, Low-Carbon, Chromium, Steel Bars for Concrete Reinforcement," ASTM International, West Conshohocken, PA, USA, 2014.

[5] Faza, S., Kwok, J., Salah, O., "Application of High-Strength and Corrosion-Resistant ASTM A1035 Steel Reinforcing Bar in Concrete High-Rise Construction," CTBUH 8th World Congress, Council on Tall Buildings and Urban Habitat, Chicago, Illinois, USA, 2008.

[6] Bowen, G.E., "Service and Ultimate Limit State Flexural Behavior of One-Way Concrete Slabs Reinforced with Corrosion-Resistant Reinforcing Bars," Thesis Master of Science in Civil Engineering, Virginia Polytechnic Institute and State University, VA, USA, 2013.

[7] Seliem, H.M.A., "Behavior of Concrete Bridges Reinforced with High-Performance Steel Reinforcing Bars," Doctor Dissertation of Philosophy in Civil Engineering, North Carolina State University, NC, USA, 2007.

[8] ACI Committee 439, "Guide for the Use of ASTM A1035/A1035M type CS Grade 100 (690) Steel Bars for Structural Concrete (ACI 439.6R-19)," American Concrete Institute, Farmington Hills, MI; 2019.

[9] Jian, L., "Based on ABQUS of Concrete Structure Nonlinear Finite Element Analysis," Advanced Materials Research, V. 756, 2013, pp. 186–189.

[10] Dawari, V.B., Vesmawala, G.R., "Application of Nonlinear Concrete Model for Finite Element Analysis of Reinforced Concrete Beams," International Journal of Scientific & Engineering Research, V. 5, No. 9, 2014, pp. 776-782.

[11] Oluwaseun, A.P., "Nonlinear Finite Element Analysis of Steel Fiber-Reinforced Concrete Beam Under Static Loading," Journal of Engineering Science and Technology, V. 11, No. 12, 2016, pp. 1669-1677.

[12] Mohamad, A.B.A.E., Chen, Z., "Experimental and Numerical Analysis of the Compressive and Shear Behavior for a New Type of Self-Insulating Concrete Masonry System," Applied Sciences, V. 6, No. 9, 2016, pp. 1–14.

[13] Musmar, M.A., Rjoub, M.I., Abdel Hadi, M.A., "Nonlinear Finite Element Analysis of Shallow Reinforced Concrete Beams Using Solid65 Element," ARPN Journal of Engineering and Applied Sciences, V. 9, No. 2, 2014, pp. 85–89.

[14] Azam, A., "Numerical Modelling of Reinforced Concrete Walls Encased in Polyviny Chloride Stay-in-Place Formwork," Thesis Master of Science in Civil Engineering, University of Waterloo, Ontario, Canada, 2015.

[15] Tyau, J.S., "Finite Element Modeling of Reinforcement Concrete Using 3-Dimentional Solid Elements with Discrete Rebar," Thesis Master of Science in Civil Engineering, University of Brigham Young, Utah, USA, 2009.

[16] Razaqpur, A.G., Nofal, M., "Analytical Modeling of Nonlinear Behavior of Composite Bridges," Journal of Structural Engineering, V. 116, No. 6, 1999, pp. 1715–1733.

[17] Helba, A., Kennedy, J.B." Skew Composite Bridges—Analyses for Ultimate Load," Canadian Journal of Civil Engineering, V. 22, No. 6, 1995, pp. 1092–1103.

[18] Lubliner, J., Oliver, J., Oller, S., Onate, E., "A Plastic-Damage Model for Concrete," International Journal of Solids and Structures, V. 25, No. 3, 1989, pp. 299–326.

[19] Thevendran, V., Chen, S., Shanmugam, N.E., Liew, J.R., "Nonlinear Analysis of Steel–Concrete Composite Beams Curved in Plan," Finite Elements in Analysis and Design, V. 32, No. 3, 1999, pp. 25–139.

[20] Hu, H.T., Lin, F.M., Jan, Y.Y., "Nonlinear Finite Element Analysis of Reinforced Concrete Beams Strengthened by Fiber-Reinforced Plastics," Composite Structures Journal, V. 63, No. 3, 2004, pp. 271–281.

[21] Metwally, I.M., "Three-Dimensional Nonlinear Finite Element Analysis of Concrete Deep Beam Reinforced with GFRP Bars," HBRC Journal, V. 13, No. 1, 217, pp. 25–38.

[22] Barth, K.E., Wu, H., "Efficient Nonlinear Finite Element Modeling of Slab on Steel Stringer Bridges," Finite Elements in Analysis and Design, V. 42, No. 14, 2006, pp. 1304–1313.

[23] Sinaei, H., Shariati, M., Abna, A.H., Aghaei, M., Shariati, A., "Evaluation of Reinforced Concrete Beam Behaviour Using Finite Element Analysis by ABAQUS," Scientific Research and Essays, V. 7, No. 21, 2002, pp. 2002–2009.

[24] Ahmed, A., "Modeling of a Reinforced Concrete Beam Subjected to Impact Vibration Using ABAQUS," International Journal of Civil and Structural Engineering, V. 4, No. 3, 2014, pp. 227–236.

[25] Sihua, D., Ze, Q., Li, W., "Nonlinear Analysis of Reinforced Concrete Beam Bending Failure Experimentation Based on ABAQUS," First International Conference on Information Sciences, Machinery, Materials and Energy, Atlantis Press, 2015, pp. 440–444.

[26] Kareem, R.S., Jones, C., Dang, C.N., Prinz, G., Hale, W.M., "Structural Performance of Concrete Bridge Decks Reinforced with Grade-830 Steel Bars," Structures Journal, V. 27, 2020, pp. 1396–1404.

[27] ASTM C39/C39M-20, "Standard Test Method for Compressive Strength of Cylindrical Concrete Specimens," ASTM International, West Conshohocken, PA, USA, 2020.

[28] ASTM C469/C469M-14, "Standard Test Method for Static Modulus of Elasticity and Poisson's Ratio of Concrete in Compression," ASTM International, West Conshohocken, PA, USA, 2014.

[29] American Association of State Highway and Transportation Officials, "AASHTO LRFD Bridge Design Specifications," Washington, DC: American Association of State Highway and Transportation Officials, 2017.

[30] Virginia Department of Transportation, "Manuals of the Structure and Bridge Division–Part 2–Design Aids–Typical Details," Richmond, 2019.

[31] Halahla A., "Identification of Crack in Reinforced Concrete Beam Subjected to Static Load Using Non-Linear Finite Element Analysis," Civil Engineering Journal, V. 5, No. 7, 2019, pp. 1631–1646.

[32] Dassault Systems Simulia Corp., "ABAQUS/CAE User's Manual 6.11," Providence, RI, USA, 2011.

[33] Beng T.P., "Finite Element Analysis of Reinforced Concrete and Steel Fiber Reinforced Concrete Slabs in Punching Shear," Master of Science in Civil Engineering, University of Newfoundland, Canada 2018.

[34] Abhaee S., "Investigation of Fiber-Reinforced Concrete Crack Width Measurement by Finite Element Method," Doctor Dissertation of Philosophy in Civil Engineering, University of Louisiana, USA 2006.

[35] Lu ZH., Zhao YG., "Empirical Stress-Strain Model for Unconfined High-Strength Concrete under Uniaxial Compression," Journal of Materials in Civil Engineering, V. 22, No. 11, 2010, pp. 1181–1186.

[36] Hsu TTC., Mo YL., "Unified Theory of Concrete Structures," John Wiley & Sons Inc, 2010.

[37] Zhao G., Xu J., Li Y., Zhang M., "Numerical Analysis of the Degradation Characteristics of Bearing Capacity of a Corroded Reinforced Concrete Beam," Journal of Advanced in Civil Engineering, V. 2018, No. 11, 2018, pp. 1–10.

[38] Yosefani, A., "Flexural Strength, Ductility, and Serviceability of Beams that Contain High-Strength Steel Reinforcement and High-Grade Concrete," Doctor Dissertation of Philosophy in Civil Engineering, Portland State University, Oregon, 2018.

[39] Shahrooz, B.M., Miller, R.A., Harries, K.A., Russell, H.G., "Design of Concrete Structures Using High-Strength Steel Reinforcement," Rep. No. 679, Transportation Research Board, National Research Council, Washington, D.C, 2011, pp. 1–72.

[40] Genikomsou, A., "Nonlinear Finite Element Analysis of Punching Shear of Reinforced Concrete Slab-Column Connections," Doctor Dissertation of Philosophy in Civil Engineering, University of Waterloo, Canada, 2015.

[41] Frosch R.J., "Another Look at Cracking and Crack Control in Reinforced Concrete," ACI Struct. Journal, V. 96, 1999, pp. 437–442.

## APPENDIX 3A

The The development length ($L_d$) was estimated by ACI 439.6R-19 as shown in **Eq. (3A-1)**, with supplementary equations shown in **Eq. (3A-2)** to **Eq. (3A-9)**. The parameters $\alpha$, $\beta_c$, $\lambda$, $\phi$, $R_p$ were considered as 1.3, 1.0, 1.0, 0.8, and 0.07, respectively.

$$L_d = \frac{\left(\dfrac{f_y}{(f_c')^{1/4}} - \phi 57.4\omega\right)\alpha\beta_c\lambda}{\phi 1.83\left(\dfrac{c_b\omega + K_{tr}}{d_p}\right)} d_p$$

**Eq. (3A-1)**

$$K_{tr} = (6.2 t_r t_d A_{tr} / sn)\sqrt{f_c'}$$

**Eq. (3A-2)**

$$t_r = 9.6 R_p + 0.28 \le 1.72$$

**Eq. (3A-3)**

$$t_d = 0.03 d_p + 0.22$$

**Eq. (3A-4)**

$$c_s = \min(c_{so}, c_{si} + 0.25)$$

**Eq. (3A-5)**

$$c_{min} = \min(c_s, c_{so})$$

**Eq. (3A-6)**

$$c_{max} = \max(c_s, c_{so})$$

**Eq. (3A-7)**

$$c = c_{min} + 0.5 d_p$$

**Eq. (3A-8)**

$$\omega = 0.1\left(\frac{c_{max}}{c_{min}}\right) + 0.9 \le 1.25$$

**Eq. (3A-9)**

where: $d_p$ is bar diameter; $A_{tr}$ is total cross-sectional area of all transverse reinforcement; $c_{si}$ is one-half of average clear spacing between bars; $c_{so}$ is clear cover of reinforcement being developed; $s$ is spacing of transverse reinforcement; n is number of bars being developed.

## APPENDIX 3B

The concrete crack width can be analytically calculated.  Frosch equation (**Eq. (3B-1)**)) is used to calculate the maximum crack width [39].

$$w_c = (2 + 0.006d_c)\frac{f_s}{E_s}\sqrt{d^2_c + \left(\frac{s}{2}\right)^2}$$                    **Eq. (3B-1)**

where: $w_c$ is concrete crack width; $d_c$ is the concrete bottom cover; $s$ is and the reinforcing bar spacing.

# CHAPTER 4:  FLEXURAL BEHAVIOR OF CONCRETE BEAMS CAST WITH HIGH-PERFORMANCE MATERIALS

Rahman S. Kareem[1], Canh N. Dang[2,3*], W. Micah Hale[1]

[1] University of Arkansas, Department of Civil Engineering, 4190 Bell Engineering Center

Fayetteville, AR 72701, USA

[2] Department for Management of Science and Technology Development, Ton Duc Thang

University, Ho Chi Minh City, Vietnam

[3] Faculty of Civil Engineering, Ton Duc Thang University, Ho Chi Minh City, Vietnam

* Corresponding author:

Emails: canhdang@tdt.edu.vn; Phone +1-479-575-6348

**ABSTRACT**

The use of ultra-high strength concrete (UHSC) is advantageous in construction.  In fact, a

combination of UHSC with regular reinforcement steel still has problems with corrosion after

years in service, typically in exposed structures.  This effect is more profound by climate

changes (i.e., extensive heat waves or unexpected long and cold winter).  This research

investigates the flexural performance of concrete beams, cast with UHSC and high-performance

reinforcement (HPR) steel; which is characterized by its high-strength and high-corrosion

resistance.  The testing matrix consisted of 8 concrete beams, cast with UHSC and high-strength

concrete (HSC), in combination with ASTM A1035 Grade 830 steel and ASTM A615 Grade 420

steel.  For each flexural test, along with measuring the applied loading and deflection, the

variation in concrete compressive strain and steel tensile strain were monitored through a number

of strain gauges.  Experimental results revealed that Grade 830 can enhance the flexural capacity

by 33% as compared to Grade 420 steel.  On the other hand, UHSC can enhance the flexural capacity by 11% and decrease the concrete strains by up to 26% as compared to HSC.

**KEYWORDS:** ultra-high strength concrete; high-performance reinforcement; flexural resistance; crack width; moment deflection curve;

## 4.1 INTRODUCTION

Over the past few years, the use of high-strength concrete (HSC) has been growing due to its efficiency in improving the structural behavior of concrete structures [1,2].  HSC is a practical solution to enhance the sustainability and performance of reinforced concrete structures [3,4].  Another type of concrete that has much potential to change the concrete industry is ultra-high strength concrete (UHSC).  UHSC typically consists of portland cement, fine quartz sand, silica fume, steel fibers and high range water reducing admixture [3], and a low water/binder ratio [5].  The addition of steel fibers aims at enhancing the concrete ductility.  To improve the concrete homogeneity, UHSC typically does not contain coarse aggregates [6].  The advanced concrete properties, such as high compressive strength, improved durability, and enhanced ductility have widened UHSC applications in high-rise building construction and long-span bridge girders [2,3].

UHSC can be developed by using local available materials.  A number of studies have been conducted to develop UHSC mixture proportions by using locally available materials [7,8,9].  In 2010, Allena and Newtson developed UHSC by using the local sand, locally available Type I/II cement, and silica fume [7].  The compressive strength and flexural strength at 28 days of age were 160 MPa and 10.9 MPa, respectively.  Likewise, Meleka et al. developed UHSC mixtures

86

by using cement, silica fume, and superplasticizer [8]. The compressive strength and flexural

strength of their mixtures at 28 days of age were 152 MPa and 14.4 MPa, respectively.

The composition of UHSC affects its mechanical and durability properties. The use of steel

fibers in UHSC improves the compressive strength and flexural strength up to 6% and 67%,

respectively [7]. Meleka et al. also concluded that increasing cement and silica fume contents as

well as adding steel fibers improves the concrete properties [8]. The authors recommended the

maximum amount of silica fume, as a replacement of cement content, of 30%. Allena and

Newtson concluded that the early-age and long-term shrinkage values for UHSC mixtures

reinforced by fiber were lower than those of plain UHSC [7]. In addition, Fang investigated the

influence of constituent materials on the compressive strength of UHSC [10]. Two types of

limestone powder were used in their mixtures; one was used as a replacement material for

cement, and the other was used as supplemental material in place of quartz powder. The

compressive strength was improved by the high intrinsic strength of the fillers and reactive

particles.

UHSC has been used in flexural members. In 2014, Kamal et al. evaluated the behavior of

concrete beams cast with UHSC and reinforced by Grade 420 steel [11]. Twelve concrete beams

were tested in flexure with and without shear reinforcement. Two types of fibers were used in

this research including steel and polypropylene fibers. The behavior of the tested beams was

investigated during different stages of loading, initial cracking, cracking pattern, and ultimate

load. The researchers showed that the 28-day compressive strength of concrete including

polypropylene and steel fibers increased by 2.5% and 6% in comparison to the counterpart

mixtures without fibers. It was concluded that concrete beams cast with UHSC containing steel

fibers have higher flexural resistance and smaller crack widths.

The technology of steel reinforcement has also advanced, which has led to the development of high-performance reinforcement (HPR). Generally, the service life of reinforced concrete structures is influenced by the severe effects of environments and freezing-thawing cycles [12,13]. In comparison to typical ASTM A615 Grade 420 steel, HPR steel is less susceptible to corrosion and has a greater yield strength [14]. The nominal yield strength of HPR steel is up to twice, and the corrosion resistance is 5 to 6 times greater of that of Grad 420 steel [15,16]. The use of HPR steel in concrete structures can reduce the reinforcement ratio, reduce labor cost, and extend the service life of concrete structures [17]. A wide variety of HPR steel options are available, such as ASTM A1035, ASTM A955, and Epoxy-Coated reinforcing bars. In comparison to ASTM A955 and Epoxy-Coated bars, the treatment and manufacturing requirements for ASTM A1035 bars are simpler [18,19]. However, ACI 439.6R-19 states that additional research is needed before ASTM A1035 Grade 830 steel can be fully utilized [20]. The stress-strain behavior of Grade 830 steel is different in comparison to Grade 420. Several researchers have shown the shear strength, flexural strength, and failure modes of concrete beams reinforced by Grade 830 steel are affected by the steel properties, and more research is needed to increase engineers' confidence in using this reinforcement [14,16,21,22].

The behavior of concrete structures reinforced by Grade 420 is improved by using UHSC. However, the corrosion problem of reinforcement steel is a challenge to overcome in concrete construction. The corrosion of reinforcement steel causes the deterioration of the concrete and affects the service and ultimate limit states of concrete structures [15,16]. On the other hand, several studies have investigated the use of Grade 830 with normal concrete strength [16,19,21]. However, the use of Grade 830 steel in flexural members of concrete structures has not yet widespread [3,20]. There is a concern when using Grade 830 steel in concrete structure due to

the higher stresses developed during the service limit state.  This high stress creates greater

tensile strains which affect crack widths and may also lead to compression failure prior to steel

yielding [3,23].

Grade 830 steel is characterized by greater corrosion resistance and yield strength in comparison

to Grade 420 steel [14-16,24].  The high corrosion resistance and strength of Grade 830 can

increase the service life and reduce the amount of reinforcement in concrete structures [17,25].

Several studies have investigated the improvement of concrete decks by using Grade 830 steel

[9,25].  Seliem tested three full-scale bridge decks reinforced with Grade 420 and Grade 830

steel [25].  It was concluded that direct replacement of Grade 420 steel with Grade 830 steel in

bridge decks is conservative.  The author also showed that the replacement of Grade 420 steel by

Grade 830 steel can be reduced by 33%.  Another research using different types of Grade 830

steel in concrete bridge deck was completed by Salomon and Moen [9].  The authors tested 36

concrete decks reinforced with different types of HPR steel, such as Grade 420 (uncoated),

epoxy-coated reinforcing Grade 420, and Grade 830.  The authors concluded that the crack

widths of concrete bridge decks reinforced by Grade 830 comply with AASHTO requirements

when the amount of steel is reduced by 36%.

The structural performance of concrete beams is enhanced by using Grade 830 steel.  Concrete

beams reinforced with Grade 830 steel resist greater flexural moments than beams reinforced by

Grade 420.  Yotakhong [26] tested four large-scale concrete beams reinforced with different

types of reinforcing steel.  One of the beams was reinforced with Grade 420, and the other three

beams were reinforced with Grade 830 steel.  The concrete beams were tested until failure to

examine the behavior during the pre-cracking, cracking, post-cracking, ultimate capacities, and

failure mode.  The author concluded that concrete beams reinforced with Grade 830 steel had

greater flexural strength and a comparable amount of ductility in comparison to control beams

reinforced with Grade 420. Likewise, Li [4] studied the dynamic and static behavior of concrete

beams reinforced with Grade 830 steel and Grade 420 steel. The dynamic and static

performance of eleven beams were investigated. In the dynamic test, the beams were tested

under simulated blast loads. In the static test, the beams were tested by four-point bending loads.

The author showed that beams reinforced with Grade 830 steel are able to resist greater blast

loads than beams reinforced by Grade 420 steel in dynamic test. During the static test, the beams

reinforced with Grade 830 steel resisted a greater peak load carrying capacity when compared to

beams reinforced with the same ratio of Grade 420 steel. However, the authors used a direct

replacement of Grade 420 with Grade 830 for the tested flexural members. The direct

replacement may cause a compression failure before the steel yields due to the high strength of

Grade 830 steel [9,17,25].

In summary, the structural performance of concrete structures can be improved by using UHSC

in combination with Grade 830 steel. UHSC has been used in most studies in combination with

Grade 420 steel. In addition to the ultra-high compressive strength, the matrix microstructure of

UHSC is characterized by low porosity. However, the concrete structure may still have

durability problems due to steel corrosion after years in service. Although UHSC has the

enhanced durability characteristics, the corrosion performance of steel bars embedded in UHSC

has still been controversial. Pyo et. al. indicated that there is no significant deterioration of

specimen, cast with ultra-high performance concrete including steel fibers and immersed in

chloride solution up to 180 days [27]. However, the randomly distribution of steel fibers having

galvanized coatings may contact the steel bars, and this process may develop galvanic corrosion

[28,29]. When two different metals contact each other in an electrolyte, one metal acts as anode

and corrodes quickly while the other metal acts as cathode and corrodes slowly [29]. Moreover, the corrosion performance of steel bars embedded in UHSC has been seldom studied [28,29]. On the other hand, several researchers have studied the improved structural behavior of concrete flexural members with Grade 830 steel. However, the flexural members reinforced by Grade 830 steel are more susceptible to compression failures before the tension steel yields due to the higher tensile strength of Grade 830 steel [9,17,25,26]. This research program aims at providing a thorough understanding about the structural behavior of flexural concrete members cast with UHSC and reinforced by Grade 830 steel.

## 4.2    RESEARCH SIGNIFICANCE

The use of high-strength concrete, in combination with high-performance reinforcement (high tensile strength and high corrosion resistance) can improve the capacity, ductility, durability, and corrosion resistance of concrete structures. Through a comprehensive test matrix, this research provides an understanding about the structural behavior of concrete beams cast with high-strength concrete and high-performance reinforcement. The concrete beams were cast with either Grade 830 or Grade 420 steel and with concrete with a wide range of compressive strengths. Three concrete mixtures included HSC1 ($f'_c$ = 75 MPa at 28 days of age), HSC2 ($f'_c$ = 107 MPa at 28 days of age), and UHSC ($f'_c$ = 145 MPa at 28 days of age). The concrete compression strain and steel tensile strain were monitored throughout the test. The deflection and maximum crack widths were measured during testing. Experimental observations are discussed in the following sections.

## 4.3 EXPERIMENTAL INVESTIGATION

### 4.3.1 Concrete properties

In addition to Type I portland cement, fly ash (Class C) and silica fume were also used to develop high-strength concrete mixtures. A series of trial batches were cast to determine the optimum mix design for the mixtures. The variables that were adjusted between batches included cement content, supplementary cementitious materials content, total water content, water/binder ratio, maximum aggregate size (MAS), and aggregate content. For all mixtures in this study, the binder consists of cement, fly ash, and silica fume. A low water/binder ratio was used to reduce the porosity and increase concrete strength. Therefore, a high range water reducer (HRWR) was added to provide the sufficient workability of the fresh concrete.

Crushed limestone, coarse aggregate having a MAS of 19 mm and smaller coarse aggregate (crushed limestone) having a MAS of 9.5 mm were used to develop the concrete mixtures. In the concrete matrix, the weakest link for both strength and permeability is the interfacial transitions zone between binder paste and aggregates [30]. In addition to developing micro cracks, interfacial transition zone is more permeable than the cement paste and aggregate particles. The elimination of coarse aggregate in high strength concrete mixtures can reduce the interfacial transitions zone, but the concrete shrinkage increases [30,31]. Therefore, the mixtures can be developed with coarse aggregate, but the MAS is minimized to reduce the area of interfacial transition zone.

**Table 4-1** shows the proportions of the eleven trial mixtures. The supplementary cementitious materials content, fly ash and silica fume, ranged from 10% to 35% of the total binder content. The water/binder ranged from 0.17 to 0.43. HRWR was used for all mixtures but at different dosages. The MAS was 19 mm for Mix.1 and Mix.2, and the percentages of coarse

aggregate/fine aggregate were 56% and 68%, respectively. For all other mixtures, the MAS was

9.5 mm, and the percentages of coarse aggregate/fine aggregate ranged from 44% to 84%. The

size distribution of fine and coarse aggregate is shown in **Appendix 4A**.

**Table 4-1 – Concrete mixture proportions.**

| Materials | Quantity per cubic meter | | | | | | | | | | |
|---|---|---|---|---|---|---|---|---|---|---|---|
| | Mix.1 | Mix.2 | Mix.3 | Mix.4 | Mix.5 | Mix.6 | Mix.7 | Mix.8 | Mix.9 | Mix.10 | Mix.11 |
| Binder (kg) | 356 | 475 | 771 | 801 | 949 | 949 | 1039 | 1127 | 1188 | 1305 | 1306 |
| Cement (%) | 80 | 80 | 70 | 70 | 65 | 70 | 80 | 80 | 90 | 90 | 80 |
| Fly ash (%) | 20 | 20 | 30 | 30 | 30 | 30 | 15 | 15 | 5 | 5 | 10 |
| Silica fume (%) | 0 | 0 | 0 | 0 | 5 | 0 | 5 | 5 | 5 | 5 | 10 |
| Coarse aggregate (kg) | 664 | 686 | 667 | 575 | 564 | 548 | 393 | 347 | 323 | 266 | 240 |
| MAS (mm) | 19 | 19 | 9.5 | 9.5 | 9.5 | 9.5 | 9.5 | 9.5 | 9.5 | 9.5 | 9.5 |
| Fine aggregate (kg) | 1212 | 1010 | 801 | 848 | 675 | 657 | 716 | 693 | 740 | 608 | 551 |
| Water/Binder ratio | 0.43 | 0.37 | 0.20 | 0.20 | 0.18 | 0.20 | 0.20 | 0.20 | 0.17 | 0.17 | 0.18 |
| Water (kg) | 153 | 176 | 154 | 160 | 171 | 190 | 208 | 225 | 202 | 227 | 235 |
| HRWR (kg) | 1.8 | 1.5 | 15.5 | 15.5 | 21.8 | 16.8 | 27.8 | 33.6 | 46.8 | 47.5 | 45.0 |
| $f_c'$ (MPa) | 59 | 75 | 107 | 109 | 117 | 119 | 123 | 128 | 145 | 137 | 132 |
| $E_c$ (GPa) | 33.7 | 38.8 | 42.8 | 43.5 | 45.1 | 44.2 | 45.5 | 46.3 | 47.6 | 46.5 | 45.7 |
| Slump flow (mm) | 595 | 610 | 635 | 630 | 670 | 630 | 650 | 670 | 625 | 710 | 625 |
| J-Ring flow (mm) | 580 | 625 | 645 | 640 | 650 | 635 | 635 | 650 | 635 | 695 | 645 |
| $T_{50}$ (sec) | 2.5 | 2.5 | 3.0 | 3.0 | 2.5 | 3.5 | 4.0 | 4.5 | 4.5 | 4.5 | 4.0 |
| Selected concrete mixtures | | HSC1 | HSC2 | | | | | | UHSC | | |

Three tests (Slump flow, J-Ring flow, and $T_{50}$) were used to measure the consistency and

flowability of the mixtures. For self-consolidating concrete, the following values are

recommended. For slump flow, a spread of 500-800 mm is recommended [32]. The difference

between slump flow and J-ring should be less than 25 mm, and the $T_{50}$ is less than 5 seconds

[32]. The results of the three tests for all mixtures met these criteria.

Concrete cylinders (100x200 mm) were cast to evaluate compressive strength at 28 days of age. The compressive strengths ($f'_c$) of the mixtures showed in **Table 4-1** are the average of 3 cylinders. The compressive strengths ranged from 59 MPa to 145 MPa. The concrete mixtures are classified as HSC and UHSC when the compressive strength is greater than 55 MPa and 120 MPa, respectively [33,34]. Therefore, Mixtures 1 through 6 and Mixtures 7 through 11 are considered HSC and UHSC, respectively. ASTM C469 [35] was used to determine the modulus of elasticity ($E_c$) for all mixtures. The modulus of elasticity was in a range from 33.7 GPa to 47.6 GPa.

Three concrete mixtures were selected from **Table 4-1** to cast the beams in this research. The selected mixtures were Mix.2, Mix.3, and Mix.9. Mix.2 and Mix.9. were selected because these mixtures had the highest compressive strengths for MAS 19 mm and MAS 9.5 mm, respectively. Mix.3 was selected because its compressive strength was approximately the average compressive strength of the combination of Mix.2 and Mix.9. Mix.2, Mix.3, and Mix.9 are designated in this research as HSC1, HSC2, UHSC, respectively.

### 4.3.2 Beam Fabrication

Eight concrete beams were cast. The cross-sections of beams were 150 mm by 300 mm, and the length was 4.0 m. The concrete cover was 25 mm on all sides. The reinforcement detail is shown in **Figure 4-1**. Two types of steel, Grade 420 and Grade 830, were used to reinforce the beams. Two different reinforcement diameters were used. Top reinforcement was No. 10 bars, Grade 420. Bottom reinforcement was No. 19 bars, either Grade 420 or Grade 830 steel. To ensure the beams achieved the nominal flexural capacity before a shear failure, stirrups No. 10,

Grade 420 bars were provided at a spacing of 100 mm as shear reinforcement along the span of the beams.
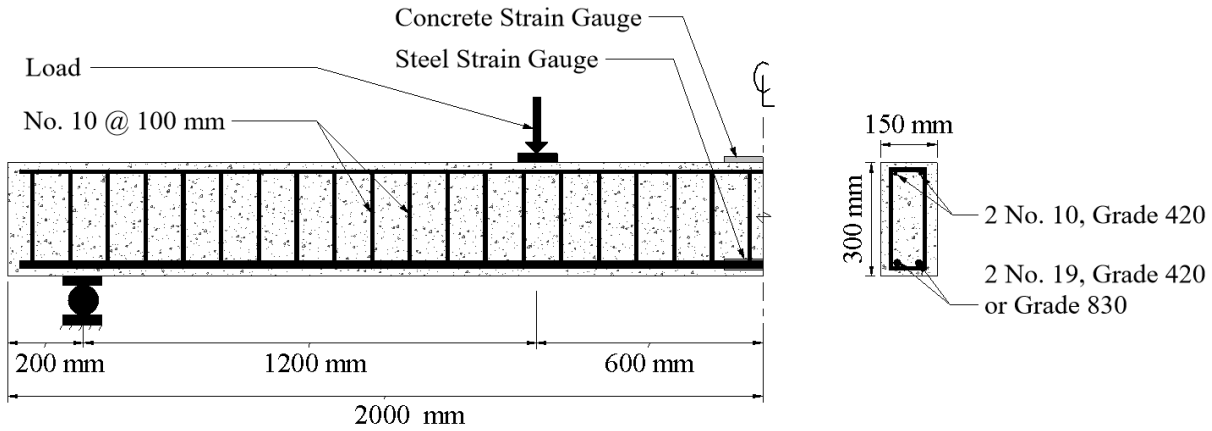


**Figure 4-1. Beam dimension and reinforcement detail.**

**Table 4-2** shows the test matrix for the concrete beams. Two beams were tested for each group to confirm the results. CH1-S420 beams were considered as control beams in this research. CH1-S420 beams were cast with HSC1 and reinforced with Grade 420 steel. CH1-S420 beams were tested to investigate the behavior of concrete beams reinforced with Grade 420 steel and cast with high-strength concrete. CH1-S830 beams were also cast by HSC1, but the beams were reinforced with Grade 830 steel. CH1-S830 were tested to investigate the effect of using Grade 830 steel. The CH2-S830 beams were also reinforced by Grade 830, but the beams were cast with higher strength of concrete (HSC2) in comparison to CH1-S830. Lastly, CUH-S830 beams were developed and tested to investigate the effect of using UHSC on the behavior of beams reinforced with Grade 830.

95

**Table 4-2** – **Testing matrix of concrete beams.**

| Beam ID | Number of beams | Concrete type | Tension reinforcement |
|---------|-----------------|---------------|-----------------------|
| CH1-S420 | 2 | HSC1 | 2 No.19, Grade 420 |
| CH1-S830 | 2 | HSC1 | 2 No.19, Grade 830 |
| CH2-S830 | 2 | HSC2 | 2 No.19, Grade 830 |
| CUH-S830 | 2 | UHSC | 2 No.19, Grade 830 |

The tensile strain of the tension steel and compressive strain of concrete were monitored during testing. A strain gauge was attached to the reinforcing steel, at the level of the bottom reinforcement, prior to casting the concrete. Two additional strain gauges were attached to the top surface of the beam to evaluate concrete compressive strain. The strain gauges were connected to data acquisition systems to monitor the results. A crack width microscope was used to measure the crack width and to count the number of cracks during the flexural test.

### 4.3.3 Test Setup

The flexural capacity of the beams was evaluated by using a four-point bending test. **Figure 4-2** shows the test system. The concrete beams were simply-supported in the test. The supports were seated under the specimen at a distance of 200 mm from the ends of the beam. The load was applied to the beam in multiple steps until failure. The loads were applied by using a 445 kN hydraulic actuator. The deflection was measured at midspan by using a linear cable encoder.
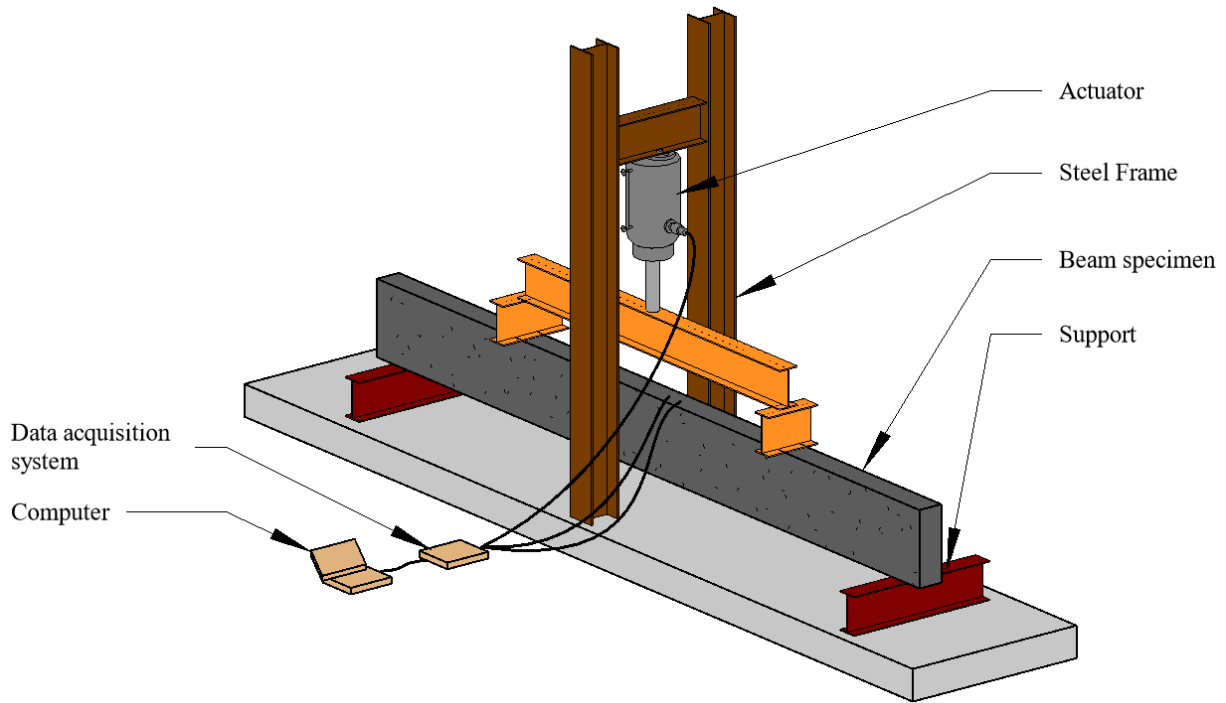
**Figure 4-2. Flexural test setup**.

## 4.4 ANALYTICAL INVESTIGATION

A computer program was developed using MATLAB to predict moment-curvature and moment-deflection curves. The moment-curvature relationship was determined based on strain compatibility and section equilibrium approach [36]. The section was assumed to be plane after loading, and the strain is uniform over section width. In addition, the reinforcement steel was fully bonded with concrete. The nonlinearity in stress-strain relationship of high-strength concrete and the yielding of the reinforcement was captured through multi-step calculations. The concrete strain ($\varepsilon_c$) was incrementally increased until reinforcement steel or concrete achieved the ultimate strain, $\varepsilon_{su}$ or $\varepsilon_{cu}$, respectively. The neutral axis depth ($c$) was determined by the applied section equilibrium for steel tension force ($T$), concrete compression force ($C_c$), and steel

compression force ($C_s$), as shown in **Figure 4-3**.  For each step, the curvature is determined as

$\theta = \varepsilon_c \big/ c$ , and the moment capacity ($M_n$) is calculated by **Eq. (4-1)**.

$$M_n = f_s \times A_s \times (d-c) + \int_0^{\varepsilon_c} f_c \times b \times x \times dx + f_s' \times A_s' \times (d'-c) \qquad \textbf{Eq. (4-1)}$$

where $x = \dfrac{\varepsilon_{cx}}{\varepsilon_c} \times c$
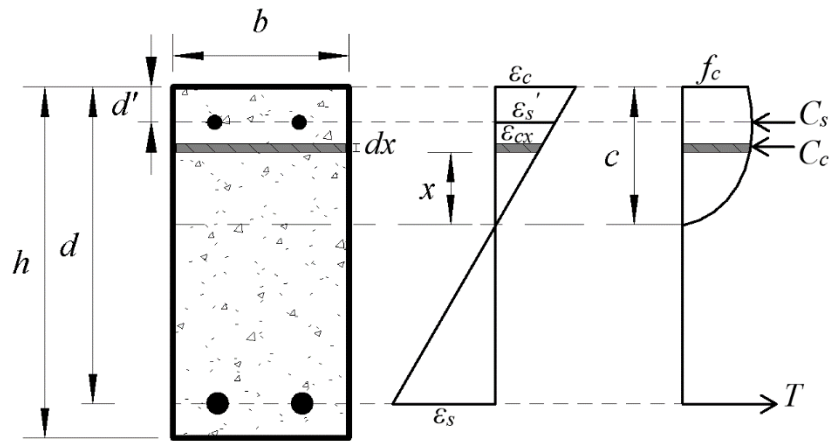


**Figure 4-3. Details of cross section.**

The steel forces for tension ($T$) and compression ($C_c$) were determined by multiplying steel

stress ($f_s$ for $T$ and $f_s'$ for $C_c$) to steel area ($A_s$ for $T$ and $A_s'$ for $C_c$).  The steel stress ($f_s$ and

$f_s'$) is calculated from the steel strain ($\varepsilon_s$ and $\varepsilon_s'$), derived from the strain compatibility method

as aforementioned, using **Eq. (4-2)** for Grade 420 and by **Eq. (4-3)** for Grade 830 [31,32].  The

steel stress-strain curves are graphically shown in **Figure 4-4**.  It should be noted that the Grade

830 steel yields gradually without an explicit yielding plateau like Grade 420 steel.  Therefore, a

multi-step calculation is needed to track the steel yielding status versus the beam deflection

during the flexural tests.

$$f_s = \begin{cases} 200000 \times \varepsilon_s & 0 \leq \varepsilon_s \leq 0.002 \\ f_y & 0.002 < \varepsilon_s \leq 0.0055 \\ f_y + (620 - f_y) \times \sqrt{\dfrac{\varepsilon_s - 0.0055}{0.0455}} & 0.0055 < \varepsilon_s \leq 0.05 \end{cases}$$  **Eq. (4-2)**

$$f_s = 200000 \times \varepsilon_s \times \left(0.0167 + \frac{0.98}{\left[1 + (191 \times \varepsilon_s)^{2.5}\right]^{0.4}}\right)$$  **Eq. (4-3)**
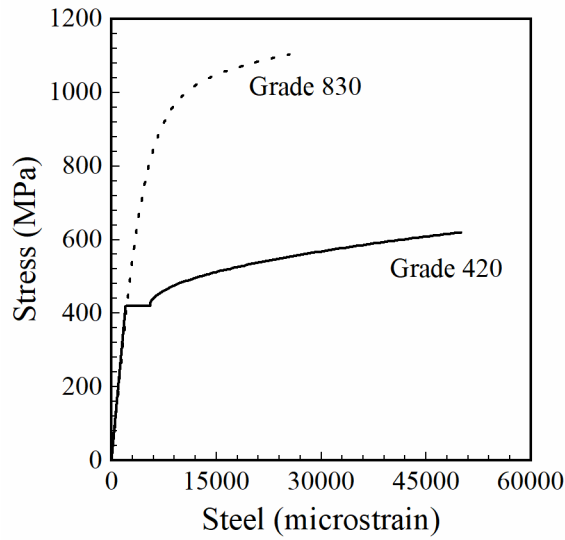


**Figure 4-4. Stress-strain relationships for Grade 420 and Grade 830 steel.**

The Lu and Zhao model captured the nonlinearity in stress-strain relationship of high-strength concrete [38]. The concrete compression force ($C_c$) was determined based on integrating the concrete stress ($f_c$), as shown in **Eq. (4-4)**. The concrete stress ($f_c$) at each step is calculated by **Eq. (4-5)**, with supplementary equations shown in **Eq. (4-6)** to **Eq. (4-9)** [38]. The model was used to generate stress-strain curve for different concrete strengths. **Figure 4-5** shows the stress-strain relationships for HSC1, HSC2, and UHSC. It is noted that steepness of the

99

ascending and descending increases with concrete strength.  This increment in steepness shows

that the brittleness intensifies with higher concrete strength.

$$C_c = \int f_c \times b \times dx \qquad\qquad \text{Eq. (4-4)}$$

$$f_c = \begin{cases} f_c' \times \left\{ \dfrac{\left(\dfrac{E_{it}}{E_0}\right) \times \left(\dfrac{\varepsilon_c}{\varepsilon_0}\right) - \left(\dfrac{\varepsilon_c}{\varepsilon_0}\right)^2}{1 + \left(\dfrac{E_{it}}{E_0} - 2\right) \times \left(\dfrac{\varepsilon_c}{\varepsilon_0}\right)} \right\} & 0 \le \varepsilon_c \le \varepsilon_L \\[4em] f_c' \times \left\{ \dfrac{1}{1 + 0.25 \times \left(\dfrac{\varepsilon_c}{\varepsilon_0} - \dfrac{\varepsilon_c}{\varepsilon_L} - 1\right)^{1.5}} \right\} & \varepsilon_c > \varepsilon_L \end{cases} \qquad\qquad \text{Eq. (4-5)}$$

$$\varepsilon_L = \varepsilon_0 \times \left[ \left( 0.1\dfrac{E_{it}}{E_0} + \dfrac{4}{5} \right) + \sqrt{\left( 0.1\dfrac{E_{it}}{E_0} + \dfrac{4}{5} \right)^2 - \dfrac{4}{5}} \right] \qquad\qquad \text{Eq. (4-6)}$$

$$E_{it} = 19350 \times \left( \dfrac{f_c'}{10} \right)^{1/3} \qquad\qquad \text{Eq. (4-7)}$$

$$E_0 = \dfrac{f_c'}{\varepsilon_0} \qquad\qquad \text{Eq. (4-8)}$$

$$\varepsilon_0 = 700 \times \left( f_c' \right)^{0.31} \times 10^{-6} \qquad\qquad \text{Eq. (4-9)}$$
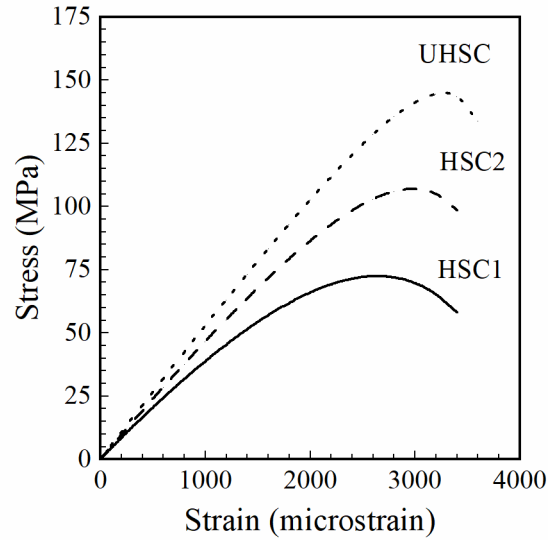
**Figure 4-5. Stress-strain relationships for HSC1, HSC2, and UHSC.**

For each step, the deflection is calculated by the numerical integration of the curvature ($\theta$) distribution up to the positions of interest (at the mid-span in this study), as shown in **Eq. (4-10)** [39].

$$\Delta = \sum \left( \frac{\theta_i x_i + \theta_{i+1} x_{i+1}}{2} \right) \Delta x_i \qquad \text{Eq. (4-10)}$$

where $\Delta$ is the mid-span deflection; $\theta_i$ and $\theta_{i+1}$ are the curvatures corresponding to distances $x_i$ and $x_{i+1}$ from the support; $\Delta x_i = x_i - x_{i+1}$.

## 4.5    RESULTS AND DISCUSSION

### 4.5.1   Flexural Capacity

**Figure 4-6** shows the moments at failure for the concrete beams at mid-span.  The average failure moment was 87 kNm for the CH1-S420 beams and 116 kNm for the CH1-S830 beams.

With the same concrete strength, the use of Grade 830 steel increased the flexural capacity by

33% as compared to Garde 420 steel. The average moment at failure for the CH2-S830 and

CUH-S830 beams were higher than that of CH1-S830 by 5% and 11%, respectively. An

increase of 48% was observed when comparing the moments at failure for CUH-S830 and CH1-

S420. The concrete beams CUH-S830, cast with UHSC in combination with Grade 830 steel,

could resist 48% additional load when compared to the control beams CH-S420. Regarding

structural applications, the use of these materials is advantageous at the areas where heavier

loads are required but have a restriction in terms of member sizes.
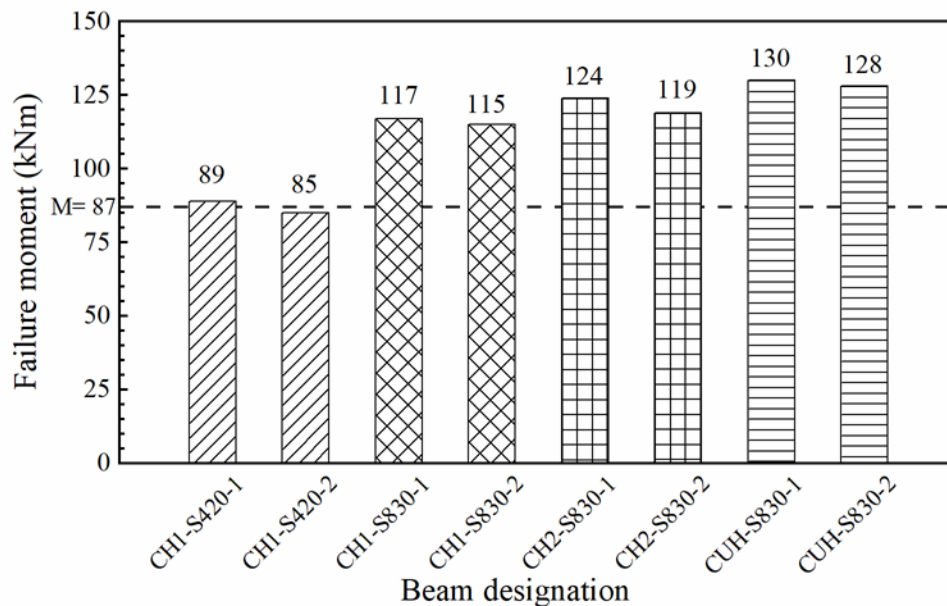


**Figure 4-6. Failure moments.**

### 4.5.2   Moment-Deflection Curve

4.5.2.1 Experimental results

Deflection is one of the design criteria at the service limit state (SLS). Deflection is a function of

steel strain at SLS [15,25]. The steel stress at the SLS was assumed to be 60% of the yield

strength ($0.6 f_y$) [15]. Accordingly, the SLS moments of CH1-S420 and CH1-S830 are 31 kNm

($M_{SLS.Grade420}$) and 62 kNm ($M_{SLS.Grade830}$), respectively. As shown in **Figure 4-7 (A)**, the

experimental relationship of the deflection and applied moments at the mid-span of CH1-S420

and CH1-S830 beams exhibited a similar trend (in the region up to the beams reach SLS

moments). The SLS deflection of CH1-S830 was approximately twice that of CH1-S420, 7 mm

($L$/515) vs. 15 mm ($L$/240); where $L$ is the support-to-support span of the beams. The SLS

moment of CH1-S830, in fact, is also as twice that of the SLS moment of CH1-S420 (62 kNm

vs. 31 kNm). The deflection at failure, on the other hand, provides a warning when the concrete

member is about to fail. This deflection was 65 mm ($L$/55) for CH1-S420 and 71 mm ($L$/50) for

CH1-S830.

**Figure 4-7 (B)** shows the experimental relationship of the deflection at mid-span and applied

moments of CH1-S830, CH2-S830 and CUH-S830 beam groups. For each group, the data

represent the average results of two beams. The deflection at each load step is the average

deflection values of two tested beams at each corresponding load step. The figure indicates that

the moments at failure were marginally different between the beam groups, but the deflections at

failure were almost identical. At failure, the concrete beams experience a significant level of

cracking. At SLS, the concrete beams partially crack, and therefore, the concrete strength is an

important factor affecting the beam stiffness (*EI*) and therefore beam deflections. As compared

to CH1-S830 beams, the deflection of CH2-S830 and CUH-S830 beams decreased by 13% and

27% at SLS, respectively.

**(A)**                         **(B)**
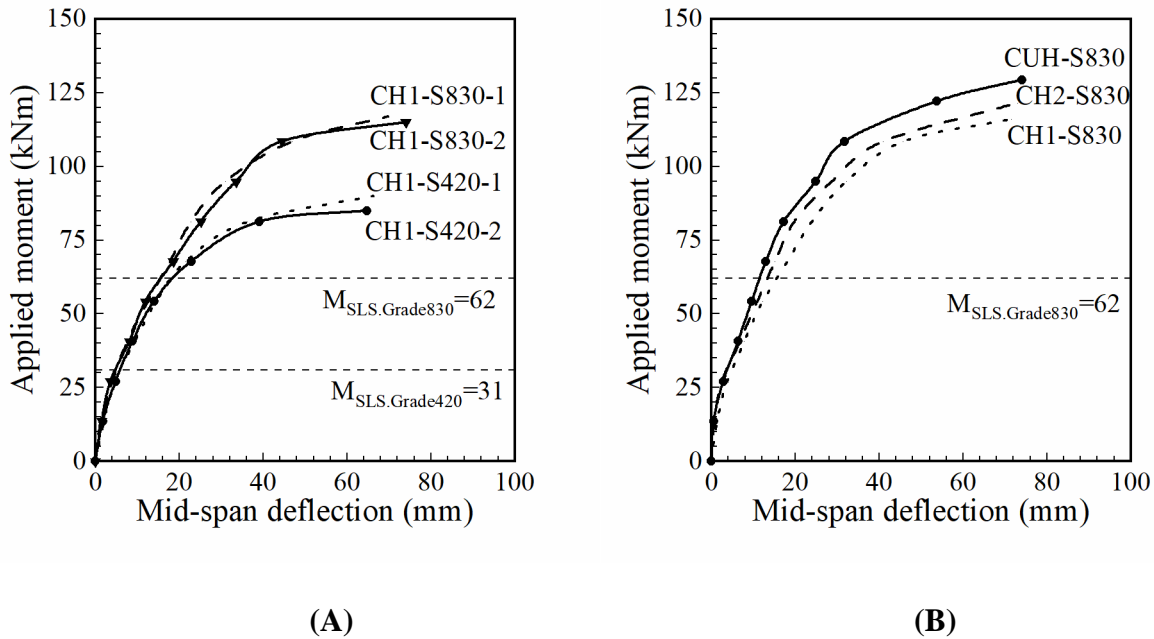
**Figure 4-7. Experimental relationship of the mid-span deflection and applied moment.**
(A) different steel grades, and (B) different concrete strengths.

4.5.2.2 Analytical results

As aforementioned, a program was developed using MATLAB to predict the moment-deflection

relationship. **Figure 4-8 (A)** shows the comparison between the analytical and experimental

moment-deflection relationships for the CH1-S420 and CH1-S830 beam group. In general, the

analytical results are in agreement with the experimental results. The analytical to experimental

failure-moment ratios for CH1-S420 and CH1-S830 are 0.98 and 1.02, respectively. In terms of

deflection, the ratios are 1.17 and 1.03, respectively. Similar results are observed for CH2-S830

and CUH-S830 on **Figure 4-8 (B)**. The failure-moment ratios are 1.04 and 1.05 for CH2-S830

and CUH-S830, respectively. The failure deflection ratios are 1.07 and 1.06 for CH1-S420 and

CH1-S830, respectively.

**(A)**          **(B)**
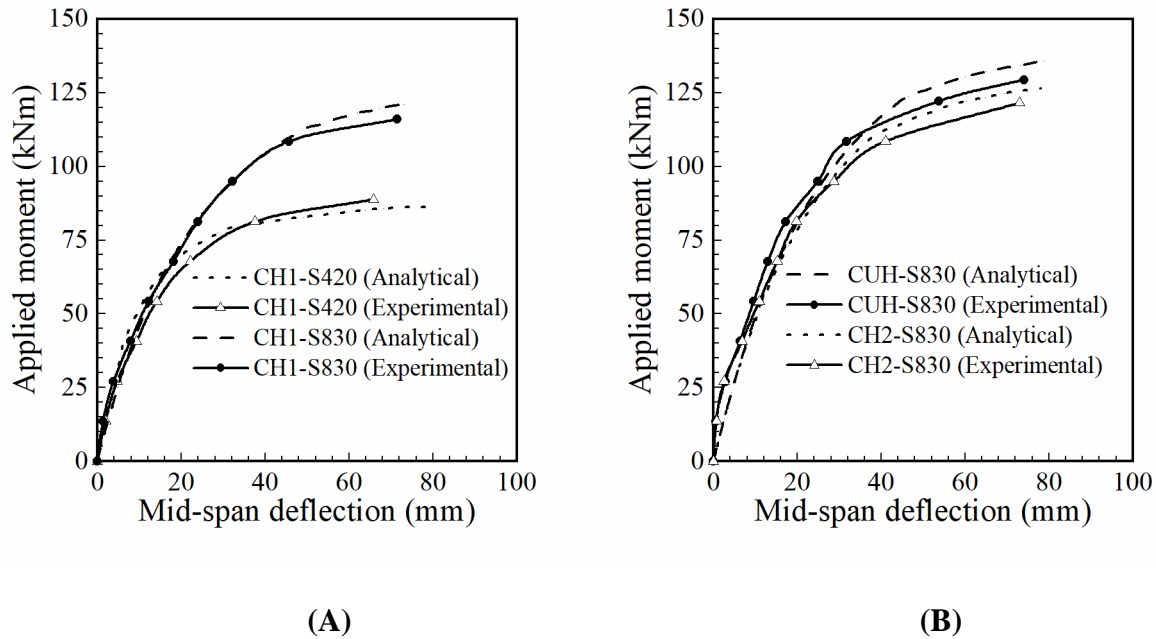
**Figure 4-8. Analytical and experimental relationship between the mid-span deflection and applied moment.**

(A) different steel grades, and (B) different concrete strengths.

The analytical results confirm that the flexural capacity of the beams reinforced with Grade 830 increases by using high strength concrete.  In comparison to CH1-S830, the moments at failure of CH2-S830 and CUH-S830 increased by 4% and 12%, respectively.  Experimentally, the increases in moments were 5% and 12%.  The analytical moment for the beams reinforced with Grade 830 is slightly greater than the measured moment.  This difference could be due to either the reduction in experimental stiffness associated with micro-cracks or the difference between actual and modeling stress-strain relationships of concrete and steel [39].

### 4.5.3    Concrete Strain

Concrete strain at the SLS on the top fiber of the beams varies, depending on the steel grades.  As shown in **Figure 4-9 (A)**, at the SLS the concrete strains of CH1-S420 and CH1-S830 were 568 and 983 microstrain, respectively.  In fact, concrete can experience an elastic behavior up to

0.4 $f_c'$ [40]. In structural design, the SLS concrete stress is typically limited to this stress level to avoid the plastic deformation of concrete. From the stress-strain curves shown in **Figure 4-5**, the corresponding concrete strains at 0.4 $f_c'$ are 597, 948, and 1153 microstrain for CH1, CH2, and UHSC, respectively. Accordingly, the concrete stress of CH1-S420 is in the elastic range at SLS because the concrete strain is less than 597 microstrain. In fact, the concrete stress of CH1-S830 is not in the elastic range at SLS since the concrete strain is more than 597 microstrain. This can be a concern for the use of HSC1 concrete with Grade 830 steel since the concrete strains exceeded the elastic limit and reach the plastic range at SLS.



**(A)**                                   **(B)**
**Figure 4-9. Relationship between concrete strain and applied moment.**
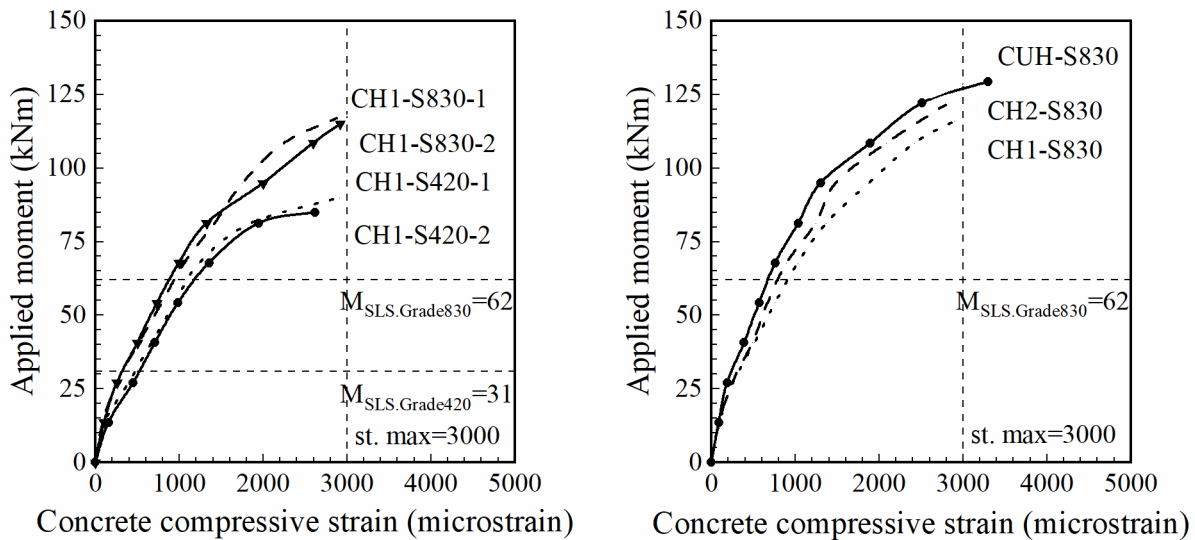(A) different steel grades, and (B) different concrete strengths.

The use of higher strength concrete improves the behavior of beams reinforced with Grade 830 steel. **Figure 4-9 (B)** shows the relationship of concrete compressive strains and applied moments of CH1-S830, CH2-S830, and CUH-S830 beams. The concrete strains of CH2-S830 and CUH-S830 at SLS were 837 and 712 microstrain, respectively. It is noted that the concrete

stress of CH2-S830 and CUH-S830 are in elastic range of concrete since the concrete strains of

the beams are less than the strains corresponding to $0.4\,f_c'$ for each type of concrete. In

comparison to CH1-S830, the concrete strains of CH2-S830 and CUH-S830 were 13% and 26%

less, respectively. The high concrete strains at SLS due to using Grade 830 can be reduced by

using higher concrete strength, so concrete experiences the elastic behavior at SLS.

At the ultimate limit state (ULS), the concrete strains of CH1-S420 and CH1-S830 were 2768

and 2901 microstrain, respectively. As shown in **Figure 4-5**, the theoretical concrete strains at

the peak stress ($\varepsilon_u$) of CH1, CH2, and UHSC were 2916, 3027, and 3381 microstrain,

respectively. **Figure 4-9 (A)** shows that the CH1-S420 beams failed before the concrete reached

the $\varepsilon_u$ of CH1. For CH1-S830, the concrete strain of at ULS was closer to $\varepsilon_u$ of CH1 than that

of CH1-S420. Accordingly, the concrete stress of CH1-S830 was around to reach the ultimate

strength before reinforcement steel Grade 830. **Figure 4-9 (B)** shows the concrete strains of

CH2-S830 and CUH-S830 at ULS were 2793 and 3301 microstrain, respectively. It is noted that

concrete strains of CH2-S830 and CUH-S830 at ULS were less than $\varepsilon_u$ of CH2 and UHSC,

respectively. Therefore, the concern of compression failure before yielding the tension steel due

to the high tensile strength of Grade 830 can be avoided by using high strength concrete.


### 4.5.4    Steel Strain

The theoretical yielding strain of Grade 420 ($\varepsilon_{y420}$) was calculated by dividing the yield strength

by the modulus of elasticity. For Grade 830, the theoretical yielding strain ($\varepsilon_{y830}$) was estimated

from the stress-strain curve shown in **Figure 4-4**. The yielding strain ($\varepsilon_{y830}$) corresponded to the

yield strength (830 MPa). The typical calculated yielding strains of Grade 420 ($\varepsilon_{y420}$) and Grade

830 ($\varepsilon_{y830}$) were 2070 microstrain and 5700 microstrain, respectively. **Figure 4-10 (A)**

illustrates the relationship of the steel tensile strains and applied moments. The steel tensile

strains were measured at mid-span from initial loading to steel yielding. The tensile

reinforcement of CH1-S420 and CH1-S830 reached the yielding strains when the applied

moments were approximately 61 kNm and 99 kNm, respectively. The required moment for steel

yielding in CH1-S830 was 54% greater than that of CH1-S420. The ratios of the failure-moment

to the yielding-moment were 1.42 and 1.18 for CH1-S420 and CH1-S830, respectively. The

capability of structural members to develop inelastic rotation capacity is a function of the length

of the inelastic region [41]. The failure strength to yielding strength ratio represents the length of

inelastic region. In comparison to CH1-S420, the length of inelastic region of CH1-S830

decreased by 17% for CH1-S830.
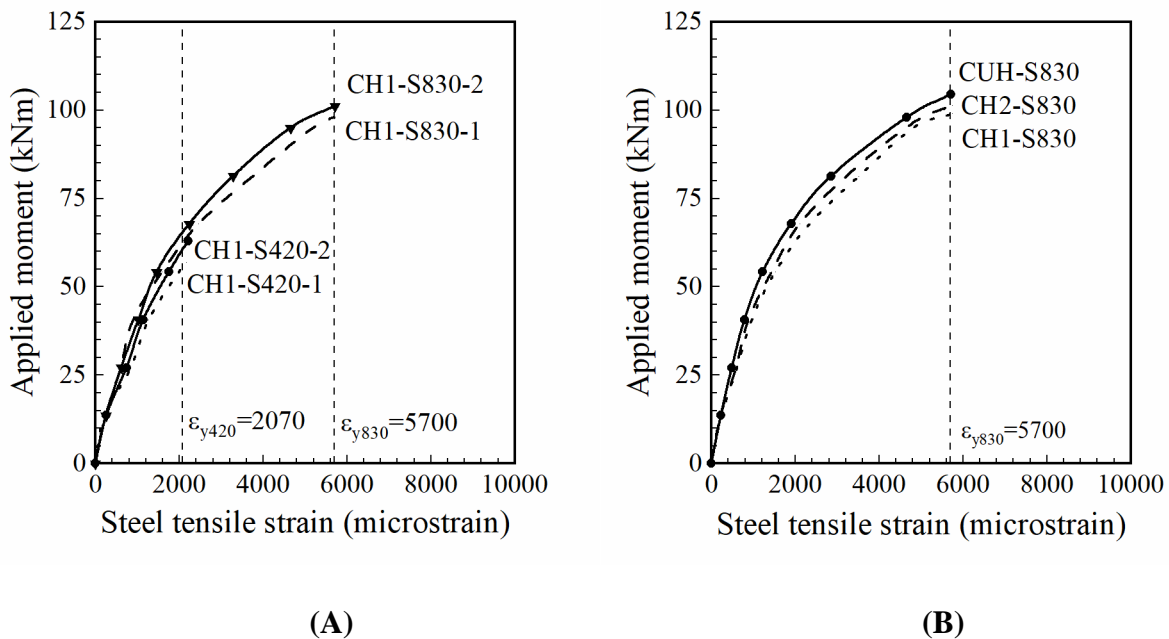


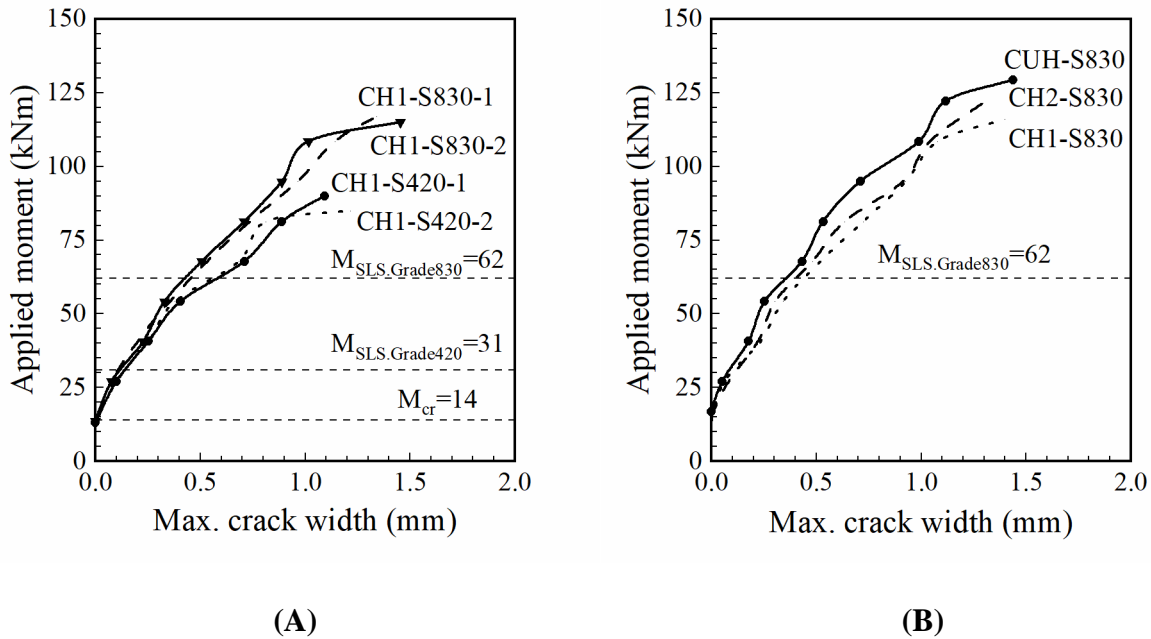(A)                                    (B)
**Figure 4-10. Relationship between tensile steel strain and applied moment.**
(A) different steel grades, and (B) different concrete strengths.

**Figure 4-10 (A)** illustrates the effect of concrete strength on the yielding of Grade 830 steel. When the concrete compressive strength increases, the applied moment required for yielding the tensile reinforcement also increases accordingly. In comparison to CH1-S830, the required moments for yielding the steel of CH2-S830 and CUH-S830 increased by 3% and 5%. The ratios of the failure-moment to the yielding-moment are 1.22 and 1.27 for CH2-S830 and CUH-S830, respectively. In comparison to CH1-S830, the length of the inelastic region for CH2-S830 and CUH-S830 increased by 3% and 8%, respectively. Therefore, the ductility of concrete beams reinforced with Grade 830 can be increased by using high strength concrete.

### 4.5.5   Crack Width

**Figure 4-11 (A)** shows that the relationship between the maximum crack widths and the applied moments. The cracks began to propagate when the applied moment exceeded 14 kNm ($M_{cr}$) for CH1-S420 and CH1-S830 beams. This experimental cracking moment was close to theoretical cracking moment calculated by ACI 318-19 (12 kNm) [41]. The replacement of Grade 420 steel with Grade 830 steel in concrete beams increased the maximum crack width at SLS. The maximum crack widths of CH1-S420 and CH1-S830 at the SLS were 0.15 mm and 0.46 mm, respectively. The maximum crack width of CH1-S830 exceeded the crack width under service loads (0.41 mm) limited by ACI 22R-01 [42]. The concrete cracks adversely affect the service life of concrete structures due to increasing the risk of corrosion of the reinforcement steel.
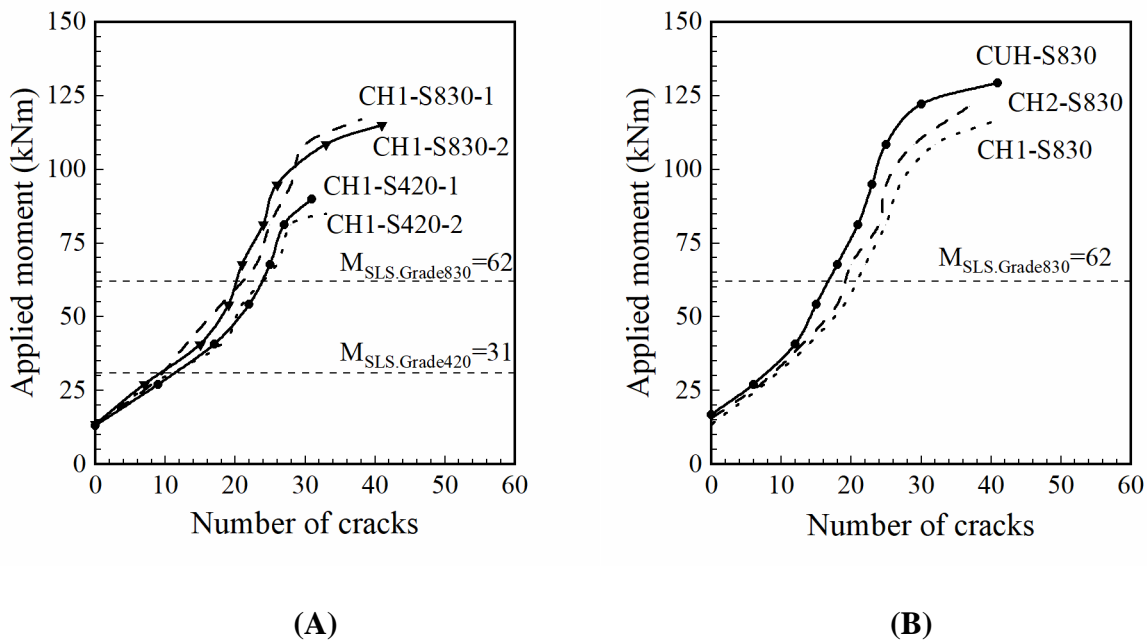
**(A)** **(B)**
**Figure 4-11. Relationship between maximum crack width and applied moment.**
(A) different steel grades, and (B) different concrete strengths.

Casting beams with higher concrete strength can reduce crack widths of beams reinforced with

Grade 830 at SLS. **Figure 4-11 (B)** shows the relationship of maximum crack widths and the

applied moments for CH1-S830, CH2-S830, and CUH-S830 beams. The first crack of CH2-

S830 and CUH-S830 beams appeared when the applied moment reached 15 kNm and 17 kNm,

respectively. The maximum crack widths at the SLS were 0.39 mm and 0.36 mm for CH2-S830

and CUH-S830, respectively. In comparison to CH1-S830, the maximum crack widths for CH2-

S830 and CUH-S830 at the SLS were reduced by 15% and 22%, respectively. These crack

widths were smaller than the 0.41 mm recommended by ACI 22R-01 [42].

### 4.5.6 Number of Cracks

**Figure 4-12 (A)** shows the relationship of number of cracks with applied moment. The number

of cracks at the SLS increases when Grade 420 was replaced with Grade 830 steel. This increase

110

in the number of cracks of CH1-S830 is due to the greater SLS moments. In comparison to CH1-S420, the number of cracks at the SLS of CH1-S830 increased by 67% (12 cracks vs. 20 cracks). When the number of cracks increases, the moisture from the surrounding environmental has a greater chance to penetrate through concrete and accelerate the corrosion of reinforcement.



**(A)**                  **(B)**

**Figure 4-12. Relationship between number of crack and applied moment.**
(A) different steel grades, and (B) different concrete strengths.

**Figure 4-12 (B)** illustrates the relationship of number of cracks and applied moment for CH1-S830, CH2-S830, and CUH-S830 beams. The results show that the number of cracks at the SLS was reduced when beams were cast with concrete having a greater compressive strength. The number of cracks at SLS was 18 for CH2-S830 and 16 for CUH-S830. The number of cracks of CH2-S830 and CUH-S830 at SLS decreased by 10% and 20% as compared to CH1-S830. In addition to increasing the risk of corrosion, the number of cracks adversely affect the bond

111

between concrete and steel reinforcement, reduce beams stiffness, and increase beams deflection [43].

## 4.6    CONCLUSIONS

Based the experimental and analytical results, the following conclusion can be drawn:

1.  The replacement of tensile reinforcement Grade 420 steel with Grade 830 steel increases the flexural resistance moment of concrete beams by 33% when using concrete with the same compressive strength.  In addition, the use of high-strength concrete in combination with Grade 830 steel improves the flexural resistance.  In comparison to CH1-S830, the flexural resistance of CUH-S830 improves by 11% when the concrete strength was increased from 75 MPa to 145 MPa.

2.  The concrete beams reinforced with Grade 830 steel have greater deflection than the control beams at the SLS and ULS.  In comparison to CH1-S420, the deflection of CH1-S830 was twice at the SLS and more by 9% at ULS.

3.  The analytical and experimental results of the failure-moments were in agreement with experimental results.  In comparison to the experimental data, the analytical failure-moments are -2% and 4% for beams reinforced with Grade 420 and Grade 830, respectively.

4.  The use of Grade 830 steel increases concrete strains at the SLS.  To avoid the plastic deformation of concrete at SLS, high strength concrete is recommended for use in combination with Grade 830 steel for reducing concrete stains.  Compressive strains at SLS of CH2-S830 and CHU-S830 are reduced by 17% and 35% in comparison to CH1-S830.

5.  The use of Grade 830 reduces the length of the inelastic region.  However, the use of high strength concrete can reduce the effect of less ductility problem for high strength steel.  The

112

ratio of the moment required for tensile steel yielding to ultimate moment is 1.18 for CH1-S830. This ratio is increased to 1.22 and 1.27 when HSC2 and UHSC are used instead of HSC1.

6.  The maximum crack width and the number of cracks increase when Grade 420 is replaced with Grade 830. Therefore, the use of high strength concrete is recommended to use in combination with Grade 830 for reducing the crack width and number of cracks. CH2-S830 and CUH-S830 comply with the requirements of ACI 224R-01 for crack width.

# REFERENCES

[1] Reis, H., Ervin, B. L., Kuchma, D. A., Bernhard, J. T., "Estimation of Corrosion Damage in Steel Reinforced Mortar Using Guided Waves," Journal of Pressure Vessel Technology, V. 127, No. 3, 2005, pp. 255-261.

[2] Darwin, D., Browning, J., Nguyen, T. V., Locke, C., "Mechanical and Corrosion Properties of a High-Strength, High Chromium Reinforcing Steel for Concrete," SM Report No. 66. University of Kansas, Lawrence KS, 2002, pp. 1-142.

[3] Aldabagh, S., Abed, F., Yehia, S., "Effect of Types of Concrete on Flexural Behavior of Beams Reinforced with High-Strength Steel Bars," ACI Structural Journal, V. 115, No. 2, 2018, pp. 351-364.

[4] Li, Y., "Blast Performance of Reinforced Concrete Beams Constructed with High-Strength Concrete and High-Strength Reinforcement," Master's Thesis, University of Ottawa, Ottawa, Canada, 2016.

[5] Mehta, P. K., Monterio, P. J. M., "Concrete: Microstructure, Properties and Materials," Third edition, McGraw-Hill, New York, 2006, 659 pp.

[6] Allena, S., Newtson, C. M., That, M. N., "Mechanical Properties of Ultra-High Strength Concrete with Local Materials," Advances in Civil Engineering and Building Materials, Taylor & Francis Group, London, ISBN 978-0-415-64342-9, 2013, pp.195-198.

[7] Allena, S., Newtson, C. M., "Ultra-High Strength Concrete Mixtures Using Local Materials," In Proceedings of International Concrete Sustainability Conference, Tempe, AZ, USA, 2010.

[8] Meleka, N. N., Bashandy, A. A., Arab, M. A., "Ultra High Strength Concrete Using Economical Materials," International Journal of Current Engineering and Technology, V. 3, No. 2, 2013, pp. 393-402.

[9] Salomon, A. L., Moen, C. D., "Structural Design Guidelines for Concrete Bridge Decks Reinforced with Corrosion-Resistant Reinforcing Bars," Rep. No. FHWA/VCTIR 15-R10, Virginia Center for Transportation Innovation and Research 530 Edgemont Road Charlottesville VA, 2014, pp. 1-49.

[10] Fang, P., "Development of Sustainable Ultra-High Strength Concretes," Master of Applied Science, Department of Civil Engineering, University of Toronto, Canada, 2013.

[11] Kamal, M. M., Safan, M. A., Etman, M. A., Salama, R. A., "Behavior and Strength of Beams Cast with Ultra High Strength Concrete Containing Different Types of Fibers," HBRC Journal, V. 10, 2014, pp. 55-63.

[12] Seliem, H., Lucier, G., Rizkalla, S., Zia, P., "Behavior of Concrete Bridge Decks Reinforced with High-Performance Steel," ACI Structural Journal, V. 105, No. 1, 2008, pp. 78–86.

[13] Chen, Y., Liu, P., Yu, Z., "Effects of Environmental Factors on Concrete Carbonation Depth and Compressive Strength," Materials Journal, V. 11, 2018, pp. 1-11.

[14] Hassan, T., Seliem, H., Dwairi, H., Rizkalla, S., Zia, P., "Shear Behavior of Large Concrete Beams Reinforced with High-Strength Steel," ACI Structural Journal, V. 105, No. 2, 2008, pp. 173-179.

[15] Harries, K. A., Shahrooz, B. M., Soltani, A., "Flexural Crack Widths in Concrete Girders with High-Strength Reinforcement," Journal of Bridge Engineering, V. 17, No. 5, 2012, pp. 804-812.

[16] Faza, S., Kwok, J., Salah, O., "Application of High-Strength and Corrosion-Resistant ASTM A1035 Steel Reinforcing Bar in Concrete High-Rise Construction," CTBUH 8th World Congress, Council on Tall Buildings and Urban Habitat, Chicago, Illinois, Dubai, 2008, pp. 1-6.

[17] Bowen, G. E., "Service and Ultimate Limit State Flexural Behavior of One-Way Concrete Slabs Reinforced with Corrosion-Resistant Reinforcing Bars," Thesis Master of Science in Civil Engineering, Virginia Polytechnic Institute and State University, USA, May 2013.

[18] Desalegne, A. S., Lubell, A. S., "Shear in Concrete Beams Reinforced with High-Performance Steel," ACI Structural Journal, V. 112, No. 6, 2015, pp. 783-792.

[19] Garay-Moran, J. D., Lubell, A. S., "Behavior of Concrete Deep Beams with High Strength Reinforcement," Structural Engineering Report 277; University of Alberta, Canada 2008.

[20] ACI Committee 439, "Guide for the Use of ASTM A1035/A1035M Type CS Grade 100 (690) Steel Bars for Structural Concrete (ACI 439.6R-19)," American Concrete Institute, Farmington Hills, MI, 2019.

[21] Graham, S. K., Paulson, C., "Mechanical Properties of ASTM A1035 High Strength Steel Bar Reinforcement," WJE No.2008.9901.0, 2008, pp. 1-47.

[22] Munikrishna, A., Hosny, A., Rizkalla, S., Zia, P., "Behavior of Concrete Beams Reinforced with ASTM A1035 Grade 100 Stirrups Under Shear," ACI Structural Journal, V. 108, No. 1, 2011, pp. 34-41.

[23] Shahrooz, B. M., Reis, J. M., Wells, E. L., Miller, R. A., Harries, K. A., Russell, H. G., "Flexural Members with High-Strength Reinforcement: Behavior and Code Implications," J. Bridge Engineering, V. 19, No. 5, 2014, pp. 1-7.

[24] Kareem, R. S., Jones, C., Dang, C. N., Prinz, G. S., Hale, W. M., "Structural Performance of Concrete Bridge Decks Reinforced with Grade-830 Steel Bars," Structures Journal. V. 27, 2020, pp. 1396-1404.

[25] Seliem, H. M. A., "Behavior of Concrete Bridges Reinforced with High-Performance Steel Reinforcing Bars," Doctor Dissertation of Philosophy in Civil Engineering. North Carolina State University, USA, 2007.

[26] Yotakhong, P., "Flexural Performance of MMFX Reinforcing Rebars in Concrete Structures," Master's Thesis, North Carolina State University, Raleigh NC., 2003.

[27] Pyo, S., Koh, T., Tafesse, M., Kim, H. K., "Chloride-Induced Corrosion of Steel Fiber near the Surface of Ultra-High Performance Concrete and its Effect on Flexural Behavior with Various Thickness," Construction and Building Materials Journal, V. 224, 2019, pp. 206-213. https://doi.org/10.1016/j.conbuildmat.2019.07.063.

[28] Fan, L., Meng, W., Teng, L., Khayat, K. H., "Effect of Steel Fibers with Galvanized Coatings on Corrosion of Steel Bars Embedded in UHPC," Composites Part B: Engineering, V. 177, 2019, 107445. https://doi.org/10.1016/j.compositesb.2019.107445.

[29] Marcos-Meson, V., Michel, A., Solgaard, A., Fischer, G., Edvardsen, C., Skovhus, T. L., "Corrosion Resistance of Steel Fiber Reinforced Concrete-A literature review," Cement and Concrete Research, V. 103, 2018, pp. 1-20. https://doi.org/10.1016/j.cemconres.2017.05.016.

[30] Ma, H., Li, Z., "Multi-Aggregate Approach for Modeling Interfacial Transition Zone in Concrete," ACI Materials Journal, V. 111, No. 2, 2014, pp. 189-199.

[31] West, M., Darwin, D., Browning, J., "Effect of Materials and Curing on Period on Shrinkage of Concrete," Rep. No. 98, University of Kansas Center for Research, Inc., Lawrence, Kansas, 2010, pp. 1-245.

[32] Shindman, B., Panesar, D. K., "Comparative Study of Plastic Property Test Methods for Self-Consolidating Concrete," Canadian Journal of Civil Engineering, V. 39, No. 8, 2012, pp. 937-950.

[33] Xiong, M., Liew., J. Y. R., "Mechanical Behaviour of Ultra-High Strength Concrete at Elevated Temperatures and Fire Resistance of Ultra-High Strength Concrete Filled Steel Tubes," Materials & Design Journal, No. 104, 2016, pp. 414-427.

[34] American Institute of Steel Construction, Inc. ANSI/AISC 360-10: Specification for Structural Steel Buildings," June 22, 2010.

[35] ASTM C469/C469M-14, "Standard Test Method for Static Modulus of Elasticity and Poisson's Ratio of Concrete in Compression," ASTM International, West Conshohocken, PA, USA, 2014.

[36] Darwin, D., Dolan, C. W., Nilson, A. H., "Design of Concrete," Fifteenth Edition, McGraw-Hill, New York, 2016, 244 pp.

[37] Yosefani, A., "Flexural Strength, Ductility, and Serviceability of Beams that Contain High-Strength Steel Reinforcement and High-Grade Concrete," Doctor Dissertation of Philosophy in Civil Engineering, Portland State University, Oregon, 2018.

[38] Lu, Z. H., Zhao, Y. G., "Empirical Stress-Strain Model for Unconfined High-Strength Concrete under Uniaxial Compression," Journal of Materials in Civil Engineering, V. 22, No. 11, 2010, pp. 1181-1186.

[39] Elgabbas, F., El-Ghandour, A. A., Abdelrahman, A. A., El-Dieb, A. S., "Different CFRP Strengthening Techniques for Prestressed Hollow Core Concrete Slabs: Experimental Study and Analytical Investigation," Composite Structures, V. 92, 2010, pp. 401-411.

[40] Barros, H., Ferreira, C., Marques, T., "Moment-Curvature Diagrams for Evaluation of Second Order Effects in RC Elements," ECCOMAS Congress, Greece 2016, pp. 1-15.

[41] ACI Committee 318, "Building Code Requirements for Structural Concrete (ACI 318R-19): An ACI Standard: Commentary on Building Code Requirements for Structural Concrete," An ACI Report, American Concrete Institute, Farmington Hills, MI, 2019.

[42] ACI Committee 224, "Control of Cracking in Concrete Structures (ACI 224R-01)," An ACI Report, American Concrete Institute, Farmington Hills, MI, 2008.

[43] Apostolopoulos, C. A., Koulouris, K. F., Apostolopoulos, A. C., "Correlation of Surface Cracks of Concrete Due to Corrosion and Bond Strength (Between Steel Bar and Concrete)," Advances in Civil Engineering Journal, V. 2019, 2019, pp. 1-12.

[44] ASTM C136/C136M-19, "Standard Test Method for Sieve Analysis of Fine and Coarse Aggregates," ASTM International, West Conshohocken, PA, USA, 2019.

**APPENDIX 4A**

The gradation of fine aggregate (FA) and coarse aggregate (CA), MAS 19 mm and MAS 9.5 mm, were determined by sieve analysis as per ASTM C136/136M-19 [44]. The gradation of fine and coarse aggregate is shown in **Figure 4A-1**.
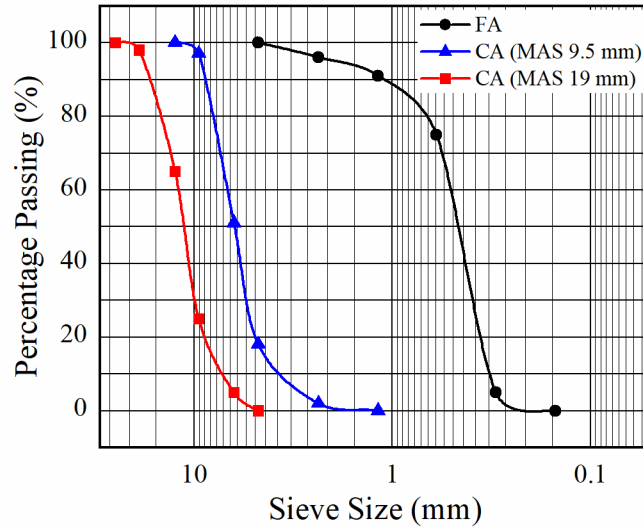


**Figure 4A-1. Gradation of fine and coarse aggregates.**

# CHAPTER 5: CONCLUSIONS, CONTRIBUTIONS, AND FUTURE WORK

## 5.1 CONCLUSIONS

The principal goal of this research was to provide further understanding of the behavior and performance of concrete structures reinforced with A1035 steel. One of the main objectives for this research is the investigation of concrete bridges reinforced with differing amounts of A1035 at both the service and strength limit states. The allowable reduction of the quantity of reinforcing steel due to the higher strength of A1035 and the effect of this reduction on cost were examined for bridge decks. Also, the effect of concrete strength was investigated for flexural members reinforced with high-performance steel (A1035) was another objective of this research. The tensile strain of steel, compressive strain of concrete, deflection, crack width, and the number of cracks were investigated. Another objective was to develop a finite element model for concrete structures reinforced with A1035. This model will allow researchers to investigate the performance of structures reinforced with A1035 analytically, instead of conducting experimental tests. The following conclusions can be drawn from this research.

1. The use of Grade 830 steel in concrete bridge decks reduced the maximum crack width, number of cracks, and deflection at serviceability. The level of reduction is dependent on the replacement ratio of Grade 830 steel to Grade 420 steel. When the amount of Grade 830 steel is 35-40% less than that of Grade 420 steel, the performance of concrete bridge decks reinforced with Grade 420 or Grade 830 steel are comparable.

2. When Grade 420 steel is replaced at a one-to-one rate with Grade 830 steel, the flexural resistance increases by 37%. However, the improvement in flexural resistance was still 19-24% even though the reinforcement ratio of Grade 830 steel was reduced 35-40%.

3. In addition to the maximum crack width, the flexural resistance, compressive concrete strain, and tensile steel strain of decks reinforced with Grade 830 can be improved by reducing the concrete cover. When the concrete cover was reduced from 50 mm to 38 mm, the improvements include decreasing the maximum crack width by 20-33%, increasing the flexural resistance by 2-5%, decreasing the maximum compressive concrete strain by 28%, and decreasing tensile steel strain at service by 24%.

4. The replacement of Grade 420 with Grade 830 steel can reduce the cost and the construction time. The reduction in the amount of steel in concrete decks reinforced with Grade 830 steel decreases the total cost and reduces the time for constructing concrete bridge decks.

5. The non-linear behavior of concrete bridge decks can be appropriately represented by finite element method using ABAQUS software. The non-linear behavior of concrete and Grade 830 steel can be displayed by the Concrete Damage Plasticity model and Plasticity option in ABAQUS, respectively.

6. The load-deflection relationship, compressive strains of concrete, and tensile strains of reinforcing steel prior to yielding in bridge decks reinforced with Grade 830 steel can be estimated using a finite element model. The model is in very good agreement with the experimental data. Also, the propagation of cracks in the concrete deck can be monitored and captured by the proposed finite element model. In the finite element model, minimal cracks widths can be visualized in cracks patterns.

7. In comparison to the concrete decks reinforced with Grade 420, the failure loads of decks containing same steel ratio and reinforced by Grade 690 and Grade 830 are greater by 29% and 41%, respectively.

8. The analytical results show the replacement of Grade 420 by Grade 690 and Grade 830 reinforcement increases the maximum deflection of concrete decks by 21% and 28%, respectively. This result is attributed to the higher tensile strength of Grade 690 and Grade 830 in comparison to Grade 420 steel even though both types of steel have same modulus of elasticity.

9. The flexural resistance of concrete beams reinforced with Grade 830 is 33% more than a control beams containing same steel ratio and reinforced with Grade 420. Also, the concrete beams reinforced with Grade 830 steel more deflection (2% more) at the SLS and 9% more at the ULS when compared to the control beams.

10. Increasing the concrete compressive strength of beams reinforced with Grade 830 can improve the flexural resistance. The flexural resistance of beams increases by 5% and 11% when the concrete strength increases from 75 MPa to 107 MPa and 145 MPa, respectively.

11. In comparison to the experimental data, the analytical failure-moments are -2% and 4% for beams reinforced with Grade 420 and Grade 830, respectively.

12. To avoid the plastic deformation of concrete beams reinforced with Grade 830 at the SLS, high strength concrete is recommended for use in combination with Grade 830 steel for reducing concrete stains. Compressive strains at the SLS of beams reinforced with Grade 830 are reduced by 17% and 35% when the concrete strength increases from 75 MPa to 107 MPa and 145 MPa, respectively.

13. When high strength concrete is used with beams reinforced by Grade 830 steel, the reduction of ductility that can be associated with the use of higher strength rebar is lessened. The ratio of the required moment for tensile steel yielding to ultimate moment

is increased from 1.18 to 1.22 and 1.27 when the concrete strength increases from 75

MPa to 107 MPa and 145 MPa, respectively.

14. The maximum crack width and the number of cracks increase when Grade 420 is
   replaced with Grade 830. Therefore, the use of high strength concrete is recommended to
   use in combination with Grade 830 for reducing the crack width and number of cracks.
   CH2-S830 and CUH-S830 comply with the requirements of ACI 224R-01for crack
   width.

## 5.2    CONTRIBUTION TO THE BODY OF KNOWLEDGE

Most of the previous research uses a direct replacement method of conventional reinforcement

with Grade 830 steel, so the higher strength of Grade 830 is not considered. This research

provides further understanding about the structural behavior of concrete reinforced with high

strength steel Grade 830. Research has suggested that using the higher tensile strength of Grade

830 steel and taking in account its improved strength, can reduce costs, material quantity, and

construction time in addition to improving the structural behavior. The following contributions

are pointed out:

1. The use of Grade 830 steel as the main reinforcement improves structural behavior of
   concrete bridge decks at the service and ultimate strength states. This includes improving
   the flexural resistance, deflection, concrete compressive strains, steel tensile strain, cracks
   width, and number of cracks. The reinforcement ratio can be reduced by 35 to 40% when
   Grade 420 steel is replaced with Grade 830.

2. When Grade 830 steel is used in combination with high strength concrete, compression
   failures and increases in crack number and width can be reduced and possibly avoided.

122

3. A finite element model was developed to represent concrete members reinforced with Grade 830 steel. The finite element model can be used as an alternative to experimental testing when investigating the behavior of concrete members reinforced with Grade 830 steel. The analytical results were in a very good agreement with experimental data.

## 5.3    RECOMEDATIONS FOR FUTURE WORK

Based on the experimental and analytical investigations of this research, additional studies may be considered to investigate the structural behavior of concrete structures reinforced with Grade 830 steel. The following recommendations are suggested:

1. Further experimental investigations may be considered for other concrete members reinforced with Grade 830 steel, such as deep beams and columns.

2. The long term performance of concrete members reinforced with Grade 830 steel.

3. The use of Grade 830 steel as shear reinforcement.

4. The behavior of concrete members reinforced with Grade 830 steel in beams cast with ultra-high-performance concrete (UHPC).

5. The flexural behavior of concrete beams reinforced with Grade 830 steel subjected to cyclic loading.

6. Analytical design equations/design process for Grade 830 steel.